UNIVERSIDADE DE BRASÍLIA

INSTITUTO DE GEOCIÊNCIAS (IG)

CARACTERIZAÇÃO DA ASSINATURA DA MINERALIZAÇÃO POLIMETÁLICA DO *GREENSTONE BELT* DE FAINA (GO)

Dissertação de Mestrado n° 478

Fernando Rossi Almeida

Orientadora: Profa. Dra. Adalene Moreira Silva
Coorientadora: Profa. Dra. Catarina Labouré Bemfica Toledo

Área de Concentração: Geologia Econômica e Prospecção Mineral

BRASÍLIA
2021

FERNANDO ROSSI ALMEIDA

CARACTERIZAÇÃO DA ASSINATURA DA MINERALIZAÇÃO POLIMETÁLICA DO *GREENSTONE BELT* DE FAINA (GO)

Dissertação apresentada ao Instituto de Geociências da Universidade de Brasília, como requisito para obtenção do grau de Mestre em Geologia.

Orientadora

Profª. Drª. Adalene Moreira Silva

Banca Examinadora

Profª. Drª. Adalene Moreira Silva (UnB)

Prof. Dr. Álvaro Penteado Crosta (UNICAMP)

Prof. Dr. Claudinei Gouveia de Oliveira (UnB)

Brasília, junho de 2021.

“As with anything creative, change is inevitable."

Enya

AGRADECIMENTOS

Agradeço aos meus pais, Silvio e Lilian pelo apoio incondicional de sempre me incentivarem a ser quem eu sou, fazer minhas próprias escolhas e seguir a carreira que escolhi. Eu sou quem sou hoje graças a vocês. Meu irmão, Daniel, e minha avó, Maria, tios e tias, obrigado pelo carinho e fé que sempre tiveram por mim.

Agradeço minhas orientadoras, Adalene Moreira Silva e Catarina Labouré Bemfica Toledo pela confiança, motivação, ensinamentos e carinho que me transmitiram durante todo esse período, vocês são grande fonte de inspiração na minha formação como geólogo, profissional e humano. Também agradeço o professor Diego Fernando Ducart e o mestrando Kawinã Araujo pelo suporte e discussões que muito contribuíram com esse presente trabalho.

Todos meus agradecimentos ao CNPq e CAPES pela concessão de bolsa de mestrado e todo o apoio financeiro dedicado os custos técnicos que viabilizaram o trabalho. E também ao Instituto de Geociências da Universidade de Brasília, que foi minha segunda casa por todos esses anos de graduação e mestrado. Sou muito grato pela oportunidade de ter aprendido tanto com toda a equipe de professores e técnicos e também pelo privilégio de poder desenvolver pesquisa em um instituto tão bem capacitado em termos estrutura técnica e de laboratórios. Enfatizo o agradecimento aos professores Paola Ferreira Barbosa, Adriana Horbe e Luís Fernando Martins Ribeiro pelas suas respectivas contribuições.

Agradeço meu grande amigo e irmão Victor Mota e Nogueira, que esteve presente e me apoiou em todos os momentos durante toda minha jornada como estudante e geólogo, enfatizo o apoio dado nesse último ano, tão difícil para todos. Acredito que minha experiência não seria a mesma sem nossa amizade, risadas e perrengues que vivemos juntos.

Agradeço às pessoas que se tornaram minha grande família em Brasília: Malú Nakamura, Caio Rodrigo Costa, Juliana Carvalho, Mariana Machado, Moniélle Martins, Joice Dias, Thassio Werlang, Vitória Flores, Deusavan Costa, Alissa Hubner, Pedro Amaral e Luana Machado. Sou muito grato pelo acolhimento e carinho de todos.

Também agradeço meus amigos de Londrina, Victor Zanin, Felipe Salerno, Fernando Nakagawa, Jéssica Koyama e Mariana Marques. Mesmo fisicamente distantes por boa parte do tempo, vocês se mantiveram presentes, me ensinaram e me ajudaram muito. Espero sempre poder retribuir essa força incondicional que vocês me transmitem.

Agradeço a empresa *Orinico Gold Limited* e toda sua equipe pelo apoio a pesquisa e por ceder as amostras e análises necessárias para a execução desse trabalho. O presente trabalho foi realizado com apoio da Coordenação de Aperfeiçoamento de Pessoal de Nível Superior - Brasil (CAPES) - Código de Financiamento 001.

RESUMO

Essa dissertação de mestrado apresenta os resultados da investigação do sistema mineral polimetálico Tinteiro mapeado no *greenstone belt* de Faina, que é associado à estruturas rúpteis que cortam as unidades litológicas e a mineralização aurífera, de idade estimada paleoproterozoica. A mineralização polimetálica é caracterizada por brechas manganesíferas/ferruginosas com teores anômalos de metais de base, tais quais Ag, Co, Cu, Ni, Ba, Mo, As, Pb, U, Fe, Mn e LREE. O *footprint* da mineralização é marcado por uma alteração hidrotermal hematítica mapeada em várias escalas, ora como vênulas milimétricas, ora presente nos contatos litológicos entre as unidades. Os resultados obtidos nesta dissertação permitiram definir o ambiente mineralizado através da análises de amostras de testemunhos de sondagem que interceptam este sistema. A análise petrográfica e de difratometria de raios-x das brechas indica uma assembleia mineral composta por quartzo, muscovita, hematita, goethita, psilomelano, romanechita e hollandita, e calcopirita. Nas porções onde a alteração hematítica é mais intensa, observa-se quartzo, muscovita, hematita, goethita, clinocloro, corrensita e caulinita. O mapeamento espectral das brechas demonstra que os minerais dos grupos dos óxidos e hidróxidos de ferro possuem composição intermediária entre goethita e hematita, e também que os de minerais do grupo das micas brancas têm sua composição intermediária entre muscovita e fengita, essas apresentando alto grau de cristalinidade. Os resultados de geoquímica de rocha total indicam valores anômalos de até 9% de Fe_2O_3, 13% de MnO, 2.790 ppm de Co, 10.000 ppm de Ba, 1.890 ppm de Cu e 1.460 ppm de Ni. Os elementos Zn e As demonstraram ser vetores de identificação da alteração hematítica proximal como *pathfinders* do sistema. A integração dos multiparâmetros coletados permitiu a caracterização do *footprint* da zona distal do sistema, que é caracterizada por alta susceptibilidade magnética (valor médio de 4,23 x 10^{-3} SI), abundancia de clorita e carbonato superior a 0,1%, teores superiores a 5% de MgO, Cao, P_2O_5 e Na_2O e pouca incidência de estruturas rúpteis. O *footprint* do halo proximal do sistema evidencia uma queda nos valores de densidade natural e susceptibilidade magnética das rochas no sentido da mineralização. A composição dos minerais do grupo dos óxidos e hidróxidos de ferro é de hematita e a cristalinidade dos minerais membros do grupo das micas brancas atinge valores superiores a 10. E quanto maior a proximidade da porção mineralizada, maior a intensidade de feições de venulações e fraturas. O *footprint* da zona mineralizada é caracterizado por queda da abundancia de minerais do grupo dos óxidos e hidróxidos de ferro (menor que 0,22), queda nos valores da densidade da rocha, mas altos valores de densidade absoluta e a susceptibilidade magnética aumenta em relação às zonas proximais (média de 0,542 x 10^{-3} SI).

PALAVRAS-CHAVE: GREENSTONE BELT DE FAINA; MAPEAMENTO ESPECTRAL; PETROFÍSICA; INTEGRAÇÃO DE DADOS; MINERALIZAÇÃO POLIMETÁLICA

ABSTRACT

This research investigates the Tinteiro polymetallic mineral system that is found in several locations in the Faina greenstone belt, which is associated with brittle structures that cut the lithological units. The polymetallic mineralization is characterized by manganesiferous/ferruginous breccias with anomalous levels of base metals, such as Ag, Co, Cu, Ni, Ba, Mo, As, Pb, U, Fe, Mn and LREE. The mineralization footprint is marked by a hematitic hydrothermal alteration mapped at various scales, sometimes as millimeter veinlets, or even present in the lithological contacts between the metachert units, muscovite schist and carbonate units. The results obtained in this dissertation made it possible to define the mineralized environment through the analysis of samples extracted from drilling cores that intercept this system. The petrographic description and x-ray diffractometry analysis of the breccias shows a mineral assemblage composed of quartz, muscovite, hematite, goethite, psilomelane, romanechite and hollandite, and chalcopyrite. In the portions where the hematitic alteration is more intense, quartz, muscovite, hematite, goethite, clinochlore, corrensite and kaolinite are observed. The spectral mapping of the breccias shows that the minerals from the group of iron oxides and hydroxides have an intermediate composition between goethite and hematite, and that the of minerals from white micas group have their composition intermediate between muscovite and phengite, these presenting a high degree of crystallinity. The results of total rock geochemistry brought anomalous values of up to 9% Fe2O3, 13% MnO, 2,790 ppm Co, 10,000 ppm Ba, 1,890 ppm Cu and 1,460 ppm N, and the elements Zn and As demonstrated to be important pathfinders of proximal hematitic alteration. The integration of the collected multiparameters data identifies that the footprint of the distal zone of the system is characterized by high magnetic susceptibility (average value of 4.23 x 10-3 SI), abundance of chlorite and carbonate greater than 0.1, contents greater than 5% MgO, Cao, P2O5 and Na2O and low incidence of brittle structures. The footprint of the proximal halo of the system shows a drop in the values of density and magnetic susceptibility of the rocks to the direction of mineralization, the composition of the minerals in the group of iron oxides and hydroxides is hematite and the crystallinity of the minerals members of the group of white micas reach values greater than 10, and the greater the proximity of the mineralized portion, the greater the intensity of venulations features. The footprint of the mineralized zone is characterized by a decrease in the abundance of minerals from the group of iron oxides and hydroxides (less than 0.22), a decrease in rock density values, but high absolute density values and magnetic susceptibility increases in relation to to the proximal zones (average of 0.542 x 10-3 SI).

***KEYWORDS**: FAINA GREENSTONE BELT; REFLECTANCE SPECTROSCOPY; DATA INTEGRATION; POLLYMETALIC HIDROTERMAL ALTERATION.*

ÍNDICE DE FIGURAS

ÍNDICE DE TABELAS

Sumário

CAPÍTULO I - INTRODUÇÃO

1. Apresentação

Os *greenstone belts* são componentes importantes na compreensão da evolução tectônica terrestre e estão presentes em vários crátons pelo mundo, materializados em uma grande variedade litológica de rochas ígneas a sedimentares (Pearce, 2014; Smithies *et al.,* 2018). Essas rochas carregam o vestígio de diferentes ambientes tectônicos e os mais variados eventos deformacionais e magmáticos, bem como hospedam mineralizações de ouro, cobre níquel, dentre outras (Mathieu *et al*., 2020).

O reconhecimento de terrenos férteis de alta concentração aurífera e de metais de base é de suma importância tanto para a compreensão cientifica da gênese desses depósitos, quanto para o desenvolvimento econômico relacionado à exploração dessas *commodities* (De With & Ashwal, 1995; Patten *et al.*, 2020; Hastie *et al.*, 2020; Katz *et al*., 2021). A prospecção mineral está cada vez mais focada em corpos não aflorantes, exigindo ferramentas mais eficazes para detectar sistemas minerais em diferentes escalas e mapear a assinatura dessas mineralizações (Lampinem *et al.*, 2019; Rieger *et al.*, 2021). Essa assinatura tem sido denominada como o *footprint* de uma zona mineralizada, termo idealizado tanto por grupos de pesquisas canadenses e australianos há mais de uma década. O NSERC-CMIC *Footprints Project* é o grupo canadense fundado em 2010 com o intuito de formar um fundo de investimento em parceria de universidades, empresas de mineração e *softwares* que viabilizasse a caracterização massiva de vários depósitos minerais importantes para a indústria do país, dividindo o projeto em três subprojectos: o *Disseminated Au Subproject*; *Basinal U Subprject*; e *Porphyry Cu Subproject*. Já o grupo australiano *Distal Footprints Research Project*, fundado em 2016, foi criado como resposta ao fato da maioria dos grandes depósitos minerais descobertos pela sua expressão direta na superfície já estarem em estágios avançados de exploração. Seu foco é fornecer uma base de conhecimento e tecnologia que visa aumentar substancialmente a taxa de sucesso da exploração mineral em depósitos que estão recobertos por espessas camadas de rochas intemperizadas e coberturas lateríticas (Lesher *et al.*, 2017).

Faz-se necessário, então, a delimitação de fatores que permitam determinar assinaturas detectáveis de sistemas mineralizados em subsuperficie. Isso consiste na integração do conhecimento geológico regional e de detalhe (estratigrafia, trama estrutural das rochas e petrografia) com todo o banco de dado de parâmetros químicos e físicos que podem ser determinados por análises diretas (geoquímica, química mineral, petrografia de detalhe, petrofísica, escaneamento espcetral) e remotas/indiretas (aerogeofísica, sensoriamento remoto, linhas sísmicas). O fato é que cada ferramenta mapeia um *footprint* específico e a integração destes multiparâmetros representam um salto para a academia e para a indústria mineral. E essa premissa tem apresentado resultados positivos que permitiram a exploração de áreas onde a extração mineral foi anteriormente considerada tecnicamente inviável, ou não econômica (Lesher *et al.*, 2017;Byrne *et al.*, 2020; Kreuzer *et al.,* 2020).

A área de estudo esta localizada dentro do Terreno Arqueano-Paleoproterozóico de Goiás (Figura 1). O mesmo possui depósitos hospedados nos *greenstone belts* de Crixás (7 Moz Au), Guarinos (6,5 Moz), Pilar (0,7 Moz) ao norte, e Faina (3 Moz) ao sul. A ocorrência de ouro associada a estas faixas é reconhecida desde o século XVIII e a mineralização aurífera desses terrenos é hospedada em rochas metavulcânicas e metassedimentares estruturalmente controladas por zonas de cisalhamento de nível crustal rúptil-dúctil, incluindo empurrões de baixo ângulo e falhas do tipo *strike-slip*, associadas a eventos orogênicos durante o Paleoproterozóico (Pulls, 1995; Resende, 1999; Marques *et al.*, 2013; Jost *et al.,* 2014).

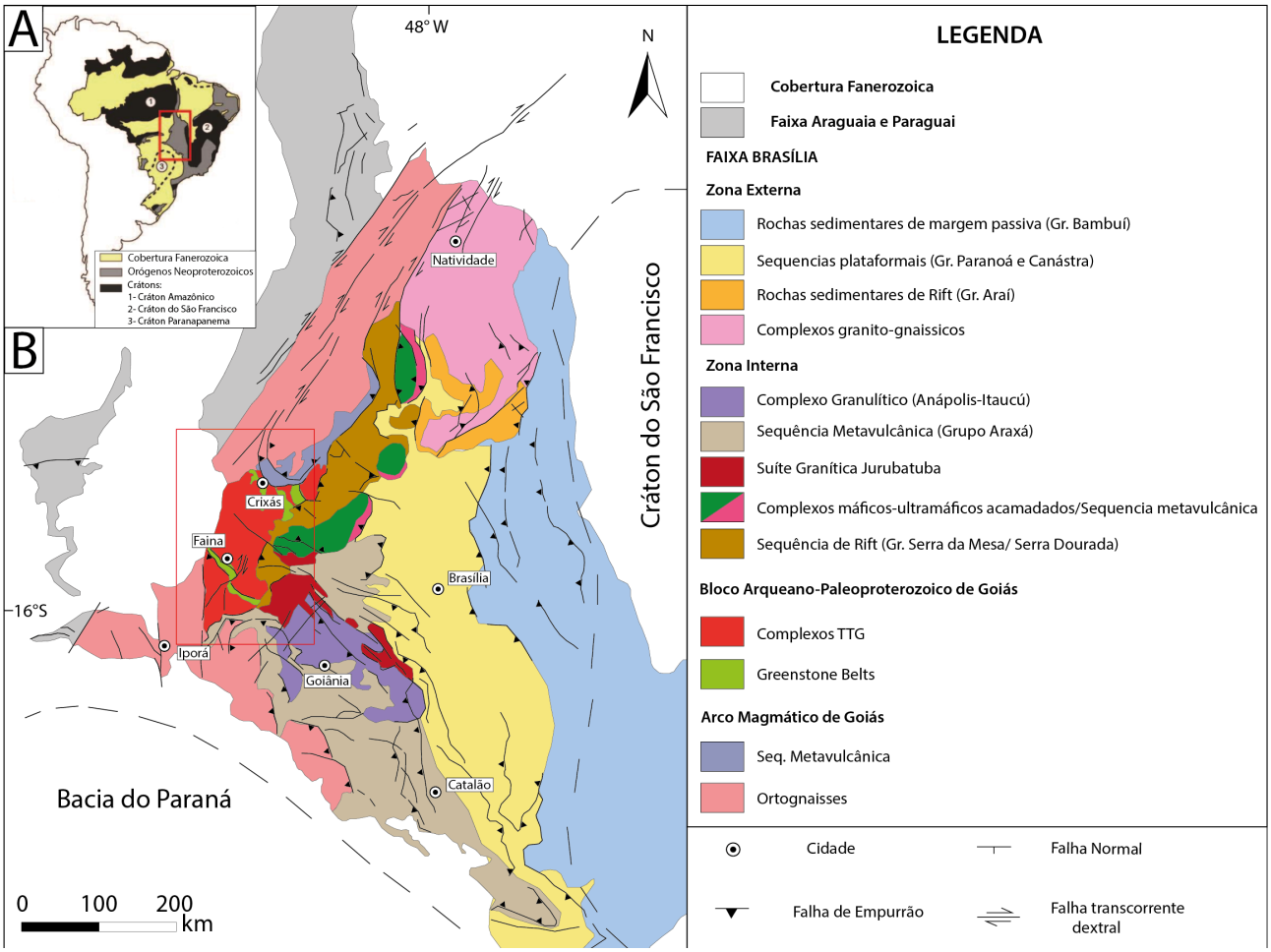

Figura 1: A) Localização da Província Tocantins no Brasil. B) Mapa simplificado da Faixa Brasília e a compartimentação de suas principais unidades geológicas, destaque em vermelho no Terreno Arqueano-Paleoproterozóico de Goiás (adaptado de Pimentel *et al.*, 2004).

O *greenstone belt* de Faina hospeda três principais depósitos auríferos de estilos mineralizantes distintos. O depósito Cascavel (Jost *et al.,* 2014; Campos *et al.*, 2017), que é caracterizado pela mineralização de ouro do tipo *vein hosted*, enquanto o de Sertão está associado a um sistema de ouro disseminado (Bogossian *et al.*, 2020) e também ocorrências de ouro hospedadas em conglomerados (Carvalho *et al,*. 2013). Porém, esses estudos independentes ainda carecem de integração regional para propor um modelo genético coerente interligado das mineralizações auríferas do *greenstone belt* de

Faina. A mina de ouro Sertão foi implantada no ano 2000 (até então explorada pela empresa Sertão Mineração Lda.), e iniciou com a extração do sistema de minério oxidado atingindo profundidades de até 40 metros e uma produção de mais de 250 Moz de ouro com o teor médio de 24,95 g/t (Silva & Rocha, 2008). (Carvalho *et al.,* 2013) também reportam mineralizações auríferas associada à sistemas detríticos, hospedado em conglomerados, e dentre os vários avanços do conhecimento metalogenético da região, destaca-se a descoberta de uma mineralização polimetálica intitulada de sistema Tinteiro pela empresa *Orinoco Gold Limited* (Campos *et al.,* 2015), ainda muito pouco estudada e é o objeto de estudo do presente trabalho.

O sistema Tinteiro é caracterizado por uma alteração hidrotermal marcada por halo de alteração muscovítica, hematítica e óxidos e hidróxidos de manganês associados aos metacherts que intercepta as unidades do *greenstone belt* de Faina (quartzitos, metapelitos e metacherts) e associadas com estruturas rúpteis de direção preferencialmente NE (mas também NW e E-W) e que seccionam toda a sequencia metavulcanosedimentar e os sistemas minerais de ouro orogênico (Campos *et al*., 2017; Bogossian *et al.*, 2020). Os dados publicados pela *Orinoco Gold Limited* destacam teores de Cu-Au associados com anomalias de Co, Ba, Ag, U e Fe e com semelhanças a um sistema de IOCG (*Iron Oxide Cupper Gold ore deposit*) (Orinoco Gold *annual report*, 2014).

Este trabalho foi realizado dentro do Programa de Pós-Graduação em Geologia do Instituto de Geociências da Universidade de Brasília sob a orientação da Professora Dra. Adalene Moreira Silva, da Professora Dra. Catarina L. B. Toledo e contribuição do Professor Dr. Diego F. Ducart da Unicamp e foi feito em parceria com a empresa *Orinoco do Brasil Mineração Ltda*.

A meta principal deste projeto é mapear o *footprint* da mineralização polimetálica do *greenstone belt* de Faina conhecida como Sistema Tinteiro. Busca-se definir os principais vetores exploratórios na área pela caracterização do arcabouço litológico interceptado pelas estruturas mineralizantes e suas zonas de alterações hidrotermais, com o interesse de diferenciar ou individualizar quais características são oriundas do evento orogênico regional do *greenstone* e as referentes ao sistema tardio de nível crustal rúptil a rúptil-dúctil. Foram utilizadas técnicas tanto convencionais quanto não convencionais para a indústria nesta caracterização, com o intuito de calibrá-las como novos instrumentos relevantes à exploração mineral

1.1 Objetivos

O objetivo central da dissertação de mestrado é caracterizar a assinatura (*footprint*) da mineralização polimetálica do *greenstone belt* de Faina conhecida como Sistema Tinteiro, a partir de técnicas espectrais para mapeamento mineral, geoquímica, propriedades físicas da rocha e sua integração com dados geológicos.

Os objetivos específicos incluem:

i. Individualização das principais zonas de alteração hidrotermal na área de estudo a partir da descrição de testemunhos de sondagem;

ii. Análise petrográfica da assembleia mineral associada à mineralização;

iii. Levantamento de propriedades físicas de rochas (densidade e susceptibilidade magnética) em testemunhos de sondagem, com o intuito de auxiliar na caracterização petrofísica qualitativa do minério e suas encaixantes;

iv. Análise de dados petrofísicos obtidos em laboratório;

v. Caracterização espectroradiométrica de todos os furos de sondagem, com foco nas zonas de alteração hidrotermal identificadas em campo e em testemunhos de sondagem;

vi. Caracterização mineralógica de domínios específicos onde o minério encontra-se friável e intemperizado por difratometria de raios-x;

vii. Integração dos dados obtidos visando a caracterização da assinatura geofísica e espectral do sistema polimetálico Tinteiro do *Greenstone belt* de Faina.

1.2 Localização e acesso

A região estudada localiza-se na porção noroeste do estado de Goiás. A distância da capital do estado (Goiânia) é de aproximadamente 200 km. Toda a amostragem foi realizada no galpão de sondagem da empresa *Orinoco do Brasil Mineração Ltda*. que pode ser acessado pela via não pavimentada que conecta os municípios de Faina e Lua Nova, ou a partir da estrada GO-230 acessada pela GO-164, no sentido de Lua Nova (Figura 2).

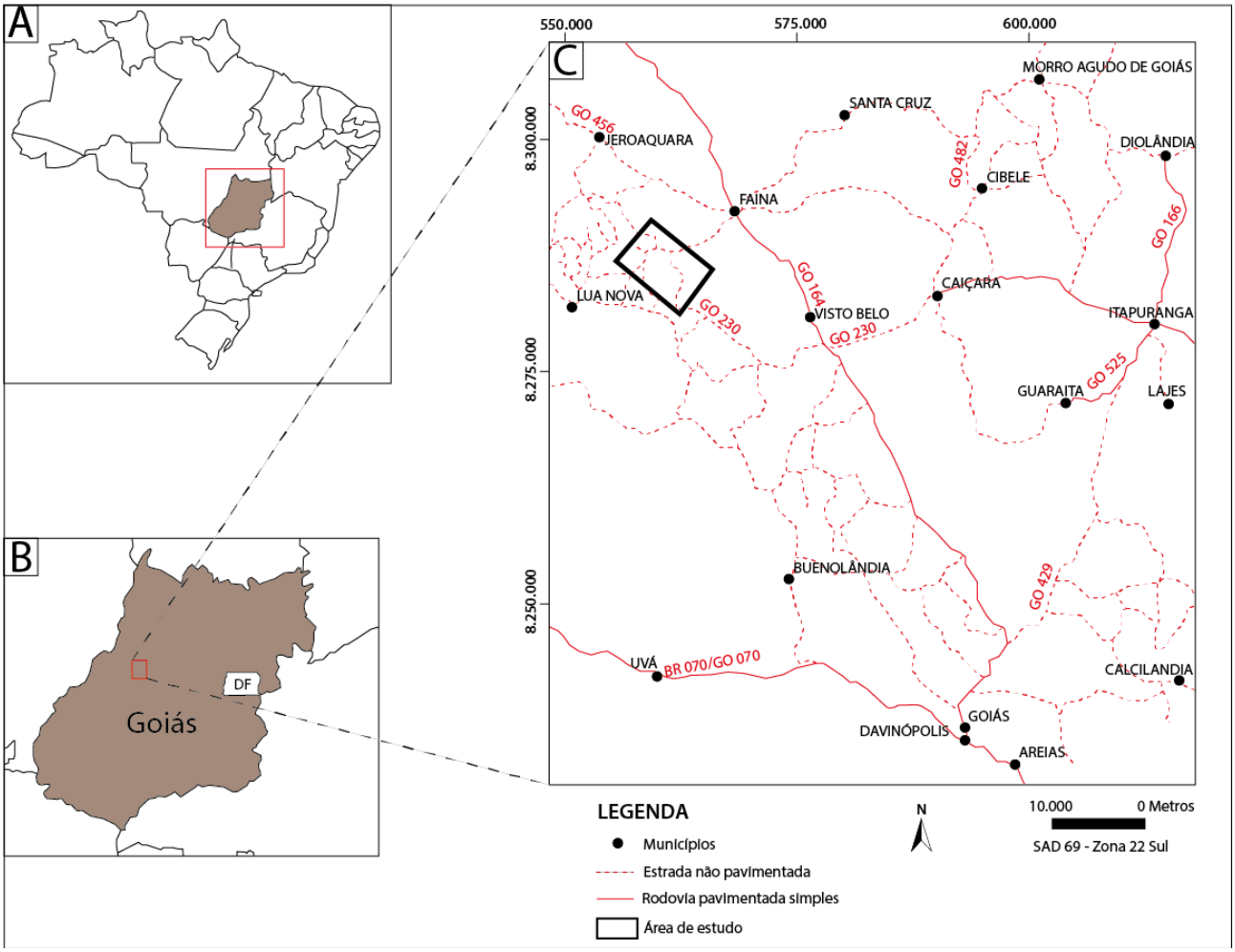

Figura 2: Mapa de localização de com rodovias e cidades principais adjacentes da área de estudo (base de dados base map - ESRI); Em (A) destaca-se o mapa simplificado do Brasil; em (B) Corte de detalhe no estado de Goiás; e em (C) mapa de localização.

1.3 Estruturação da Dissertação

A estrutura da dissertação foi dividida em três segmentos: a primeira parte consiste nos Capítulos I e II, em que se apresenta as metas e hipóteses para este projeto de pesquisa, e por consequência, toda a metodologia envolvida neste processo. O Capítulo III é elaborado na forma de artigo científico de título: *"THE FOOTPRINT OF THE POLYMETALLIC MINERALIZATION OF THE FAINA GREENSTONE BELT, BRAZIL"*. Este segmento apresenta os resultados centrais do projeto e suas seguintes discussões e conclusões. Por último, o Capítulo IV é referente às considerações finais da pesquisa e dos dados obtidos e aborda projeções de estudos futuros para serem sugeridos na área.

CAPÍTULO II - MATERIAIS E MÉTODOS

1. Trabalho de campo e amostragem

O trabalho de campo foi realizado durante a primeira quinzena do mês de novembro de 2018 e contou-se com o total apoio da *Orinoco Gold* Ltda. em relação a transporte, alimentação e logística na coleta das amostras. Foi disponibilizada uma base de furos de sondagem, com descrição geológica prévia e resultados geoquímicos, pertencentes ao alvo Tinteiro que interceptem intervalos mineralizados. Destes, foram selecionados 5 furos: (1) TIN-001, (8.285.222,5 N e 564.011,5 E, cota 637 m, azimute 280° e inclinação de -70°) com 31,83 metros de profundidade; (2) TIN-001A (8.285.236,8 N e 564.015,3 E, cota 637,4 m, azimute 275° e inclinação de -90°) com 74,5 metros de profundidade; (3) TIN-002 (8.285.184,7 N e 563.985,38 E, cota 641 m, azimute 0° e inclinação de -58,7°) com 100,17 metros de profundidade; (4) TIN-004 (8.286.761,8 N e 559.707,1 E, cota 516,5 m, azimute 5° e inclinação de -60°) com 110 metros de profundidade e (5) TIN-006 (8.286.729,38 N e 560.390,83 E, cota 590 m, azimute 17° e inclinação de -59°) com 100 metros de profundidade.

A rotina de amostragem empregada foi através da coleta de amostras de 1 (um) em 1 (um) m, excetuando nas zonas mineralizadas, onde foi efetuada de 0,5 em 0,5 m, totalizando um número de 225 amostras.

2. Petrografia

A descrição petrográfica macroscópica do material coletado foi realizada previamente em campo, com o intuito de distinguir o arcabouço mineralógico e textural. Posteriormente, foram confeccionadas 29 lâminas polidas que foram analisadas no Laboratório de Microscopia do Instituto de Geociências da Universidade de Brasília. Tanto para a análise com luz transmitida e refletida, utilizou-se o microscópio Olympus (modelo BX60FS - *Olympus Optical Co. Ltda.*). Adicionalmente, foi confeccionada uma seção polida de fragmento de rocha de amostra de brecha manganesífera, no Laboratório de Preparação de Amostras do Instituto de Geociências da Universidade de Brasília sob a supervisão da Professora Dra. Paola Barbosa.

Toda a nomenclatura utilizada para nomear os litotipos e suas siglas foram estabelecidas pela empresa *Orinoco Gold* Ltda., e os mesmos receberam as seguintes siglas: Brecha - BCH; Metachet - MECH; Muscovita xisto - MX; Clorita-quartzo xisto - CQS; Veio de Quartzo - QZ. A mesma lógica foi aplicada também nas zonas de alteração hidrotermal: Zona de alteração polimetálica/*Polymetallic Zone* – PZ (Tabela 1).

Tabela 1: Tabela indicando as amostras enviadas para laminação e seus respectivos litotipos.

Sigla	Litotipo	N° de amostras	Amostras
BCH	Brecha Manganesífera	2	T1/05; T1A/07
MECH	Metachert	12	T1/15; T1A/14; T1A/16; T2/13; T2/16; T4/31; T4/33; T4/36; T6/20A T6/20B; T6/28
CQS	Carbonato-quartzo xisto	8	T1/32; T1A/31; T2/30; T2/43; T4/45; T6/40A; T6/40B; T6/45
MX	Muscovita xisto	3	T1A/25; T1A/26; T2/25
PZ	Metachert alterado	3	T1/28; T1A/29; T2/26
QZ	Veio de quartzo	1	T4/38

3. Geoquímica

A análise química das amostras foi efetuada no Laboratório Comercial de Geoquímica ALS do Brasil LTDA. (Rocha Total, ICP-MS), contando com dados de dosagens de elementos maiores, menores e traços de 170 amostras. Estes resultados foram disponibilizados em novembro de 2018 pela empresa *Orinoco Gold* Ltda para este trabalho. Posteriormente (em 2019), outras 13 análises adicionais foram realizadas usando o mesmo padrão analítico das primeiras amostras e complementar os resultados anteriores.

O método de análise ICP - *Mass Spectometry* (MS) envolve o uso de dosagem de óxidos e vários elementos menores em amostras de 0,25g. Uma vez que estão preparadas, é realizada a diluição por ácidos tais quais o perclórico, nítrico, fluorídrico e clorídrico. O resíduo é posteriormente reagido com ácido clorídrico e analisado pelo ICP - *atomic emission spectroscopy* (AES). Estes resultados prévios são revisados em relação a concentrações anômalas de Bi, Hg, Mo, Ag e W, e quando conferidos, as amostras são analisadas para ICP – MS (ALS *Geochemistry*, 2017).

O tratamento e processamento dos dados utilizando o *software* ioGAS (versão 7.2 - *Trial*). Este permitiu elaborar perfis de composição química de todos os furos de sondagens e suas respectivas zonas mineralizadas. Os perfis gerados neste programa foram posteriormente importados e vetorizados no programa Adobe Illustrator 2020 (versão 24.2.1) e assim, exportados no formato png.

4. Espectroscopia de Reflectância

A análise espectroscópica se refere ao estudo da luz como um agente do comprimento de onda que é emitido, refletido e espalhado por um sólido, líquido ou gás (Meer & Jong, 2004). Segundo Meneses e*t al.* (2001), há três fatores principais que afetam diretamente a qualificação da composição mineralógica das rochas pela espectroscopia de reflectância: o tipo de superfície, a granulometria e forma das partículas, e a geometria da iluminação. A superfície uma vez que é lisa, cria o efeito de reflectância especular, onde a maior parte da energia incidente será refletida numa única direção, e quando o mesmo não acontece, a radiação incidente é refletida em várias direções diferentes. Quando as partículas do material são menores, há o aumento de albedo (valor médio da reflectância medido em um especifico intervalo de comprimento de onda). E a geometria de iluminação interfere de maneira que intervalos angulares entre 15 e 30 graus de iluminação resultam em maiores valores de reflectância e de absortância. A reflectância espectral de rochas e minerais em várias regiões do espectro eletromagnético é resultante das diferenças entre suas propriedades químicas e físicas. Estas propriedades refletem em feições de absorção (Figura 3) controladas pela sua posição no comprimento de onda, forma, profundidade e largura (Thompson *et al.,* 1999).

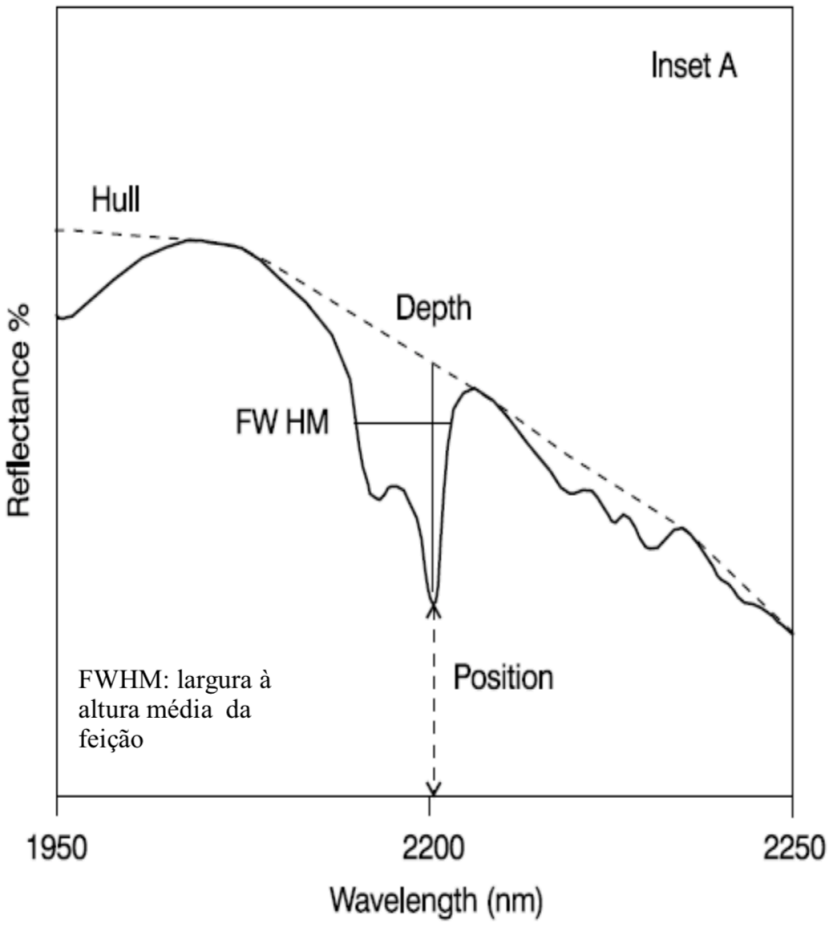

Figura 3: Destaque nos principais fatores determinantes na identificação de feições de absorção de minerais: posição, forma, profundidade e largura (Thompson *et al*., 1999).

Bandas de transferência de carga referentes ao resultado da troca de elétrons entre íons vizinhos de metais, criam feições de absorção entre de 0,4 µm e 1 µm do espectro eletromagnético (Goetz *et al*., 1983). A figura 4 ilustra intervalos de absorções espectrais de minerais de interesse comum à exploração mineral.

Transições eletrônicas em íons de metais de transição (Fe, Cr, Co, Ni, por exemplo; Burns, 1993; Adams, 1974), resultam em mudanças no nível de energia nas camadas eletrônicas (Hunt, 1977) e em feições de absorção especificas. O elemento ferro, dada a sua distribuição abundante na superfície terrestre é uma das causas mais comuns de feições neste domínio do comprimento de onda em várias rochas e tipos de solos. Tanto a presença quanto a ausência de água, hidroxila, carbonatos e sulfatos podem também determinar feições no domínio do SWIR (infravermeho de ondas curtas), e relaciona-se a processos vibracionais (Hunt, 1977).

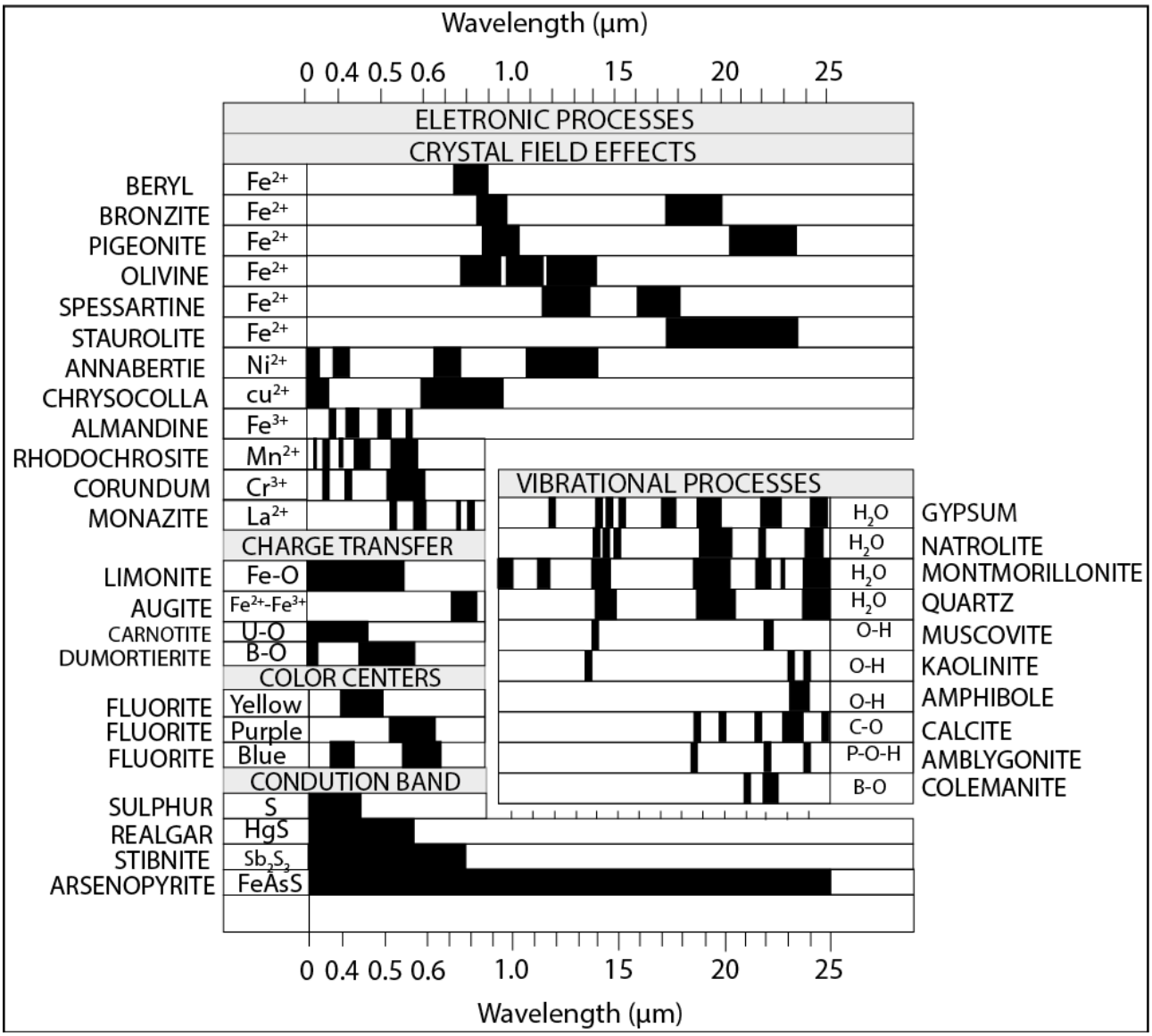

Figura 4: Diagrama que ilustra os principais intervalos de assinaturas espectrais de minerais comumente analisados na indústria mineral (Hunt, 1977).

A hidroxila comumente ocorre em múltiplos sítios cristalográficos de um mineral e normalmente está ligada a íons metálicos, o que gera absorções em 1,4 μm, e quando somada à outras -OH em outras camadas da estrutura mineral, em 2,2-2,3 μm. A somatória de H_2O intersticial com hidroxilas adicionais eleva a valores próximos a 1,9 μm (Hunt, 1977). Carbonatos também apresentam bandas de absorção vibracional diagnósticas devido ao íon $CO3^{2-}$ em regiões de 2,50-2,55 e 2,30-2,35 μm, e outras três bandas de menor intensidade próxima a 2,12-2,16 μm, 1,97-2,00 μm e 1,85-1,87 μm (Van der Meer, 2004).

A aquisição de imagens registradas em centenas bandas diferentes são disponibilizadas de maneira que possibilite em cada pixel das mesmas seja possível derivar uma curva de reflectância espectral completa (Van der Meer, 2000). A maior parte dos materiais geológicos analisados na exploração mineral possuem feições de absorção espectral com larguras entre 0,02 e 0,04 μm, e as bandas espectrais dos sensores espectrais dos sensores difundidos no mercado tendem a serem estreitas (de 0,01 a 0,02 μm de largura) e contínuas, de maneira que sejam adjacentes umas as outras, o que permite a extração de figuras de absorção dos materiais a partir de cada pixel que compõe a imagem. Estes dados extraídos podem ser calibrados e comparados diretamente por espectros medidos em campo por sensores ultraespectrais, pela petrografia, dados geoquímicos, difratogramas de raios-x e entre outros métodos.

Há décadas, vários tipos de sensores vêm sido utilizados como agente de aquisição deste tipo de informação e os mais comuns são os orbitais e os aerotransportados. Sensores portáteis de campo são também tecnologias muito difundidas a partir da década de 90. Estes sensores portáteis são relevantes devido ao fato de serem capazes de coletar dados ultra e hiperespectrais de amostras de rochas, solos, e testemunhos de sondagem. Esses instrumentos disponibilizam informações instantâneas sobre a assembleia mineral e suas variações químicas como descrito por Thompson *et al.* (1999).

Nesta presente pesquisa, utilizou-se o se o espectrorradiômetro de reflectância *FieldSpec3HiRes* (ASD) para a coleta dos dados espectrais. Neste instrumento os espectros são obtidos a partir da sonda de contato composta por uma lâmpada de halogênio (janela de aquisição de 1 cm de diâmetro) como apresentado na figura 5. Cada dado salvo representa a média de 50 espectros coletados na mesma área. No total contabilizou-se 1468 medidas em 225 amostras. O processamento e tratamento destes dados foi efetuado pelo *software* TSG - *The Spectral Geologist*, o qual fornece ferramentas de visualização e quantificação da mineralogia presente na rocha por parâmetros preestabelecidos no banco de dados do programa e outras bibliotecas espectrais.

Figura 5: O espectrorradiômetro de reflectância FieldSpec3HiRes (ASD) utilizado neste trabalho na coleta de dados espectrais.

5. Petrofísica

As propriedades físicas das rochas são analisadas em relação ao seu comportamento físico oriundo das características geológicas que as compõem. Tais propriedades como velocidade de propagação de ondas sísmicas, resistividade elétrica, porosidade, magnetismo e densidade são fundamentais para a caracterização da subsuperfície por meio de métodos indiretos (Schön, 2011). O presente trabalho priorizou duas destas propriedades apresentadas: a densidade e a susceptibilidade magnética. A aquisição desses dados foram todos realizados na Universidade de Brasília (Instituto de Geociências - IG e Faculdade de Tecnologias - FT). Foram todos métodos de fácil acesso, rápida aquisição e baixo custo, ou seja, calibra-los em um sistema de mineralização aurífera e polimetálica pode trazer benefícios às empresas e a exploração em si. O resultado do tratamento de todos são

apresentados em perfis do tipo *scatterplot*, e diagramas do tipo *boxplot* abarcando todo o conjunto analisado. Estes gráficos e perfis foram todos gerados nos *softwares Microsoft Excel* e ioGAS (versão 7.2 – *Trial version*), e posteriormente vetorizados no programa Adobe Illustrator.

5.1 Densidade

A densidade de uma rocha é definida como a razão da massa dos minerais que a compõe e dos fluidos presentes nos poros, pelo volume total. Por consequência, a densidade das rochas deve ser estimada considerando sua origem e os processos submetidos. Como este parâmetro depende de dois valores, a acurácia do valor diminui de forma que os valores tabelados nem sempre são indicados para usar como base, mediante ao fato de que a rocha não é isotrópica e pode variar conforme submetida ao intemperismo. De forma que há diversos tipos de densidades para reconhecer cada situação das rochas. Sua unidade no sistema internacional é quilograma por metro cúbico (kg/m^3), sendo que grama por centímetro cúbico (g/cm^3) é mais comumente usada em corpos mais densos. Esta propriedade é extremamente importante e é utilizada como parâmetro físico no método geofísico gravimétrico (Hinze *et al.,* 2013). Diferente de outras propriedades físicas, a densidade apresenta variação em um intervalo de ordem de magnitude menor: valores de 2 a 3,5 g/cm^3 na maior parte das rochas encontradas (Figura 6). Valores fora deste intervalo normalmente são associados à rochas já muito intemperizadas/fraturadas (quando muito baixo), ou então, eventos geológicos que propiciam formação de minerais muito densos, como sulfetos maciços (para valores muito altos).

Rochas sedimentares, geralmente, apresentam maiores valores de porosidade primária, fator que obrigatoriamente reflete em mais baixa densidade (1,8 a 2 g/cm^3). Rochas vulcânicas piroclásticas podem também apresentar valores mais baixos de densidade, mesmo que sua composição apresente um arcabouço mineral mais denso, ainda estará associada à contextos de fluxo e exsolução de voláteis durante o processo extrusivo, o que por consequência gera vesículas e interstícios "vazios" em sua estrutura. O processo metamórfico tende a ser responsável pelo o aumento da densidade em relação ao seu protólito, uma vez que o aumento da pressão e temperatura implica no aumento do empacotamento dos átomos e redução da porosidade intersticial. Já as rochas intrusivas apresentam linha muito tênue entre a variação de densidade de seus *endmembers. Rochas* ultramáficas tendem a ser mais densas, dado seu arcabouço mineral ser rico em elementos densos por natureza tais quais Fe e Mg. Consequentemente, rochas félsicas tendem ser as menos densas neste contexto (Dentith & Mudge, 2014).

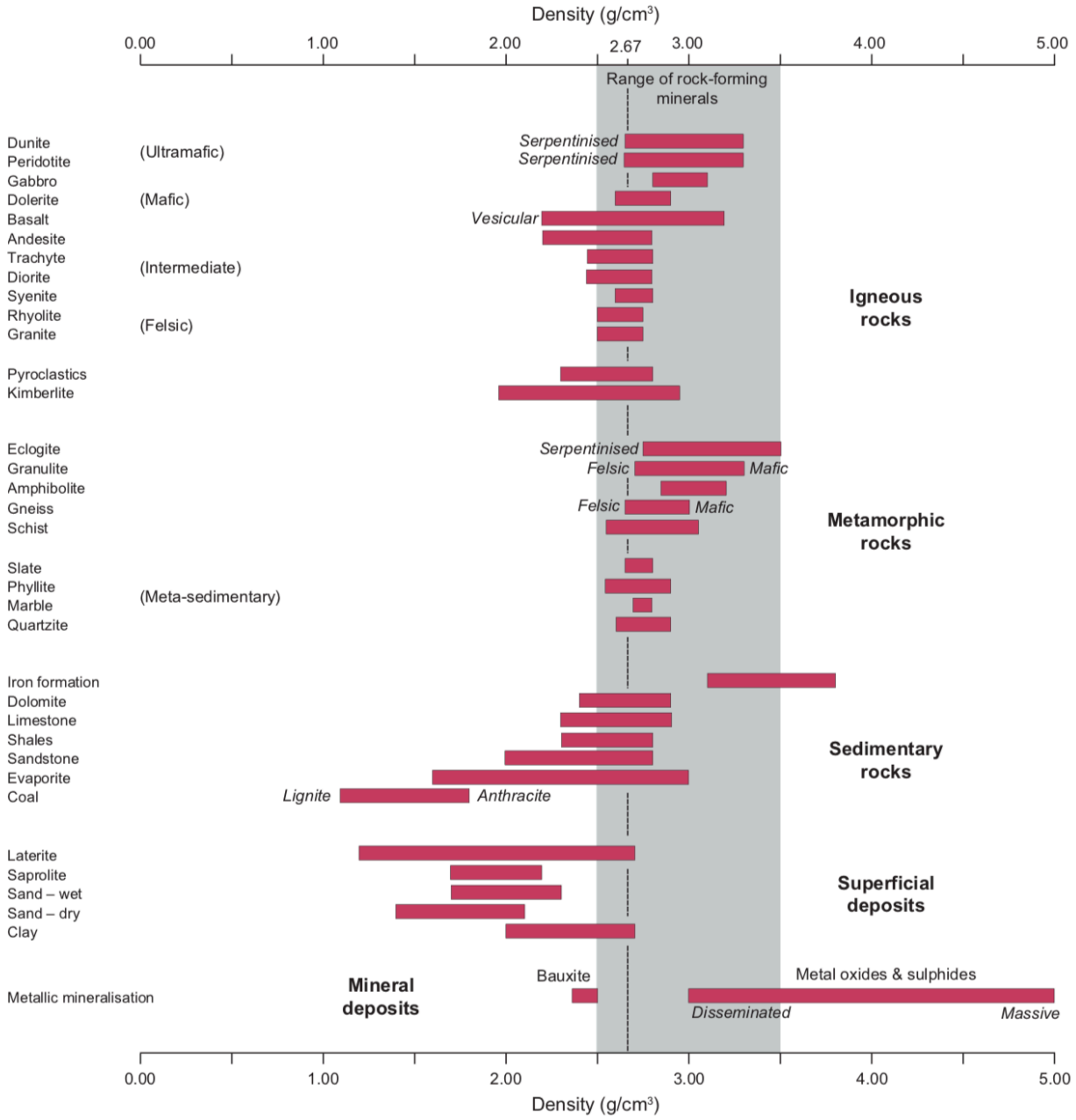

Figura 6: Esquematização da variação da densidade entre os diversos tipos de rochas e possíveis processos e minerais associados (retirado de Dentith & Mudge, 2014).

5.1.1 Método Hidrostático

Os valores de densidade das amostras compactas foram obtidos com base no princípio de Arquimedes: "*Todo corpo mergulhado num fluido em repouso sofre, por parte do fluido, uma força vertical para cima, cuja intensidade é igual ao peso do fluido deslocado pelo corpo".* Assim o processo se baseia no peso da amostra a seco e no peso da amostra "molhada", submersa na água, na qual este segundo equivale um peso aparente. Então a fórmula foi utilizada para calcular o valor da densidade final:

$$DA = MS / (MS - MM)$$

DA = densidade da amostra
MS = Massa da amostra a seco
MM = Massa da amostra submersa

Hinze *et al.* (2013) denominam essa densidade como "densidade natural" da rocha. Os valores de densidade das amostras compactas foram coletados utilizando-se da balança Toledo-IND560 do laboratório de Propriedades Físicas de Rocha do Instituto de Geociências da Universidade de Brasília. O equipamento apresenta de três partes (Figura 7): uma base seca, compreendida como uma superfície que se apoia na mesa e mede a massa da amostra seca; uma base imersa, a qual encontra-se imersa em um líquido, no caso água, e mede a massa da amostra imersa; e um painel, que indica os valores da massa medidos por cada base. As amostras foram pesadas e os dados adquiridos foram incorporados em planilhas do software *Microsoft Excel* e, posteriormente, calculou-se a densidade utilizando-se a equação acima.

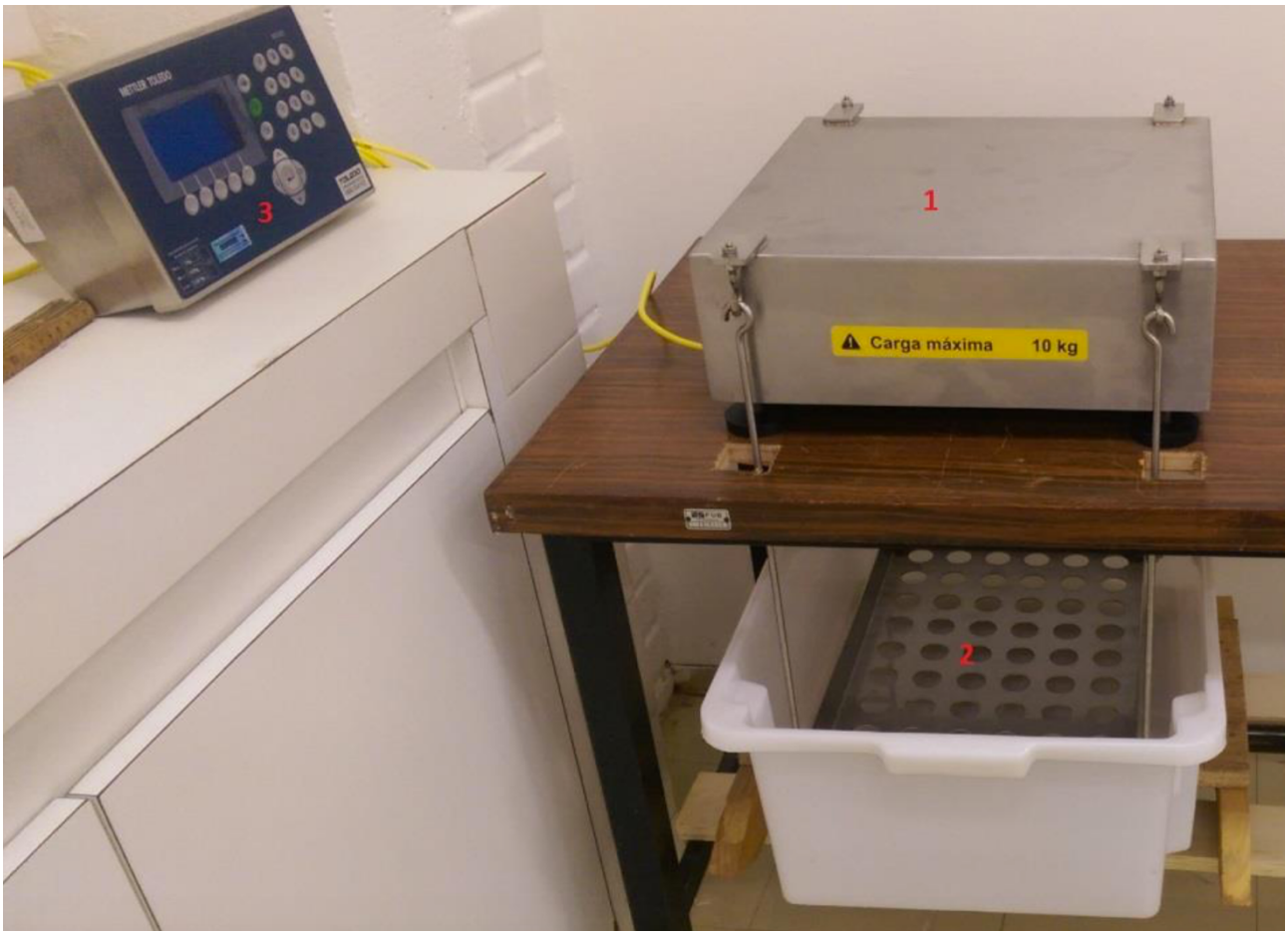

Figura 7: Balança Toledo - IND560 usada para a realização do trabalho. 1-Base a seco; 2-Base submersa; 3- Painel de visualização dos valores da massa do corpo em questão.

5.1.2 Método Pentapicnômetro

Todos os testemunhos de sondagem do alvo Tinteiro apresentam espesso perfil de intemperismo. Devido a esse fator, pelo menos de 5 a 10 metros iniciais do material interceptado pelos furos escolhidos são constituídos por material muito friável/saprolitizado em estado parcialmente ou totalmente pulverizado. E como não é possível executar o cálculo de densidade da rocha pelo método da balança hidrostática de amostras friáveis, as mesmas tiveram seus dados de densidade absoluta coletados com o uso do equipamento pentapicnômetro *Pentapyc 5200e* (Figura 8). Este equipamento foi utilizado sob a orientação do Professor Dr. Luís Fernando Martins Ribeiro, no Laboratório de Geotecnia, que faz parte da Faculdade de Tecnologia (FT) da Universidade de Brasília. Este equipamento possui cinco cápsulas de acoplamento de amostras, nas quais todo o volume disponível é preenchido por gás Hélio durante o processo de medição. Cada uma das cinco amostras é automaticamente analisada e o resultado é fornecido na tela do aparelho para a disposição do usuário. Os parâmetros obtidos são os de densidade verdadeira (no caso das amostras utilizadas, densidade mineral) e volume da amostra.

Juntamente com o pentapicnômeto utilizou-se a balança de alta precisão Shimadzu AUW2200, semi-micro com dupla escala de cinco casas decimais, para realizar a individualização constante de aproximadamente 20 gramas de amostra friável por análise (padrão da rotina do laboratório). O equipamento quantifica o volume de um material sólido pelo princípio de Arquimedes de deslocamento de fluidos e de expansão de gases (Lei de Boyle). Neste contexto, o fluido utilizado (gás Hélio) apresenta dimensão atômica pequena e poder ocupar menores cavidades (garante maior precisão na análise), com pressão alvo de zero *psi*. A análise é automática e o % de desvio padrão é informado pelo próprio usuário, neste caso, de 0,005. O método fornece apenas a densidade absoluta dos sólidos constituintes da amostra, uma vez que todas as estruturas primárias não estão mais presentes na trama da amostra (porosidade, e estruturas petrográficas).

Figura 8: Pentapyc 5200e, equipamento utilizado na coleta da densidade absoluta do material friável dos níveis saprolíticos encontrados nos testemunhos de sondagem utilizados nessa pesquisa.

5.2 Susceptibilidade Magnética

Diferente dos valores de densidade, a variação do campo magnético está estritamente ligada com a capacidade dos materiais terrestres de se magnetizar, ou seja, a susceptibilidade magnética presente nas rochas (Hinze, 2013). A susceptibilidade magnética varia com a intensidade do campo magnético, e por consequência, existem diversos fatores que podem influenciar no dado, que na prática classificam seus tipos. A susceptibilidade é expressa em termos de volume, pois a relação deve ser feita conforme o tamanho do corpo em questão. No entanto, independente da relação do tamanho do corpo com a susceptibilidade a quantidade de materiais ferromagnéticos ou até mesmo alguns paramagnéticos presentes na composição podem influenciar no valor final medido (Figura 9). Além disso, também há

relação da anisotropia dos minerais presentes, isto é, a susceptibilidade magnética se distingue conforme os eixos dos minerais. Essas características restritas a cada mineral e formação da rocha influência nos valores de susceptibilidades nas rochas, como se apresenta na figura 8. Percebe-se também, a amplitude de valores que podem ser obtidos em comparação à densidade, apresentando maior ordem de magnitude de valores para cada tipo de rocha.

Os materiais diamagnéticos são aqueles que geram um campo magnético oposto ao aplicado sobre eles. Quartzo, feldspato e halita são exemplos, pois eles produzem um campo contrário o que torna a susceptibilidade magnética menor que zero (Dentith & Mudge, 2014). Assim, o efeito geológico em depósitos de sal, resulta em um contraste a susceptibilidade magnética positiva de rochas presente ao redor. Diferentemente, materiais com a formação de um leve campo magnético que atrai imãs, os materiais paramagnéticos compreendem sua susceptibilidade na dimensão de 0 a 10^{-6}. O campo fraco ocorre, pois é formado por íons de ferro e magnésio normalmente. Já os materiais ferromagnéticos e ferrimagnéticos possuem suas propriedades magnéticas regulares, excetuando quando submetidos à alta temperatura (Temperatura Curie). Além disso, possuem alta susceptibilidade magnética, pois quando submetidos a um campo externo seus átomos interagem gerando um campo também (Hinze, 2013).

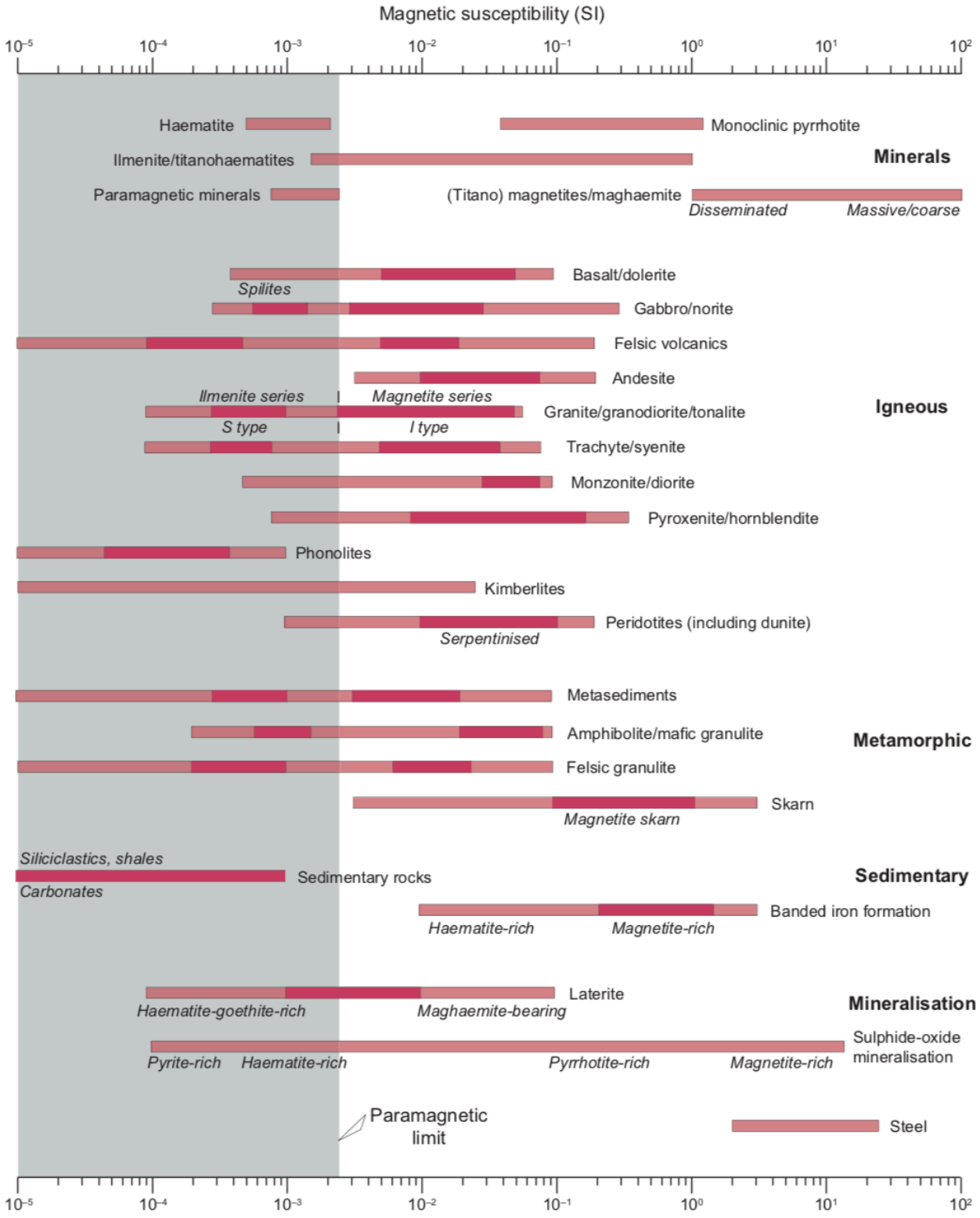

Figura 9: Diversidade da variação dos valores de susceptibilidade magnética nos diferentes tipos de rochas (retirado de Dentith & Mudge, 2014).

Neste trabalho, as medidas de susceptibilidade magnética das amostras dos furos de sondagem foram feitas com o uso do susceptibilímetro portátil da Terra Plus modelo KT-10S/C+ (Figura 10) que foi cedido pela CPRM em abril de 2019. As medidas são feitas em contato do aparelho com as amostras

e captura as medidas de susceptibilidade magnética em unidades do SI. A cada ponto medido, 3 medidas distintas foram realizadas para obter-se resultados mais precisos pelo cálculo de sua média. O aparelho conta com um oscilador LC de 10kHz, com uma bobina para medir as variações de suscetibilidade, calculada a partir das diferenças medidas entre o ar livre e a amostra. As medidas foram feitas em um ambiente com temperatura constante, uma vez que o oscilador é muito sensível a variações de temperatura e pode afetar a sensibilidade do aparelho. A frequência de medição é de 20 vezes por segundo, sendo que 4 leituras por segundo são armazenadas. As leituras foram realizadas com o sensor em contato com o plano de serragem do testemunho. A sistemática das medições consiste medir a frequência e amplitude do oscilador no ar livre, logo após a bobina é colocada em uma amostra de rocha ou pó, logo após a frequências e amplitude são novamente medidas no ar livre, após as medidas são exibidas do visor do equipamento.

Figura 10: Fotografia do susceptibilímetro portátil da Terra Plus modelo KT-10S/C+, utilizado neste trabalho.

6. Difração de Raios-X (DRX)

Com o intuito de identificação de fases minerais, especificamente das amostras altamente intemperizadas em estado friável, a análise de difratometria de raios-X (DRX) fez parte da rotina de caracterização dos furos principalmente nas porções mais superficiais dos mesmos. A rotina foi realizada sob a orientação da Professora Dra. Adriana Maria Coimbra Horbe e toda a equipe do laboratório de Raios-X do Instituto de Geociências da Universidade de Brasília. Foi utilizado o difratômetro RIGAKU, modelo ULTIMA IV. O equipamento possui um tubo de cobre e filtro de níquel sob 35kV, 15mA e detector DTEX/ULTRA com passo de 0.05, velocidade de 5°/min e varredura no intervalo 2Θ de 5° a 60°. A identificação dos minerais foi realizada com o auxílio do programa DIFFRAC.SUITE EVA com banco de dados PC- PDF (Powder Diffraction File – PDF para PC – ICDD).

CAPÍTULO III – ARTIGO CIENTÍFICO

"THE FOOTPRINT OF THE POLYMETALLIC MINERALIZATION OF THE FAINA GREENSTONE BELT"

Fernando Rossi Almeida[1], Adalene Moreira Silva[1], Catarina Labouré Bemfica Toledo[1], Diego Fernando Ducart[2], Kawinã Araújo[1]

[1]Istituto de Geociências, Universidade de Brasília (UnB);

[2]Istituto de Geociências, Universidade Estadual de Campinas (UNICAMP).

Abstract

The Faina Greenstone Belt (FGB) is one of the five greenstone sequences occurring in the Goiás Archean-Paleoproterozoic Block, in central Brazil. Exploration studies revealed the new Tinteiro polymetallic system, which spreads through several locations, but especially nearby the Cascavel mine. The Tinteiro system is controlled by NE-SW trending brittle structures that present muscovite and hematite alteration halos, and anomalous levels of base metals, such as Ag, Co, Cu, Ni, Ba, Mo, As, Pb, U, Fe, Mn and LREE accumulated in hydrothermal breccias. This article characterizes the mineralization footprint of the Tinteiro system by integrating geological data from previous maps and core samples from 5 drill holes with multi-source data set of spectral mapping, lithogeochemistry, and analysis of rock physical properties. Spectral data of the mineralized samples indicated an intermediate composition between goethite and hematite for the iron oxides and hydroxides and an intermediate composition between muscovite and phengite, with a high degree of crystallinity, for the minerals of the white mica group. Whole-rock geochemistry shows values of up to 9% Fe_2O_3, 13% MnO, 2790 ppm Co, 10,000 ppm Ba, 1890 ppm Cu, and 1460 ppm N, while Zn and As are vectors for identifying proximal hematite alteration as system pathfinders. The footprint of the proximal halo system shows a drop in density and magnetic susceptibility values in the direction of mineralization; spectral data shows that hematite is the main phase identified from the group of iron oxides and hydroxides, while the crystallinity of the white mica group mineral reaches values greater than 10. Furthermore, the greater the proximity of the mineralized portion, the greater the intensity of venulation features. The mineralized zone footprint is characterized by a decreasing abundance of minerals from the group of iron oxides and hydroxides (less than 0.22), decreasing density values, but high absolute density values while magnetic susceptibility increases next to the proximal zones (average of 0.542 x 10^{-3} SI).

***KEYWORDS**: FAINA GREENSTONE BELT; REFLECTANCE SPECTROSCOPY; DATA INTEGRATION; POLLYMETALIC HYDROTHERMAL ALTERATION.*

1. Introduction

Tropical countries such as Brazil and Australia face two major difficulties in the early development stages of the exploration process in both greenfield and brownfield: (1) acquire a better understanding of the almost ubiquitous regolith coverage in places where both geomorphology and climate cause intense supergenic alteration profile, and (2) make the best use of this knowledge to develop new sources of mineral wealth within or below this coverage (Caritat *et al.,* 2016). These questions arise especially because the efficiency of most traditional geochemical and geophysical exploration methods are initially based on areas where rocky outcrops with shallow layers of supergene alteration are abundant. The ambiguity of interpretation and understanding is attenuated with the increasing thickness of the weathered or simply transported material found on possible new deposits.

In other words, it is extremely important to develop techniques that allow determining detectable signatures of outcropping or non-outcropping mineral systems. This objective requires integrating the regional and detailed geological knowledge (stratigraphy, structural structure of the rocks and pedology) with the entire database of physical parameters that can be determined by direct analysis (lithogeochemistry, mineral chemistry, petrophysics, spectral scanning) and remote/indirect (airborne data, remote sensing, seismic lines) thus integrating an extensive local dataset of factors that correlate with mineralization (Lesher *et al.,* 2017; Lampinem *et al.,* 2019; Rieger *et al.,* 2020). Each of these tools maps a specific footprint and integrating these various parameters translates into a major advance for mineral research and the mineral industry. This premise has shown positive results that enabled exploration in areas where mineral extraction was considered technically unfeasible or uneconomical (Byrne *et al.,* 2020; Kreuzer *et al.,* 2020).

This article aims at applying a methodology or routine for characterizing the polymetallic mineralization of the Tinteiro system that occurs in the Faina Greenstone Belt (FGB, in central Brazil). The polymetallic system comprises anomalous contents of base metals such as Ag, Co, Cu, Ni, Ba, Mo, As, Pb, U, Fe, Mn, and rare earths. This system was discovered and recorded by Orinoco Gold Limited, ASX:OGX (2014) through the detection of surface geochemical anomalies and mapping of hydrothermal breccias and gossans related to late brittle structures concerning the main mineralizing events of the FGB. Although research dedicated to understanding this system is still incipient, Campos *et al*. (2017) discuss the possibility that this system represents the distal facies of an IOCG system.

This study proposes to characterize the main lithotypes affected by this system at shallow and outcropping levels, based on five drill holes that intersect the mineralized zone. The data generated include measurements of physical (petrophysical), spectral and geochemical parameters of drill cores. The work aims to help understand the signature of this mineral system and generate subsidies for mineral exploration in the Archean-Paleoproterozoic Terrane of Goiás.

2. Regional Geology

The study area is in the domain of the Archean-Paleoproterozoic Terrane of Goiás (Figure 11), which was amalgamated during the Brasiliana/Pan-African orogeny, west of the Brasília Fold Belt (Pimentel *et al*., 2000; Jost *et al*., 2008; Pimentel *et al*., 2016). About 80% of the area consists of TTG (tonalite-trondhjemite-granodiorite) terrains, whose composition ranges from tonalitic to granodiorite orthogneisses, divided into six complexes (Queiroz *et al*., 2008). They all exhibit general similarities but differ regarding the mineralogical/structural framework and age. These terrains are divided from north to south as Hidrolina, Moquém, Caiamar, Anta, Uvá and Caiçara (Jost *et al.*, 2008). The Uvá Complex is defined by two groups of orthogneisses (Jost *et al*., 2005), of which the dominant group is the oldest. This group comprises polydeformed gneisses with a composition ranging from tonalitic to granodioritic and ages of 3.0 – 2.9 Ga (Jost *et al.,* 2013) and diorite composition stocks with an age of 2.9 Ga (Pimentel *et al.,* 2003). The second group corresponds to old tonalite and monzogranite sills of age 2.8 Ga (Jost *et al*., 2013). The Caiçara Complex consists predominantly of tonalitic orthogneisses of 3.1 Ga, intruded by smaller bodies of granodiorites, granites and charnockites (Beghelli Junior, 2012) of 2.8 Ga.

The other 20% of the area corresponds to the narrow and elongated greenstone belts that are interstitially amalgamated between the TTG complexes (Pimentel *et al.,* 2003; Rodrigues, 2011; Borges *et al*., 2017; Borges *et al*., 2021). The Faina (FGB) and Serra de Santa Rita (SRGB) Greenstone Belts are observed to the south of the block, and the other three, Crixás, Guarinos and Pilar de Goiás to the north (Jost *et al*., 2005). Jost *et al.* (2014) concluded that the contacts between the greenstone belts and the TTGs are tectonic, while the occurrence of klippe in orthogneisses suggests that the supracrustal rocks are allochthonous. This same work shows that the five greenstone belts present a cohesive stratigraphy while their metamorphism varies from greenschist to amphibolite facies.

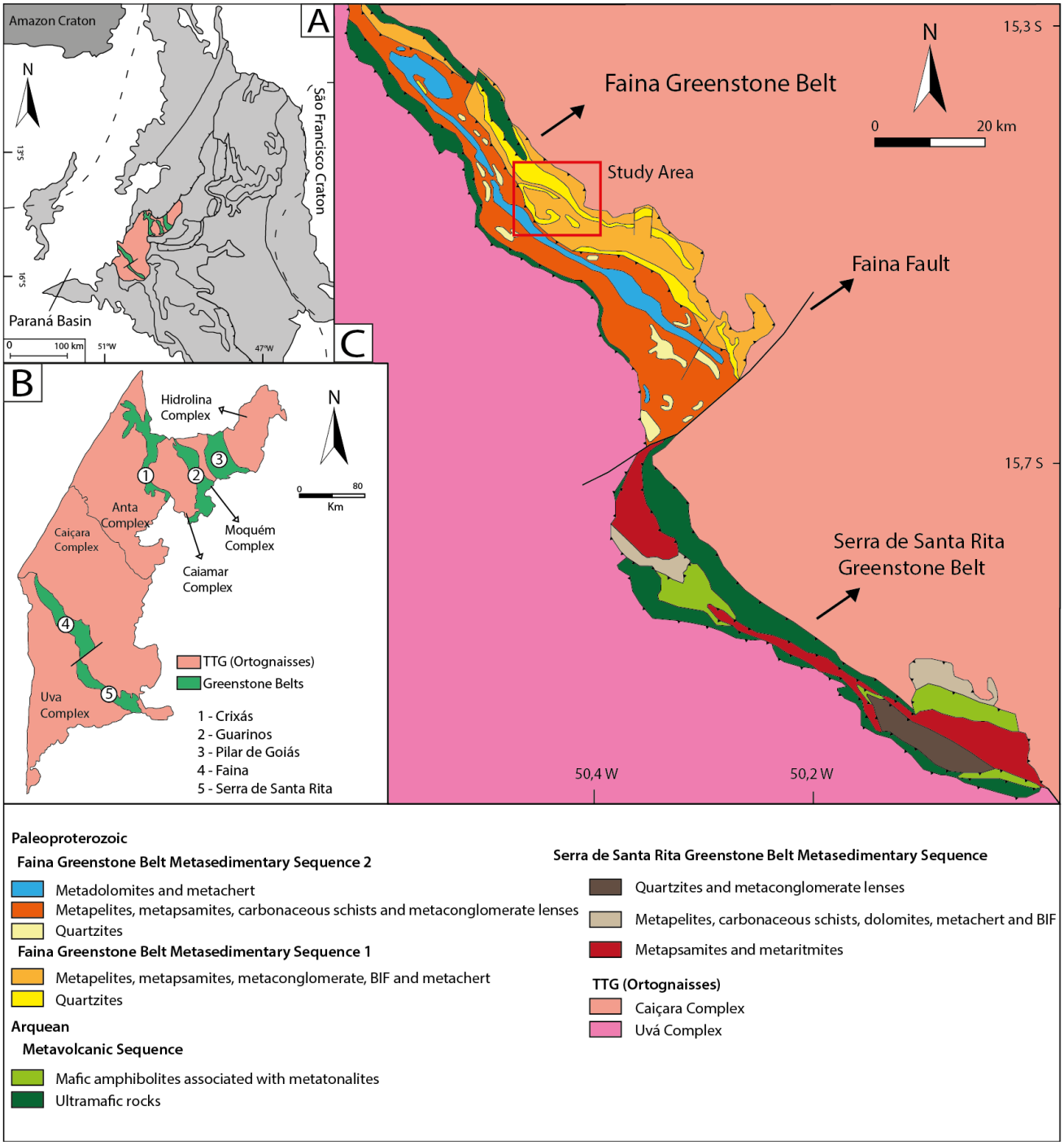

Figure 11: The Archean-Paleoproterozoic Terrane of Goiás and the Faina and Serra de Santa Rita greenstone belts, in the southern portion. (A) Location of the Archean-Paleoproterozoic Terrane of Goiás. (B) Distribution of the greenstone belts and TTG complexes that make up the Archean-Paleoproterozoic Terrane of Goiás. (C) Geological map of the Faina and Serra de Santa Rita Greenstone Belts (Modified from Baêta Júnior *et al*., 2000 and Toledo *et al*., 2014); the outlined red rectangle indicates the study area.

The base of all these belts consists of metakomatiites and metabasalts, superimposed on several successions/layers of metasedimentary rocks with gold potential (Jost *et al*., 2014). Lenses of metavolcanic and metavolcanoclastic rocks are unique features of the SRGB (Resende *et al*., 1998; Borges *et al*., 2017). Intercalations of banded and chert iron formations occur in different proportions

between levels of volcanic rocks (Resende *et al.,* 1998). Whole-rock Sm-Nd data from metakomatiites and metabasalts of the Crixás greenstone belt show an isochron age of 3.0 Ga (Fortes *et al*., 2003). Similarly, U-Pb zircon dating yielded ages of 2.96 Ga for amphibolite and chloritite from the FGB and SRGB (Borges *et al*., 2017). Several isotopic ages of the rocks from the five greenstone belts have indicated Archean and Paleoproterozoic sources (Resende *et al.*, 1999; Fortes *et al.,* 2003; Tassinari *et al.*, 2006; Jost *et al.,* 2014; Borges *et al*., 2021).

2.1 Faina Greenstone Belt Geology

The 150km-long FGB and SRGB are located in the southern region of the Archean-Paleoproterozoic Terrane of Goiás, structured by an NW-SE trending syncline. Resende *et al.* (1999) individualized these Greenstone Belts based on the interpretation that the lithological contrast in the units results from the deposition of two paleo basins in different geographic contexts that underwent different depositional regimes. In Serra de Santa Rita, the sedimentation environment was related to a gradual marine platform depositional regime from deep to shallow while in Faina, the platform arrangement evidences two transgressive cycles that culminate in an environment favorable to forming chemical sediments (Resende *et al*., 1998).

The belts are separated by the N30°E trend strike-slip Faina Fault and the contact between the adjacent tonalite-trondhjemite-granodiorite (TTG) complexes, Caiçara and Uvá, which are marked by inverse shear zones with a high angle that converge to NE and completely obliterates the original architecture of the greenstone belts (Jost *et al*., 2005). The GB lower stratigraphic sections are similar and include metakomatiites and metabasalts from bottom to top (Resende *et al*., 1998). While the SRGB exhibits a graded sequence from carbonaceous pellets to cherts, banded iron formations (BIF), and dolomites, separated by a superior turbidite unconformity, the FGB metasedimentary unit has, from base to top, two sedimentary transgressive shekels with quartzites, metapelites, carbonaceous shales and BIFs superimposing an angular nonconformity on the metavolcanic unit (Resende *et al*., 1999). The second cycle is represented by metaconglomerates, quartzites and metapelites covered by marbles and BIFs. The two sedimentary cycles are separated by an erosive nonconformity like the metasedimentary units A and B (Jost *et al*., 2014).

The sedimentation ages of all greenstone belts of the Archean-Paleoproterozoic Terrain of Goiás have are Rhyacian (Paleoproterozoic; Fortes *et al.,* 2003; Tassinari *et al.*, 2006; Borges *et al.*, 2021), and the same age was obtained for the Guarinos and Pilar de Goiás volcanic sequences. On the other hand, the volcanic rocks from Crixás, Faina and Serra de Santa Rita indicate Archean ages (Borges *et al*., 2017). Sm-Nd models of detrital zircon ages suggest maximum values ranging from

3200 to 2800 Ma for sedimentary rock protoliths (Resende *et al*., 1998; Brant *et al*., 2015). Furthermore, carbon isotopes of marbles from the first sedimentary package of the Southern greenstone belts yielded positive values of δ^{13} ranging from +10 to +14% (Fortes, 1996; Santos *et al*., 2008), suggesting that sedimentation was completed during glaciation in the Huronian, early Rhyacian. The values of δ^{13} in marbles from the second sedimentary cycle of the FGB ranged from -0.6 to +0.6%, suggesting a minimum age of deposition during late Rhyacian and early Orosian (Resende *et al.*, 1999; Jost *et al.*, 2014).

2.2 Mineralizations in the Faina Greenstone Belt

The FGB has two main deposits characterized by orogenic gold mineralization: Cascavel and Sertão. The mineralization in both deposits is structurally controlled, the alteration is marked by white mica, ± pyrite ± chalcopyrite, and an increase in iron (predominantly magnetite) concentration in the proximal parts of both deposits (Campos *et al*., 2017). Bogossian *et al*. (2020) estimate temperatures ranging from 330 to 430 °C and from 320 to 430 °C in the auriferous hydrothermal fluids of the Cascavel and Sertão deposits, respectively. This mineralization is widely distributed and observed in basal metavolcanic, ultramafic and mafic rocks, as well as higher/superior siliciclastic and chemical metasedimentary rocks. Jost *et al.* (2014) describe the continuity in the gold trends as parallel to regional shear zones, thus generating a system of superposed quartz veins. The two systems, Mestre-Cascavel and Cuca, are approximately 50 cm thick, and exhibit N60°/40°W and 25°SW trends, respectively. The main host rocks are quartzites, which, due to their low reactivity, form hydrothermalized halos with more discrete features, whose external/distal halo exhibits ocher, ferruginous color, disseminated in transversal fractures parallel to the rock foliation. The inner/proximal halo has levels of millimeter pockets composed of biotite and fuchsite. The mineralized bodies occur as ore-shoots of free gold nuggets of 2-3 mm up to 3 cm approximately every 3 meters, with grades ranging from 39.3 g/t to 24.14 g/t (DNPM, 2007). In June 2017, the Sertão deposit recorded inferred resources of 223t Au at 6.9 g/t for approximately 50 Koz of gold in subsurface open mineralization (Orinoco Gold Ltda., June 2017 ASX report).

From 2002 to 2007, the Sertão Mineração Ltda. explored gold related to paleoplacer deposits in the same stratigraphic horizon of the basal conglomerate of the second sedimentary cycle of Faina (Carvalho *et al*., 2013). The interval is described as 40 km long and 90 meters thick, consisting of orthoconglomerates, meta-sandstones, metapelites, and informally named as Arraial Dantas Formation (Carvalho *et al.,* 2013).

Jost *et al*. (2014) also reported the occurrence of Algoma-type banded iron formations in the FGB, referring to iron formations that are intercalated at stratigraphic levels below the volcanic rocks. These rocks crop out in lenses between the upper portions of the first and second sedimentary cycle (Resende *et al*., 1998), where the iron formations occupy the top of a dolomitic level and, specifically, when occurring in rocks of the first cycle, layered to the base conglomerate of the second cycle. Geographically, these lenses are more abundant in the FGB southeast and central domains.

The first references to faults, veins and hydrothermal alterations with enrichment of anomalous elements (such as Ag, Mo, Pb, W, U, Co, Fe, etc.) are found in Orinoco Gold Limited (ASX:OGX, 2014) and were classified as the late Tinteiro mineral system (possible IOCG), arranged in various FGB locations (Figure 13). This same report presents the drilling campaign carried out at the site and outlines three main exploratory trends/targets where this system is continuous: North, Central, and South Tinteiro. This occurrence predominates in the greenstone belt central region, west of the Cascavel deposit, especially among the lithological contacts found in the metasedimentary sequence of the first depositional cycle.

Campos *et al.* (2017) integrated the products derived from ETM+/Landsat 7 and geophysical (magnetometry and gamma spectrometry) data and delimited one more target in this system (Southeast Tinteiro), highlighting the contrast of mineralizing contexts concerning other prospective targets of the FGB. The study deepens the discussion of how mineralization behaves in the system, concentrated in gossans, and hematite and manganesiferous breccias, permeated by alteration halos rich in hematite and muscovite. Lineaments extracted from the first vertical derivative (Dz) indicate structural trends associated with brittle features in the E-W and NW-SE directions. The North Tinteiro target is intersected by an N50°E sinistral fault, parallel to the Faina Fault. The structural control of this system is ambiguous and difficult to understand, since the mineralization is sometimes found lodged in ductile structural features (shear zones), and sometimes associated with the structural features of the brittle regime (faults and fractures).

Bogossian *et al.* (2020) classify this system as part of the last deformation event in the area (D_4). This greenstone belt has a complex polyphasic structural evolution, where the primary bedding (S_0) is preserved only in restricted lithological domains as a compositional component with varying quartzites and metamorphic rhythmic successions. An extensive succession of events marked by the ductile regime predominates from D_1 to D_3, generating successive S_n foliation planes, anti- and syncline folds, shear zones, and also the V_2 veins, responsible for the gold mineralization in the system. The last deformation stage, D_4, is characterized by NE-SW to E-W shortening and includes moderate south-dip thrusts with north trend, high-angle reverse faults with west-dip, and fault-fill veins and breccias. Locally, directional shear zones with NNW trends are observed.

The targets delimited by the Tinteiro System are to the west of the Cascavel deposit, where metasedimentary sequences A and B, chemical, psamopelitic and psammitic units crop out. The main lithotypes consist of quartzite, feldspathic quartzite, metapelite, metachert, chlorite-quartz (± muscovite ± biotite ± carbonate ± magnetite) schist, metarhythmite, breccias and small lenses of ultramafic rocks (talc schist). The 1:10,000 scale map in figure 13 shows the arrangement of all these lithologies and structures.

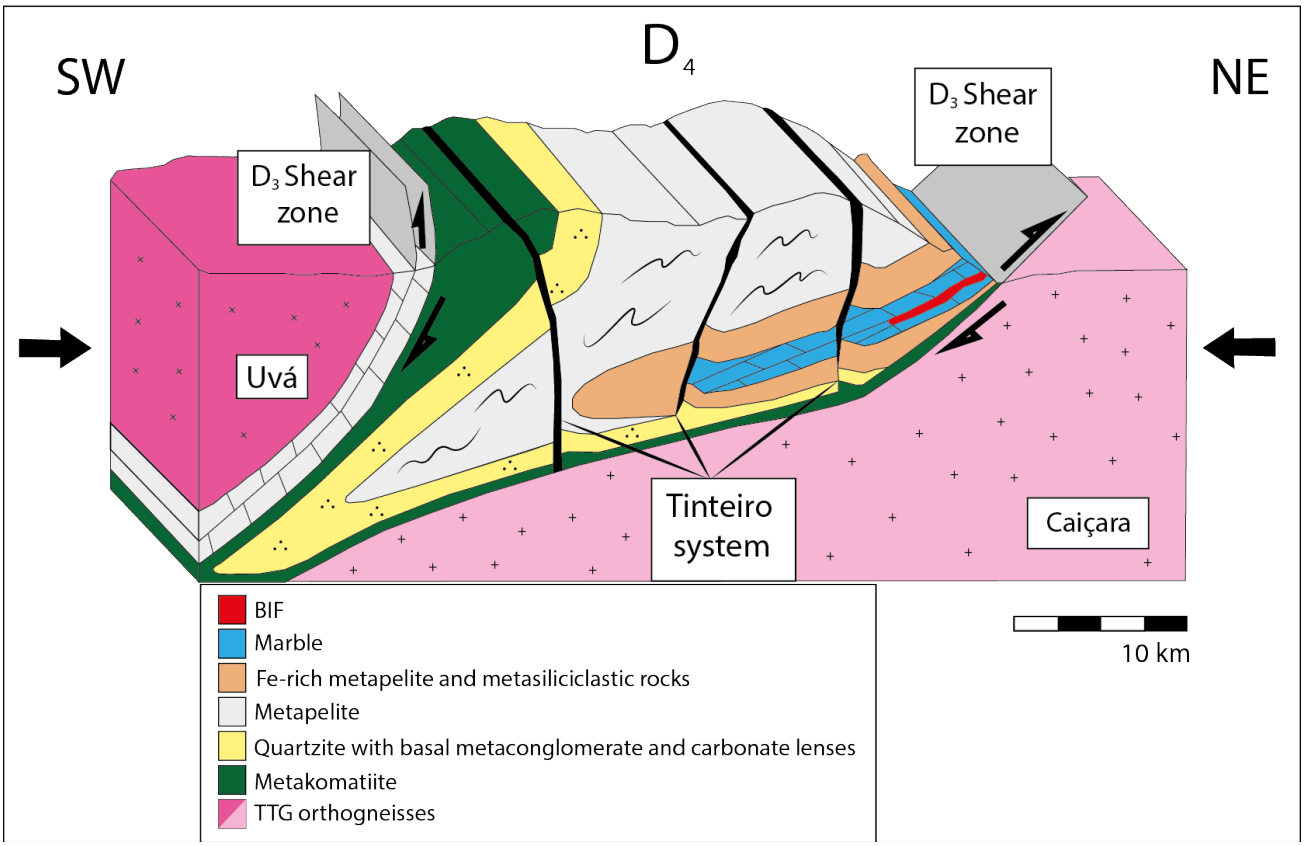

Figure 12: Schematic block diagram of the last deformation cycle (D_4) of the Faina greenstone belt illustrating how the Tinteiro system behaves geometrically (modified from Bogossian *et al.*, 2020).

In an overview of the area, quartzite and metarhythmite are fine to medium-grained and occur as massive outcrops usually found in a wide range of colors (white, yellow, light pink, and greyish) exposed by drainage. The main mineral assemblage consists of quartz (60-85%) and muscovite (5-30%), with a predominantly granoblastic texture. Magnetite, tourmaline, and sulfides occur as subordinate minerals while alterations rich in iron oxides are common. Feldspathic quartzite lenses occur in the Central Tinteiro domain and the Cascavel deposit region.

The metapelites have a predominant lepidoblastic texture, forming schists generally consisting of muscovite (20-60%), chlorite (5-20%), and quartz (10-30%). The foliation is marked by fine millimetric planes of mica. Pyrite, chalcopyrite and magnetite crystals are found in restricted levels. In the South Tinteiro target, fine-grained lenses of rocks rich in chloritoid occur.

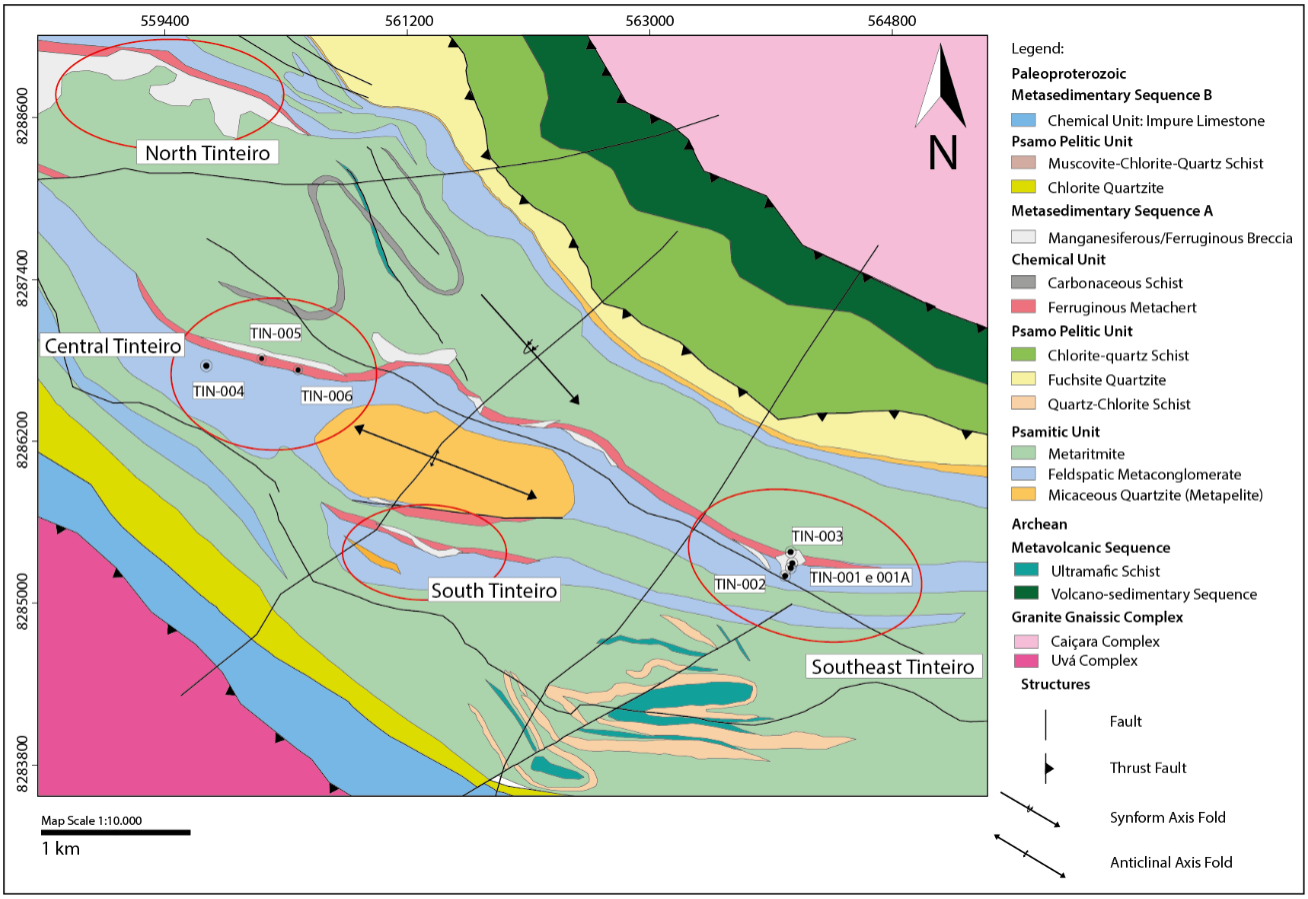

Figure 13: Geological map of the study region in 1:10,000 scale indicating the exploration targets of the Tinteiro system and the analyzed drillholes (modified from *Orinoco Gold Limited*, ASX:OGX, 2014).

The banded ferruginous metacherts from the chemical unit are grayish, with granoblastic texture, consisting predominantly of quartz (60-90%) and muscovite (5-20%). They usually occur as lenses ranging from a few centimeters up to 500 meters thick, housed both inside quartzite rocks and at the contacts between quartzites and metapelites. In the North Tinteiro target, very compacted and silky-looking talc schist lenses, with cubic pyrite crystals are observed.

Campos *et al.* (2017) reported that the hydrothermal alteration features in all targets of the Tinteiro System are similar. Both metapelites, quartzites and metacherts present hematite alteration that is marked by the formation of hematite and goethite, and also intense silicification. This alteration generates a banded appearance that can be easily confused with banded iron formations (BIF). Also, green muscovite of hydrothermal origin can be found both at levels close and coinciding with these alterations. Polymetallic mineralization occurs mainly in breccias, characterized by its matrix, sometimes rich in hematite and goethite, sometimes rich in manganese oxides and hydroxides, and angular clasts of lithic fragments of quartzite, metachert and quartz veins. Additionally, polymetallic alterations are observed at greater depths, marked by the contact between the metapelitic unit and the metachert. The authors also define two main alteration zones: proximal and mineralized zones.

3. Sampling and Methodology

The flowchart in Figure 14 summarizes the sampling and techniques used in this research work that focused on integrating multisource data. Based on previous geological models and airborne data, drill cores from field campaigns were systematically selected to determine a specific routine appropriate for the geological system in question. The methodological routine applied to the selected samples involved collecting chemical, petrophysical and spectral data, as well as microscopic petrographic analysis and X-ray diffraction. The databases previously obtained and the new ones were integrated, thus generating integrated models of the system. Finally, the footprints of the distal, proximal and mineralized zones of the Tinteiro system were delimited.

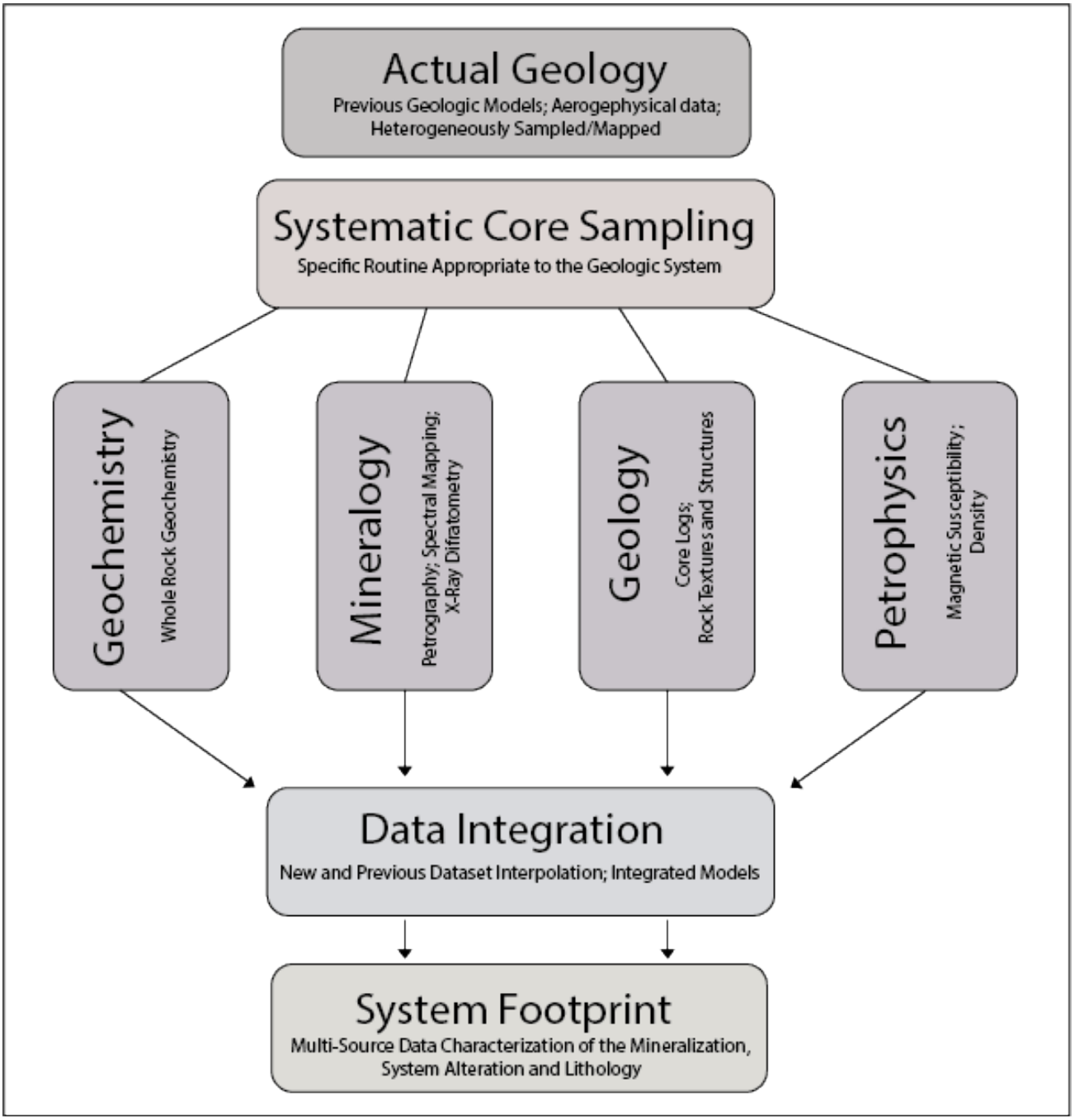

Figure 14: Flowchart of the methodological routine applied in this work (adapted from Lesher et al., 2017).

To conduct this research, a database of drill cores with a previous geological description of the Tinteiro System targets intercepting the mineralized intervals was provided. Of these, 5 drillholes were selected: (1) TIN-001, 31.83 m deep; (2) TIN-001A, 74.5 m deep; (3) TIN-002, 100.17 m deep; (4) TIN-004, 110 m deep, and (5) TIN-006, 100 m deep. The samples were collected every 1 meter, except in the mineralized zones, where it was every 0.5 m, totaling 225 samples. Of these samples, 29 were selected for making the polished blades while one sample was turned into a polished rock fragment of manganese breccia. The nomenclature used and their acronyms were established by the Orinoco Gold Ltda., as follows: BCH - manganesiferous breccia; MECH - metachert; MX - muscovite shale; CQS -

chlorite-quartz shale; QZ - quartz vein. The same logic was also applied in the hydrothermal alteration zones: PZ – polymetallic alteration zone (Table 2).

Table 2: Table indicating the samples sent for lamination and respective lithotypes.

Acronym	Litothype	Sample number	Samples
BCH	Manganesiferous breccia	2	T1/05; T1A/07
MECH	Metachert	12	T1/15; T1A/14; T1A/16; T2/13; T2/16; T4/31; T4/33; T4/36; T6/20A T6/20B; T6/28
CQS	Carbonate-quartz schist	8	T1/32; T1A/31; T2/30; T2/43; T4/45; T6/40A; T6/40B; T6/45
MX	Muscovite schist	3	T1A/25; T1A/26; T2/25
PZ	Altered Metachert	3	T1/28; T1A/29; T2/26
QZ	Quartz vein	1	T4/38

The sample chemical analyses were carried out in the Commercial Laboratory of Geochemistry ALS do Brasil Ltda. (Whole Rock, ICP-MS), relying on data of major, minor and trace elements from 170 samples. These results were provided by Orinoco Gold Ltda. for this work in November 2018. Later (in 2019), another 13 additional analyses were performed using the same analytical standard as the first samples to complement previous results.

In this specific research, the FieldSpec3HiRes (ASD) reflectance spectroradiometer was used to collect spectral data. The device collects reflectance data in two spectral ranges: in the visible to the near-infrared region (VNIR: 350-1,000 nm), and the short-wave infrared region (SWIR: 1,000-2,500 nm). In this instrument, the spectra are obtained from a contact probe consisting of a halogen lamp (1 cm diameter acquisition window). The spectral resolution is 3 nm and 8 nm in the VNIR and SWIR domains, respectively. Each recorded data represents the average of 50 spectra collected in the same area. In total, 1468 measurements were recorded in 225 samples. The data analysis obtained in the VNIR and SWIR intervals allowed identifying five mineral groups: iron oxides and hydroxides (the abundance ratio between hematite and goethite); kaolinite (identification and crystallinity degree); chlorite (identification and chemical character concerning the proportion of iron or magnesium); carbonates (abundance ratio between carbonate and dolomite); and white mica (chemical relationship between fengite-muscovite endmembers and their crystallinity degree). The data were processed and treated using The Spectral Geologist (TSG) software provided by the Geosciences Institute of Unicamp.

The natural density values of the compact samples were determined using the Toledo-IND560 scale in the Laboratory of Physical Properties of Rocks of the Institute of Geosciences, University of Brasília. And the absolute density values of the friable samples were collected using the Pentapyc 5200e in the Geotechnics laboratory of the School of Technology (FT), University of Brasília. The equipment has five capsules for placing the samples, in which gas is released during the measurement process. The pentapycnometer was used together with a high-precision Shimadzu AUW2200 balance, semi-micro with a double scale of five decimal places, to separate approximately 20 grams of friable sample per analysis (standard laboratory routine). The magnetic susceptibility measurements of the drillhole samples were conducted in a Terra Plus portable susceptibility meter, model KT-10S/C+. The measurements are made at the contact between the device and samples while the magnetic susceptibility measurements are captured in SI units. To identify mineral phases (above 1%), specifically of highly weathered samples, X-ray diffractometry (XRD) analysis was part of the drillhole characterization routine, especially in the most superficial portions. The routine was performed in the X-Ray Laboratory of the Institute of Geosciences, University of Brasília, using the RIGAKU diffractometer, model ULTIMA IV, which has a copper tube and a nickel filter set at 35kV, 15mA and a DTEX/ULTRA detector with a step of 0.05, 5°/min speed, and scanning range of 2Θ from 5° to 60°.

4. Results

The Tinteiro polymetallic mineralization is controlled by brittle mineralized structures that cut through the different FGB stratigraphic levels. The petrographic description of the sampled drillcores allowed characterizing the lithotypes and zones of hydrothermal alteration and mineralization. The TIN-001, TIN-001A and TIN-002 cores show great lithological conformity with each other since they are distant a few meters only (found in the Southeast Tinteiro target). On the other hand, TIN-004 and TIN-006 drill cores in the Central Tinteiro target, are geographically more distant from each other (Figure 13).

In all five drilling holes, it is observed a layer of soil and saprolite ranging from 1 to 5 m, which marks the beginning of each hole (Figure 15). In the drillholes TIN-001 and TIN-001A, ferruginous/manganese breccia (BCH) 3 to 4.5 m thick occurs, followed by muscovite schist layers with thickness varying from 50 cm (holes TIN-001 and 001A) up to 10 meters (holes TIN-002 to TIN-006). In all drillholes, except for the TIN-004, the muscovite schist repeats in/as less thick layers, after a thick layer (up to 17 meters) of metachert. The drillhole TIN-004 intersects two quartz vein systems (Figure 15B): one approximately 30 cm thick at 22.5 m deep, and another approximately 5 m thick at 31 m deep. The last unit mapped is the chlorite-quartz schist that extends to the end of the holes.

Polymetallic mineralization occurs associated with breccias, which may be accompanied by varying degrees of hydrothermal alteration. Two halos were observed: the distal, rich in muscovite and the proximal, rich in hematite (+ goethite), both predominantly at the contacts between the metachert and adjacent lithotypes. Muscovite-rich alteration occurs frequently in shales, but the alteration process is also observed to be imprinted in other lithotypes. Holes TIN-001 and 002 intersect a level enriched in euhedral magnetite within the chlorite-quartz shale. In hole TIN-006, a level of metachert with chloritoid was identified in its mineralogical composition.

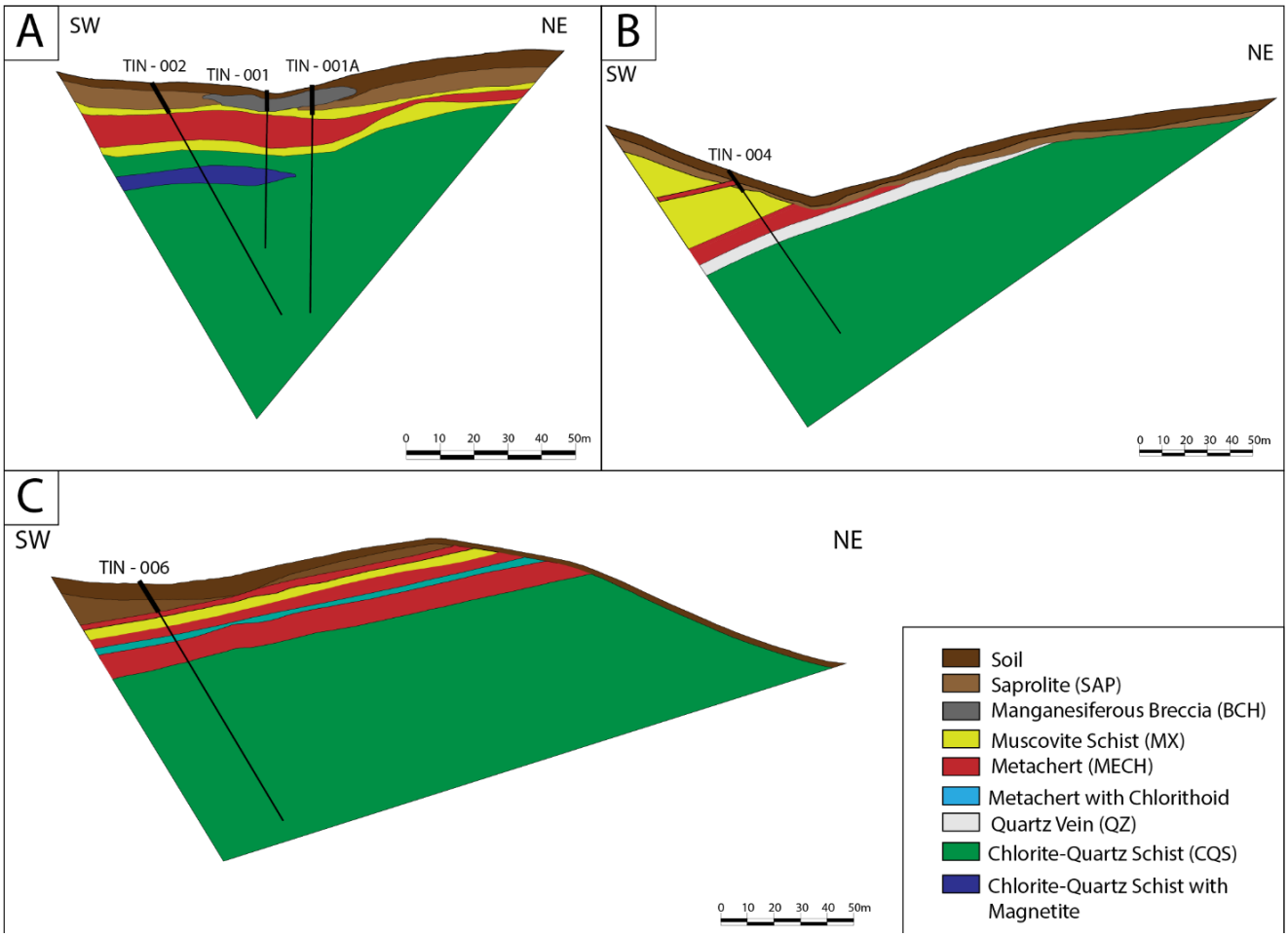

Figure 15: Schematic geological sections, with SW-NE direction, showing the location of drillholes TIN-001, TIN-001A and TIN-002 (A), TIN-004(B), and TIN-006 (C) illustrating the main lithotypes studied.

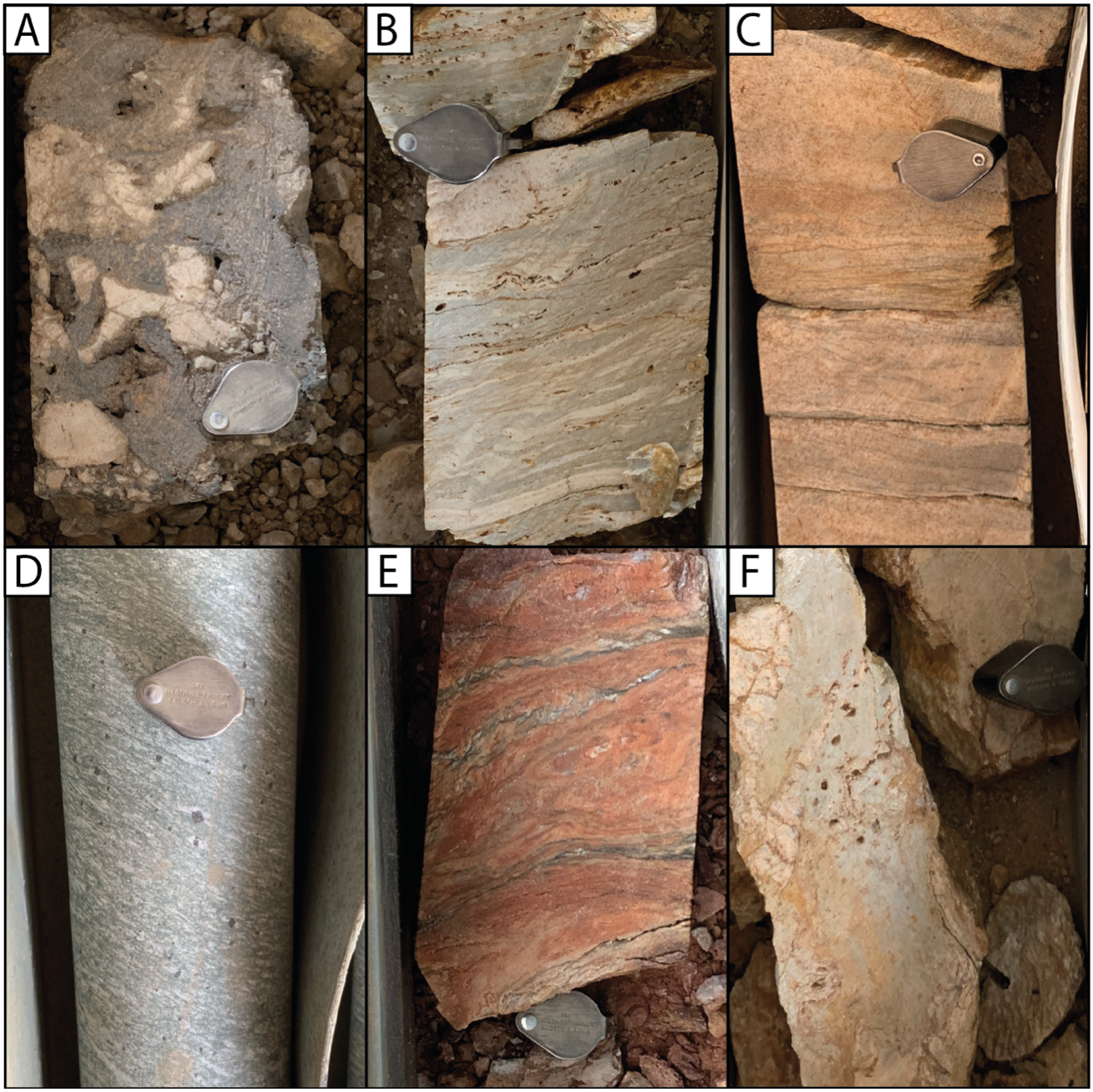

Figure 16: Mapped lithotypes and hydrothermal alteration zones: A) ferruginous/manganese breccia that hosts the polymetallic mineralization; B) muscovite shale (MX); C) metachert (MECH); D) chlorite-quartz shale (CQS) with magnetite crystals; E) metachert affected by hematite and muscovite hydrothermal alteration; F) fractured quartz vein associated with muscovite.

Metachert - MECH

In the studied drill cores, the metachert is normally semi-altered (Figure 16C). The rock is white to slightly grayish with a granoblastic texture. When altered, it shows ocher and reddish tones. Mineralogy consists of quartz >95% and muscovite <5%. The equigranular quartz crystals are fine-grained (Figure 17 A) while some muscovite-enriched levels exhibit domains with a lepidoblastic texture (<0.1 mm), highlighting the main foliation plane (Figure 17 B). In some portions, chloritoid

occurs associated with chlorite and iron oxides (TIN-004 and TIN-006; Figure 17 C and D), providing textured nematoblastic features. The iron oxides are hematite and goethite, associated with pressure remnants involving the chloritoid porphyroblasts.

At more altered levels, the rock mineralogical composition suggests the action of the hydrothermal process in this portion, where some mineralogical modifications can be observed concerning the metachert, such as muscovite enrichment in the distal portion and hematite in the proximal halo (Figure 18), giving a friable, reddish appearance with muscovite bands. At these levels, the proportion of minerals changes tending toward a greater amount of micaceous minerals and iron oxides and hydroxides.

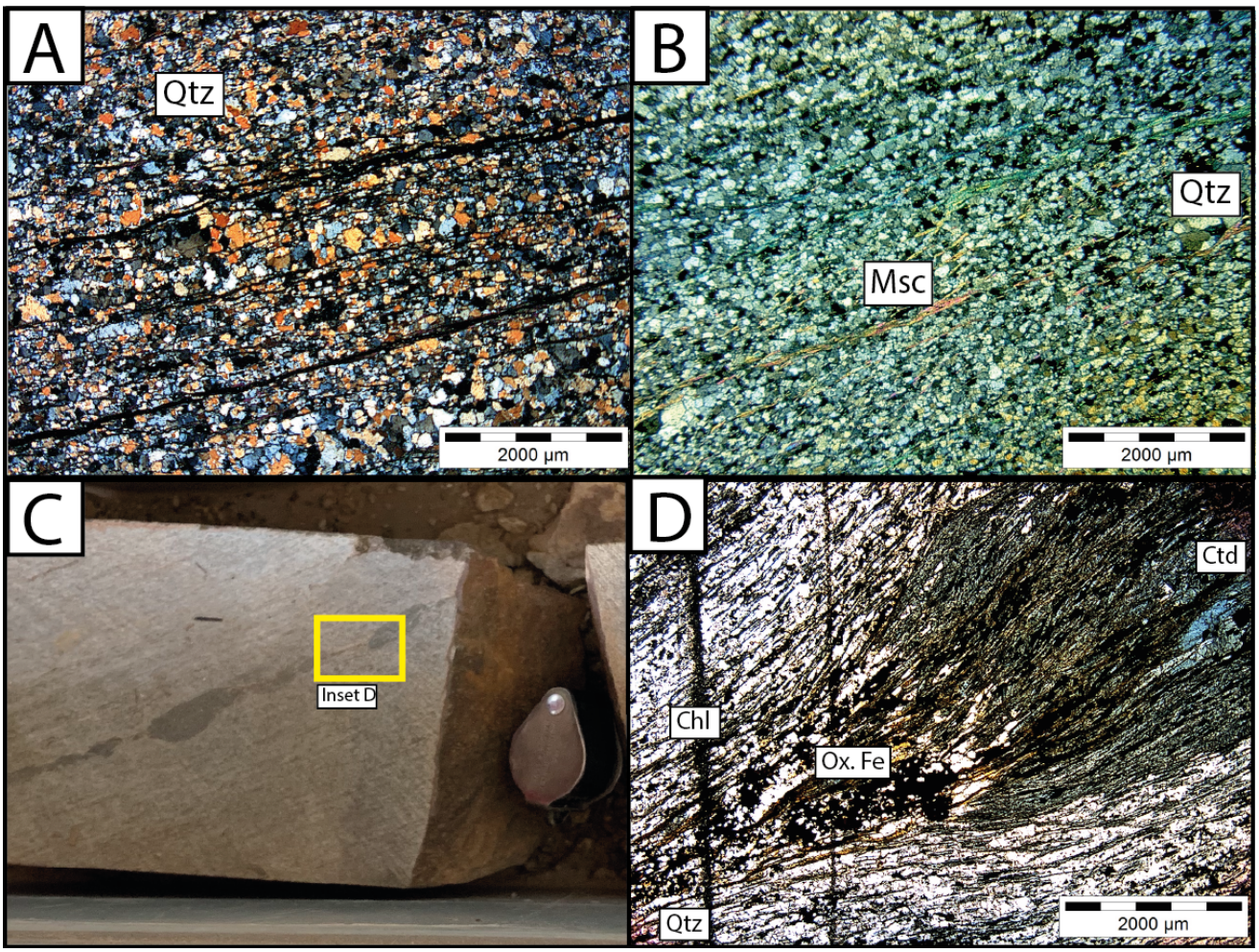

Figure 17: Metachert samples intercepted by the drillholes: A) polygonal granoblastic texture in metachert; B) muscovite films delimiting the rock foliation plane; C) Drill core metachert sample from Hole TIN-004 showing millimetric lenticular levels rich in chloritoid and chlorite; D) Photomicrograph of the same sample with chloridoid porphyroblasts wrapped in chlorite films. Iron oxides are concentrated in the pressure shadow. Qtz - quartz; Chl - chlorite; Ctd - chloritoid; Ox. Fe - iron oxides; Msc - muscovite.

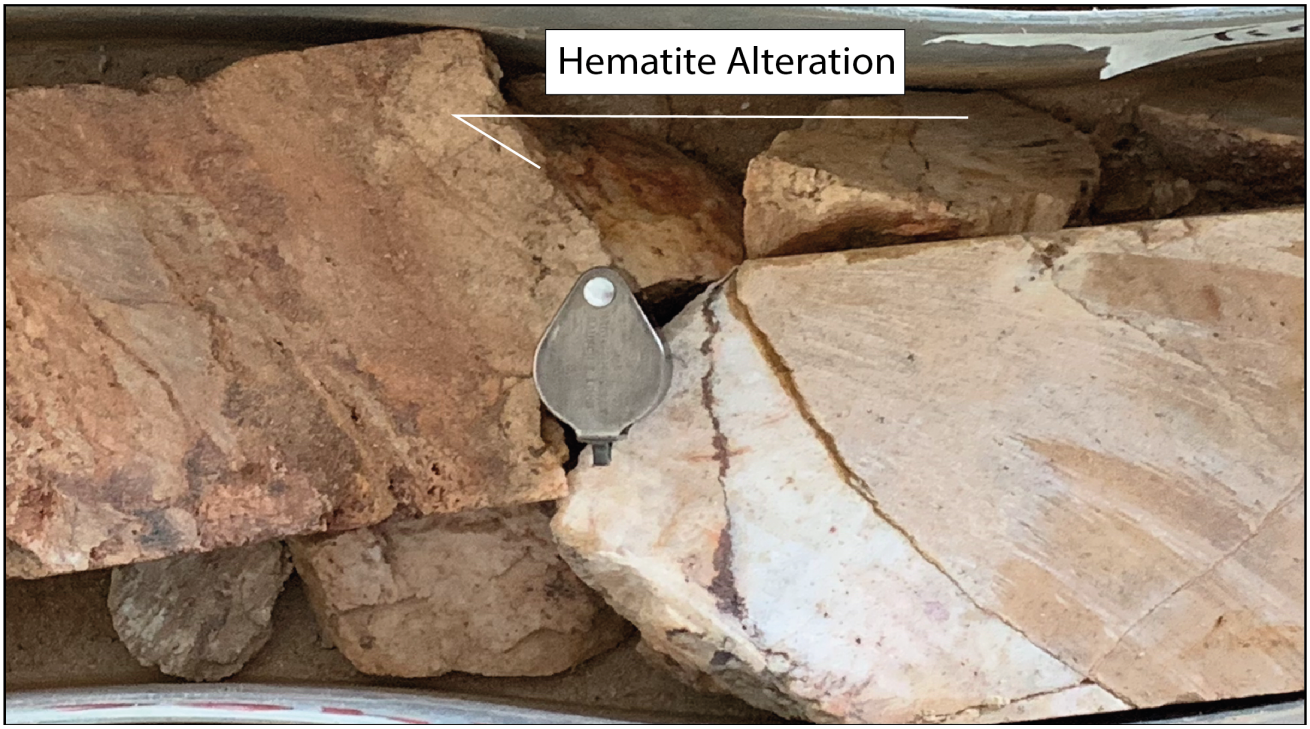

Figure 18: Drillcore samples (TIN-002/25) highlighting the effect of hematite alteration on the metachert (MECH), macroscopic scale.

Chlorite-Quartz Schist (± Carbonate and Muscovite) - CQS

Chlorite-quartz schist is a greenish rock, fine to medium-grained and very foliated. The texture is marked by alternating millimeter quartzose levels interspersed with chlorite levels (Figure 19). Magnetite disseminated (Figure 16D) in euhedral crystals (up to 5mm) and quartz and carbonate venules (up to 4 centimeters) are common in this unit. These rocks are quite friable and highly fragmented over all the intervals intersecting them in drillholes from TIN-001 to TIN-006.

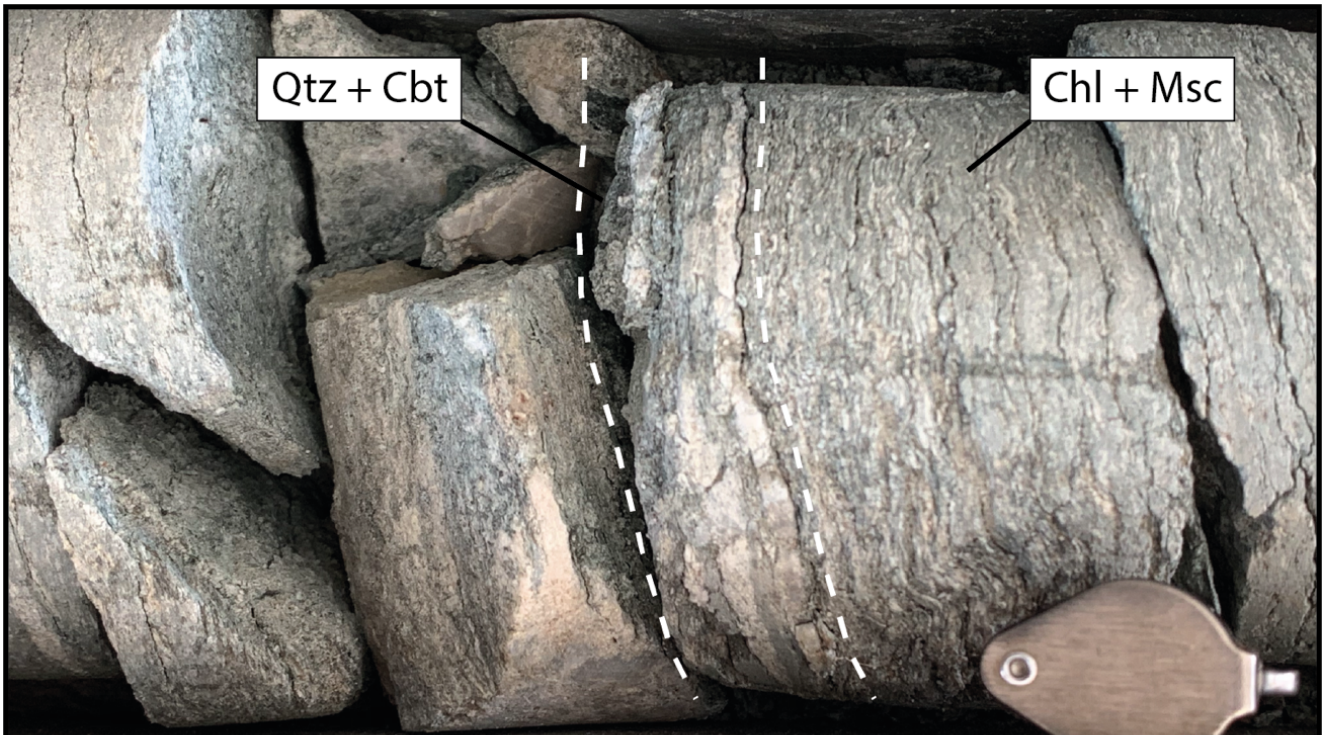

Figure 19: Sample TIN-001A/34. Strongly foliated chlorite-quartz schist with a texture marked by alternating greenish levels rich in chlorite and whitish levels of quartz and carbonate.

The mineral assemblage consists of chlorite, muscovite, quartz and carbonate, whose proportions vary greatly for the different rock facies: chlorite varies from 50 to 5%, quartz from 35 to 15%, muscovite from 40 to 5%, and carbonate from 35 to 15%. Thus, this lithology includes the following classifications: carbonate-chlorite-quartz-muscovite schist, muscovite-carbonate-quartz-chlorite schist, muscovite-quartz-carbonate-chlorite schist, and so on. Epidote (< 4%) and plagioclase (< 1%) crystals occur subordinately at specific levels, and the same applies to accessory minerals (1%), oxides and sulfides (pyrite, magnetite, chalcopyrite and hematite). The texture is predominantly lepidoblastic, marked by the preferential orientation of phyllosilicates (chlorite and muscovite). A second granoblastic textural domain is observed and characterized by levels of anhedral and equigranular quartz and carbonate crystals (0.5 mm), and plagioclase in a few samples (TIN-001/28 and TIN-001/32) (Figure 20 D). The rock is mylonitized and the carbonate is often contained in venulations stretched in the direction of foliation (Figure 20, Item B). Drillholes TIN-001 (from 25 to 30 m) and TIN-002 (from 32 to 40 m) exhibit constant euhedral crystals of chalcopyrite and pyrite (Figure 20 C), and magnetite (Figure 20 A), these minerals are late concerning the tectonic foliation, which is consistent with the hydrothermal alteration related to late structures.

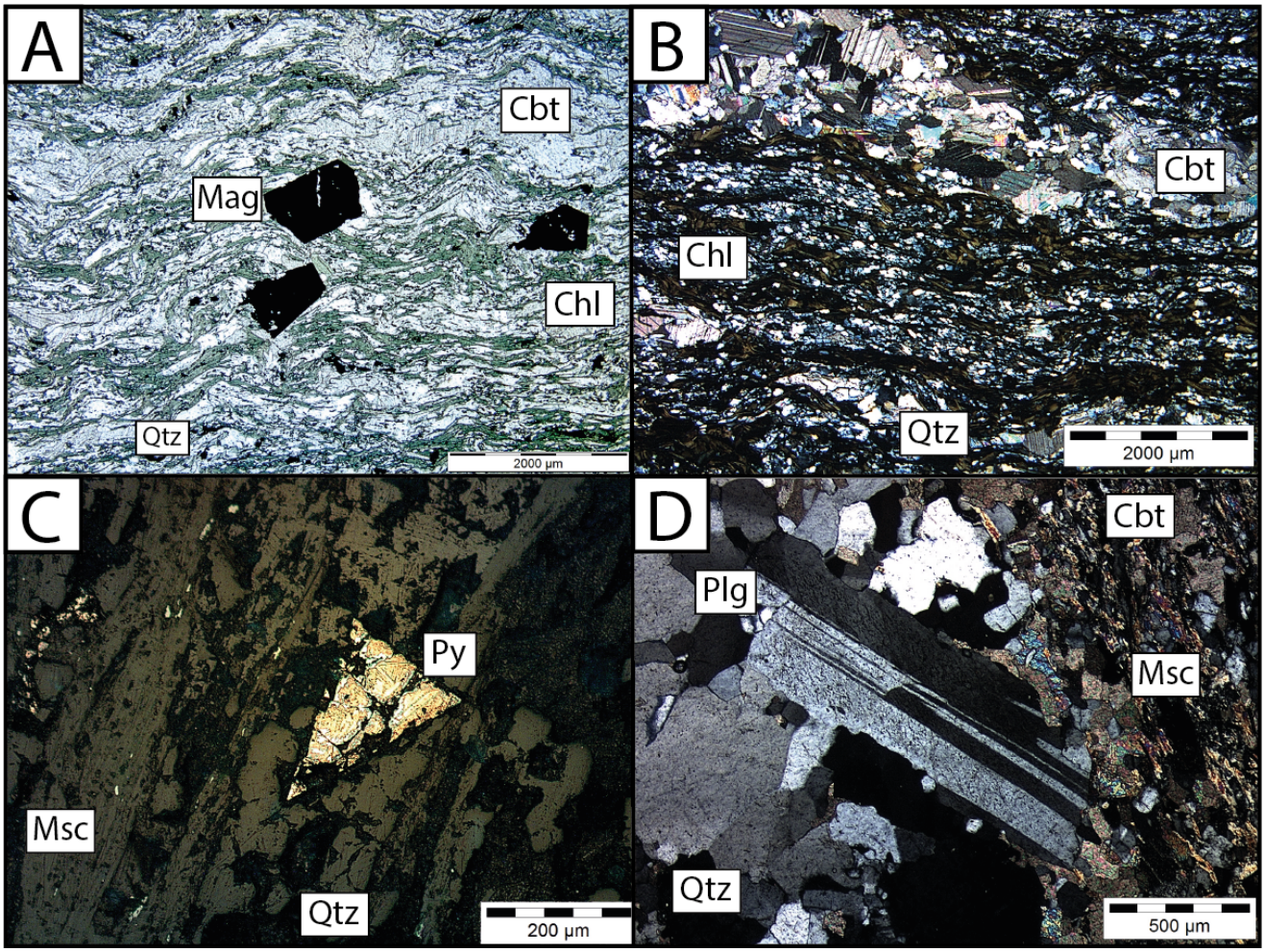

Figure 20: Photomicrographs of chlorite-quartz schist (CQS). A) Chlorite-quartz schist with late to post-tectonic porphyroblasts of magnetite; B) Carbonatic venule concordant with the main tectonic foliation in chlorite-quartz schist; C) pyrite euhedral crystal; D) anhedral plagioclase crystal at quartz-rich levels in quartz-chlorite schist. Qtz - quartz; MSc - muscovite; Cbt - carbonate; Chl - chlorite; Plg - plagioclase; Py - pyrite.

Quartz vein - (QZ)

In the drillcore TIN-004, two quartz veins are observed intersecting the units: one 30 cm thick and another, 5 m thick, at depths of 20 and 32.5 m, respectively. These veins consist mostly of quartz, found in uniform domains that extend over meters but also exhibit portions very enriched in muscovite, oriented according to the tectonic foliation (Figures 21 A and B).

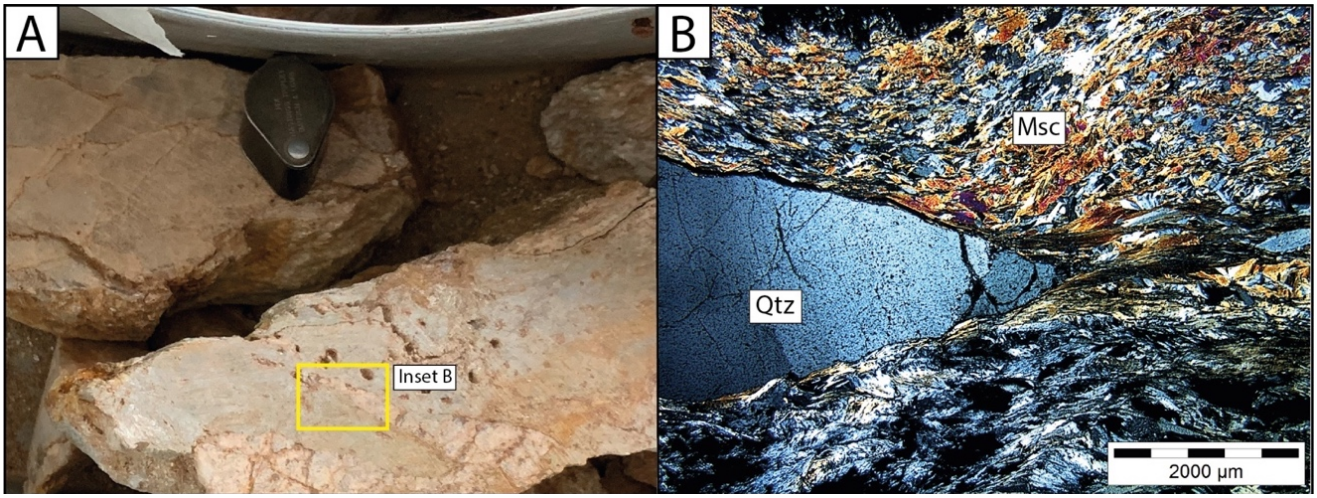

Figure 21: Quartz vein (QZ). A) drillcore sample which presents muscovite aggregates; B) Photomicrograph of the quartz vein indicating domains rich in quartz and muscovite. Qtz - quartz; Msc - muscovite.

Zones of Hydrothermal Alteration and Polymetallic Mineralization

The petrographic analysis allowed recognizing the distal and proximal hydrothermal alteration zones, marked by textural and mineralogical transformations up to the mineralized zone. Campos *et al*. (2017) identified the two types of hydrothermal alteration with the more distal muscovite-rich alteration and the more proximal hematite alteration. The analyzed data show a varying amplitude of the alteration halos presented in products derived from geophysical data interpreted by Campos *et al*. (2017) and also observed in the drill cores.

The distal hydrothermal alteration halo is marked by muscovite-enriched zones that are well registered in various portions of the metachert (see Figure 22B) and in general, millimetric to centimetric levels are observed with muscovite occupying lamellar interstitial spaces. With the expansion of the alteration, the obliteration of the mineralogical and primary textural features is observed, until the transformation into muscovite schist (MX) (Figures 16 B and 22 A). In these portions, the rock mineralogical composition consists of muscovite (95%) with a lepidoblastic texture, and quartz (5%).

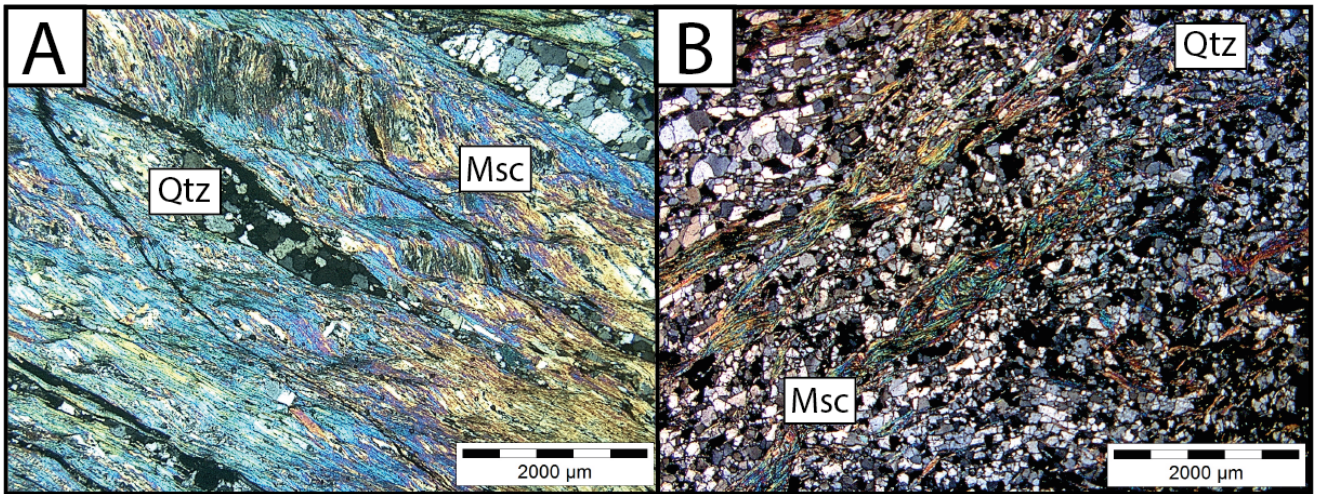

Figure 22: Polished blades from samples TIN-001/25 and TIN-002/13 illustrating the muscovite hydrothermal alteration. A) Muscovite schist foliated with small, recrystallized quartz lenses. B) Metachert with oriented muscovite lamellar aggregates resulting from muscovite alteration.

The hematite hydrothermal alteration halo is characterized by hematite and goethite enriched zones, where the alteration is seen filled in planes of preexisting structures in the rocks and also associated with brittle structures that intersect the orogenic gold system described by Campos *et al*. (2017). Images A and B of figure 23 (photographed in the Cascavel mine) highlight the hematite halo and the cut and superposition relationships, evidencing the later nature of the Tinteiro system.

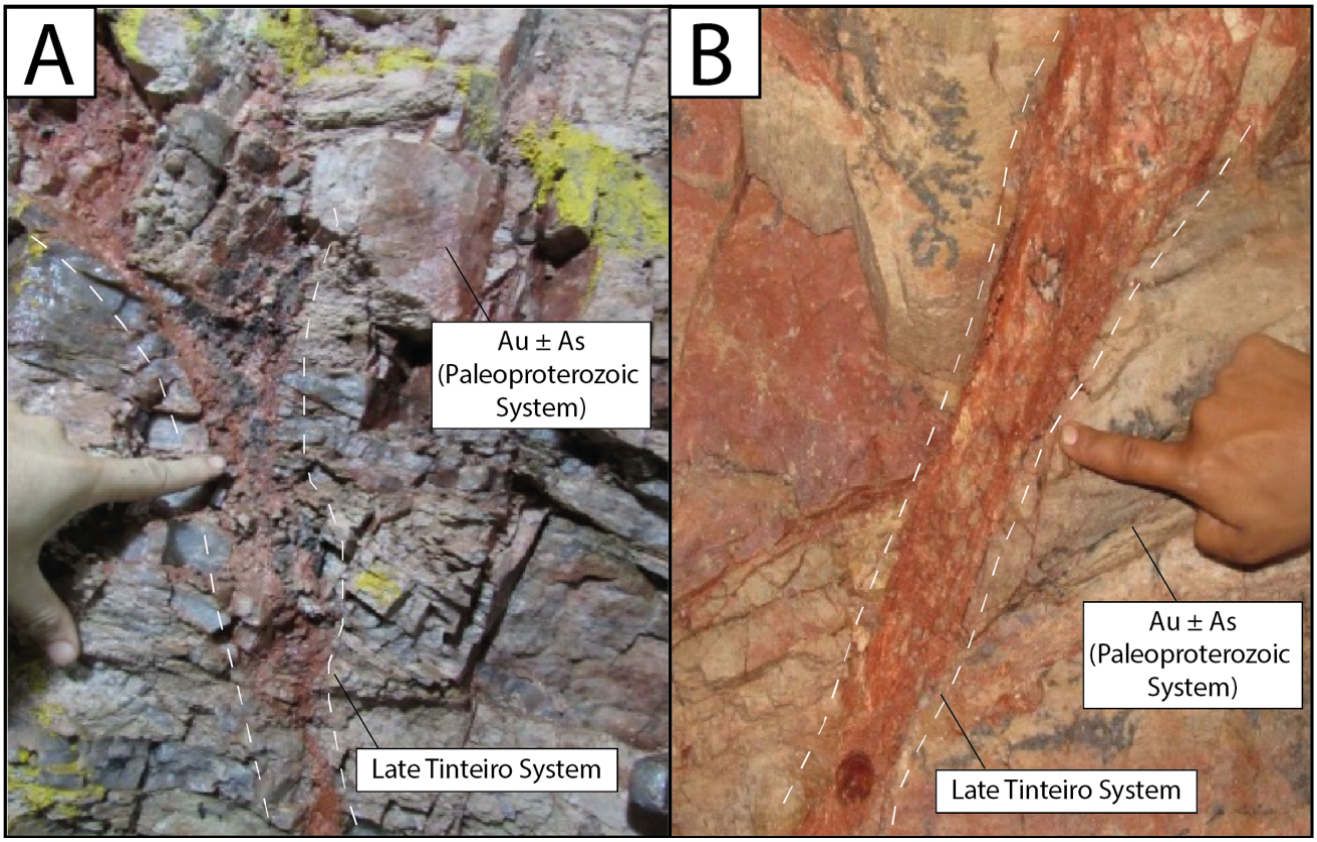

Figure 23: Photo showing the expression of the hematite halo mapped in the Cascavel mine. (A) and (B) both show the hematite alteration halo of the Tinteiro system that cuts the Paleoproterozoic orogenic auriferous system (Au ± As).

Figure 24A demonstrates the hematite hydrothermal alteration taking advantage of preexisting planes in the rock enveloping the edges of hematite lamellae and quartz grains. The hydrothermal alteration is also observed in millimeter venulations discordant from the preexisting planes, forming angles close to 90° that penetrate the rock through foliation (Figures 24 B, C and D). Among the samples collected, metachert (MECH) is the lithology that best registers this change, since there is a lot of color contrast compared to the unaltered rock (Figures 16 E and 18).

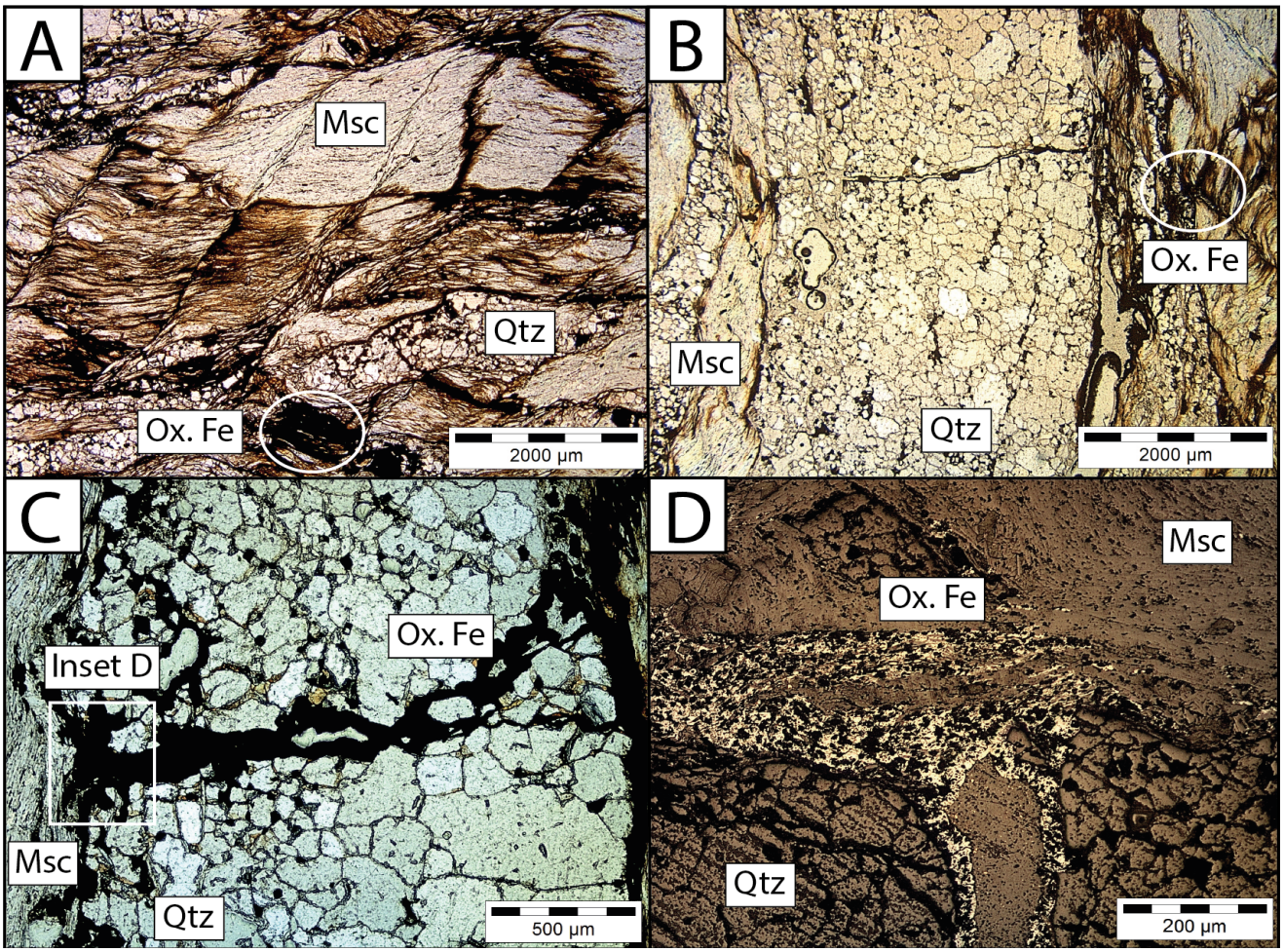

Figure 24: Photomicrographs of rocks altered by the hematite halo: A) muscovite schist with the interaction record of the hematite halo, where the ferruginous material envelops the edges of the muscovite lamellae, highlighting the behavior of well-registered alteration along the foliation planes; B, C and D) systems of discordant venules concerning the preexisting foliation. Msc - muscovite; Qtz - quartz; Ox. Fe - iron oxide (hematite and goethite).

Levels, where the rocks are intercepted by both hydrothermal alterations, were also mapped. These rocks consist of quartz (35%), muscovite (30%), iron oxides and hydroxides (goethite and hematite, 30%), and clay minerals (5%). The rock texture is very irregular due to highly foliated levels demarcated by muscovite, granoblastic levels associated with quartz, and irregular to granoblastic texture domains with a disseminated aspect related to hematite and goethite (Figures 25 A and B). The phases defined by X-ray diffraction are quartz, muscovite, hematite, goethite, clinochlore, corrensite and kaolinite (Figure 26).

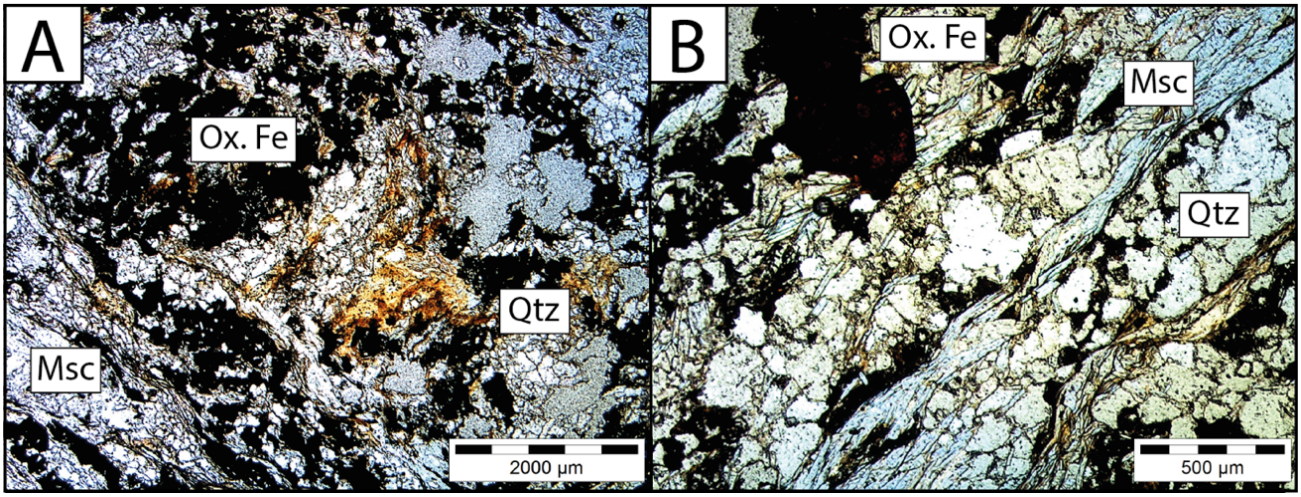

Figure 25: A) and B) Rock samples showing the superimposition of both hydrothermal alterations (muscovite and hematite). Msc - muscovite; Qtz: quartz; Ox. Fe: iron oxides (hematite and goethite).

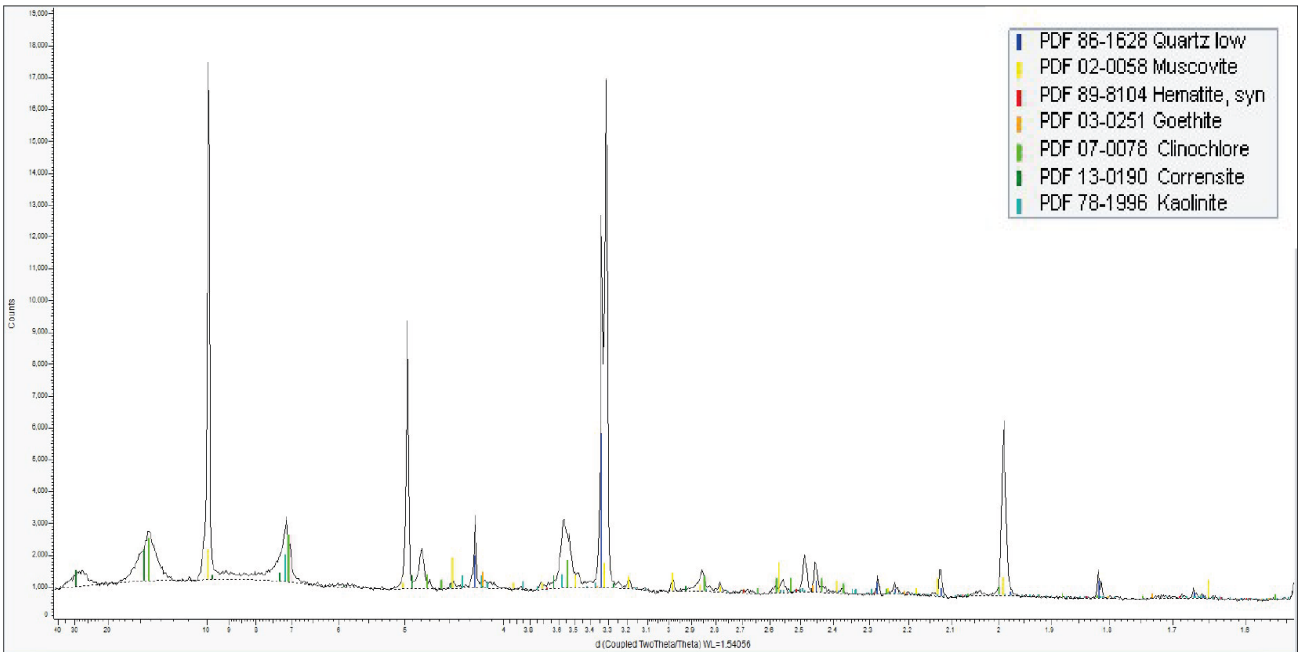

Figure 26: DRX diffractogram of the TIN-001A/27 sample, the detected phases (greater than 1% of the total sample) are: quartz, muscovite, hematite, goethite, clinochlore, corrensite and kaolinite.

The mineralized zone of the Tinteiro system was mapped in the field through the identification of breccias and gossans (Figures 27 A and B). Holes TIN-001 and TIN-001A intersect manganesiferous breccias (BCH) that represent the mineralized range mapped in the drillholes. The breccia has a dark and thin matrix with quartz clasts and angular metachert lithic fragments ranging from millimeter to centimeter scale. These rocks are usually indented by quartz veins up to 4 centimeters thick.

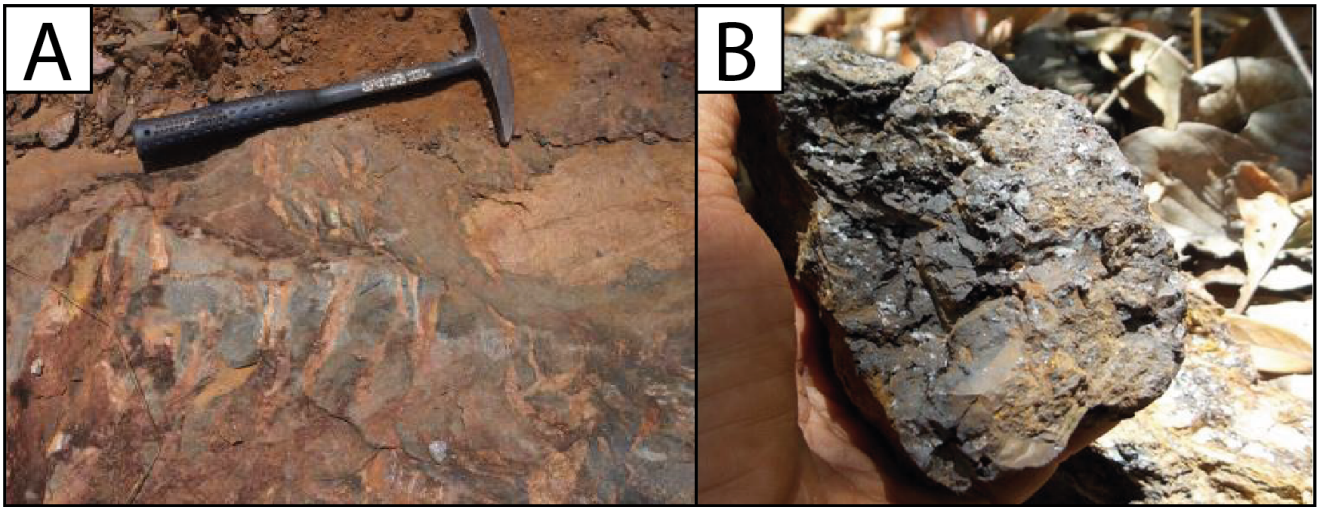

Figure 27: Surface occurrence of the Tinteiro system as hematite/manganesiferous breccias (A) and gossans (B).

The breccia matrix is composed of aggregates of manganese (60%) and iron (30%) oxides and hydroxides, muscovite (5%), and clay minerals (5%). Occasionally, pyrite and chalcopyrite (millimeter crystals) are observed (Figure 28 B). Manganese oxides and hydroxides occur as amorphous aggregates (Figure 28 A) with a dark gray tone, and, in some samples, they form aggregates with a botryoidal habit (Figure 28 C and D). Iron oxides and hydroxides are also present as amorphous aggregates, with more reddish tones and muscovite appear as very thin lamellae (<0.5mm). The breccia clasts are centimetric, angular and poorly selected, consisting of quartz and metachert lithic fragments. Analysis of the X-ray diffractometry data for the manganese breccia matrix shows quartz, muscovite, hematite, goethite, psilomelane, romanechite and hollandite (Figure 29).

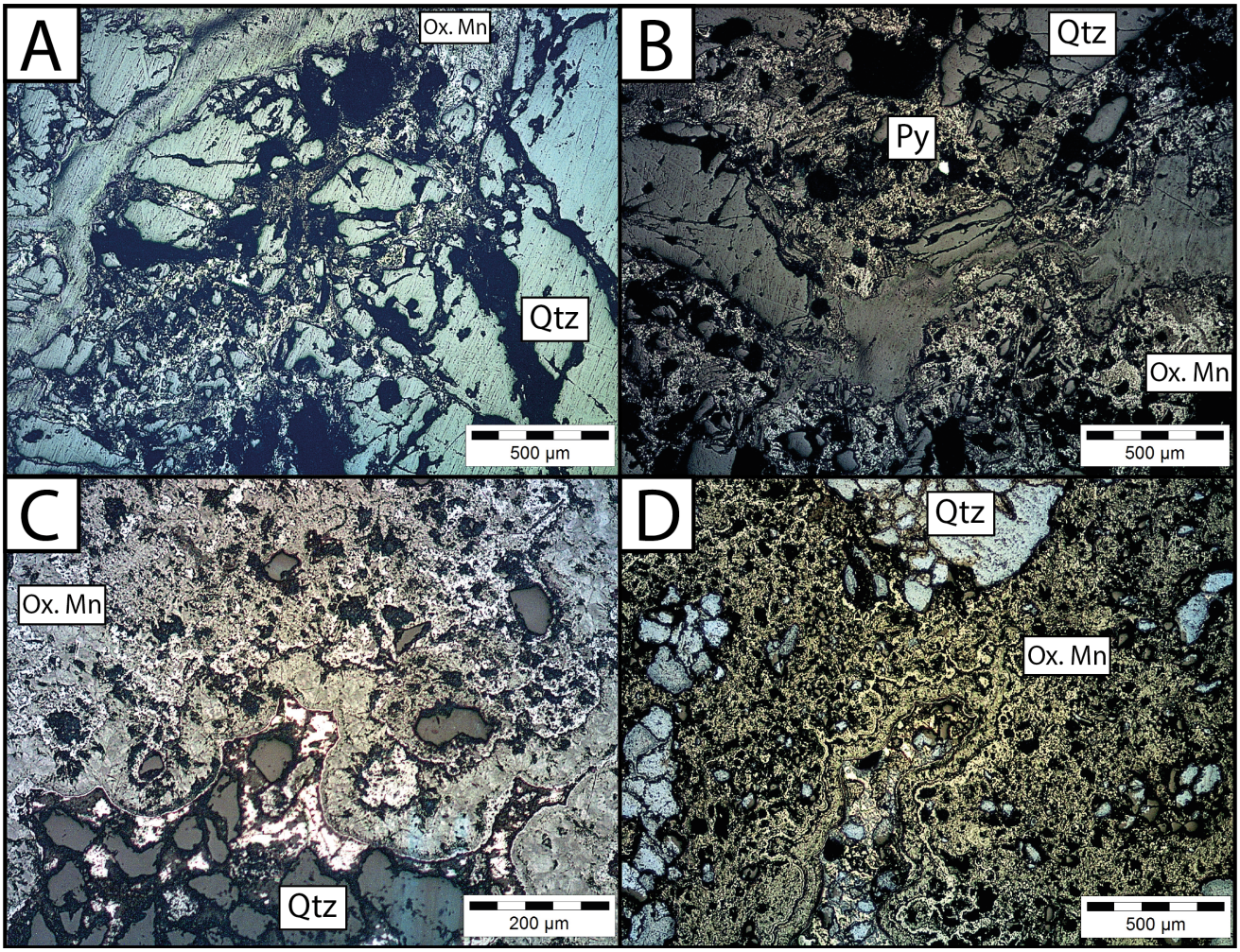

Figure 28: Polished sections of manganesiferous breccia (BCH; sample TIN-001A/5). A) It is observed very angular quartz fragments and a very fine heterogeneous matrix composed of aggregates of manganese oxides and hydroxides, in B), pyrite crystal in the breccia matrix; C) matrix with manganese oxides and hydroxides with the botryoidal habit; D) Detail of the manganese oxides present in the matrix. Qtz - quartz; Ox. Mn - manganese oxides; Py - pyrite.

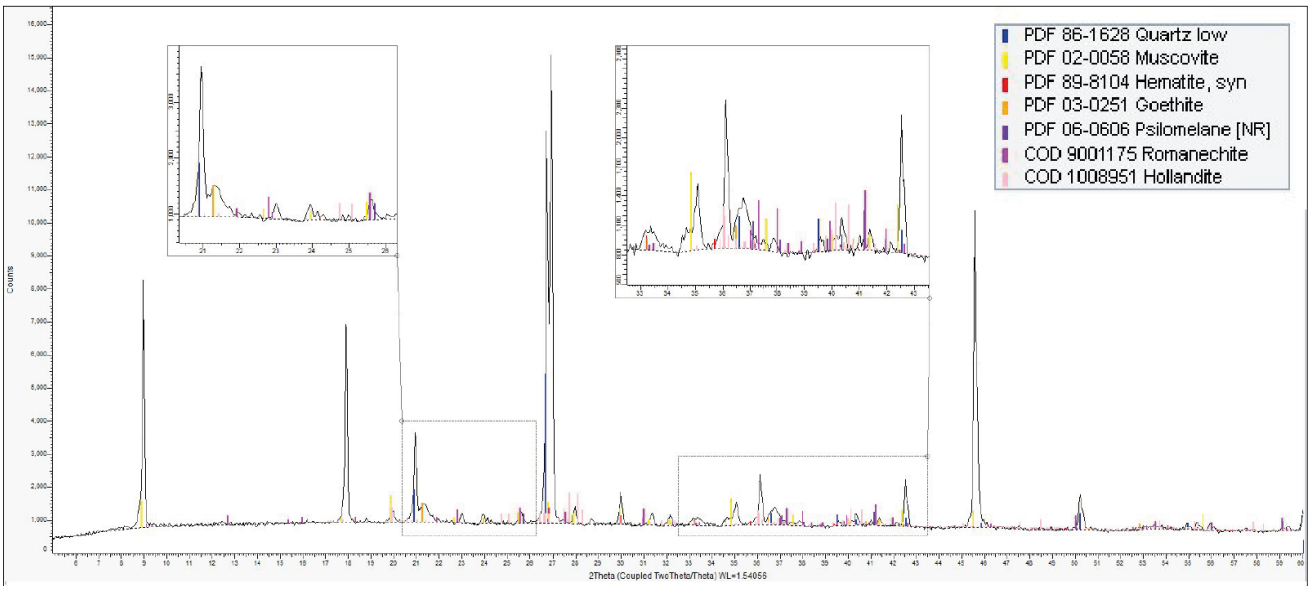

Figure 29: X-ray diffractogram of the manganesiferous breccia matrix (sample TIN-001/5). The emphasized areas highlight the peaks of the Mn-rich mineral paragenesis.

4.1 Reflectance Spectroscopy

The algorithms and parameters used for extracting the spectral data were taken from Prado *et al*. (2016), Campos, L.M. (2019) and Pereira, H.S. (2017) as follows: (1) 600_700SL, identification of Fe oxides and hydroxides; (2) 900D, identification and quantification of the relative abundance of Fe oxides and hydroxides; (3) 900Wvl, differentiation between hematite and goethite; (4) 2335D, relative abundance of chlorite; (5) 2335Wvl, chlorite composition; (6) 2330D relative abundance of carbonates; (7) 2330Wvl, the composition of carbonates; (8) 2164Dk, identification of kaolinite; (9) 2200Dk, identification and relative abundance of kaolinite; (10) 2170SL, kaolinite crystallinity index; (11) 2200Dwn, identification and quantification of white mica; and (12) 2200Wvl, white mica composition. This processing allowed us to identify all spectral members present in the samples. Figures 30 and 31 show the spectral endmembers of the white mica group, iron oxides and hydroxides, chlorite, carbonates and kaolinite found in the rocks analyzed in this work.

Iron oxides and hydroxides produce characteristic absorption features in the VNIR region, due to electronic processes involving Fe^{3+}, which can be linked to an octahedral site and with oxygen bonds (hematite) or linked to hydroxyl (-OH) and oxygen also (goethite) (Hunt, 1977). The spectral domains of 880 nm and 1008 nm define the mineral characterization of hematite and goethite, respectively (Figure 30B) and are expressed as the inflection points of the diagnostic curves of the features (Van der Meer, 2004). The histogram in Figure 32 presents the general distribution of this group members in the samples and demonstrates a high frequency of occurrence of both hematite and goethite in the analyzed rocks. Furthermore, phyllosilicates and carbonates present their diagnostic absorption features in the SWIR region, due to the bonds between H_2O molecules, metals linked to hydroxyl (-OH) and CO^{2-}_3. Chlorite has a diagnostic feature at 2253 nm, Fe Chlorite at 2350 nm and Fe-Mg Chlorite at 2340 nm (Figure 30 C), related to the MgOH and FeOH present in the mineral structure (Pontual *et al*., 2008). Samples from this work, shows that Fe Chlorite is more abundant, with only a few occurrences of Mg Chlorite.

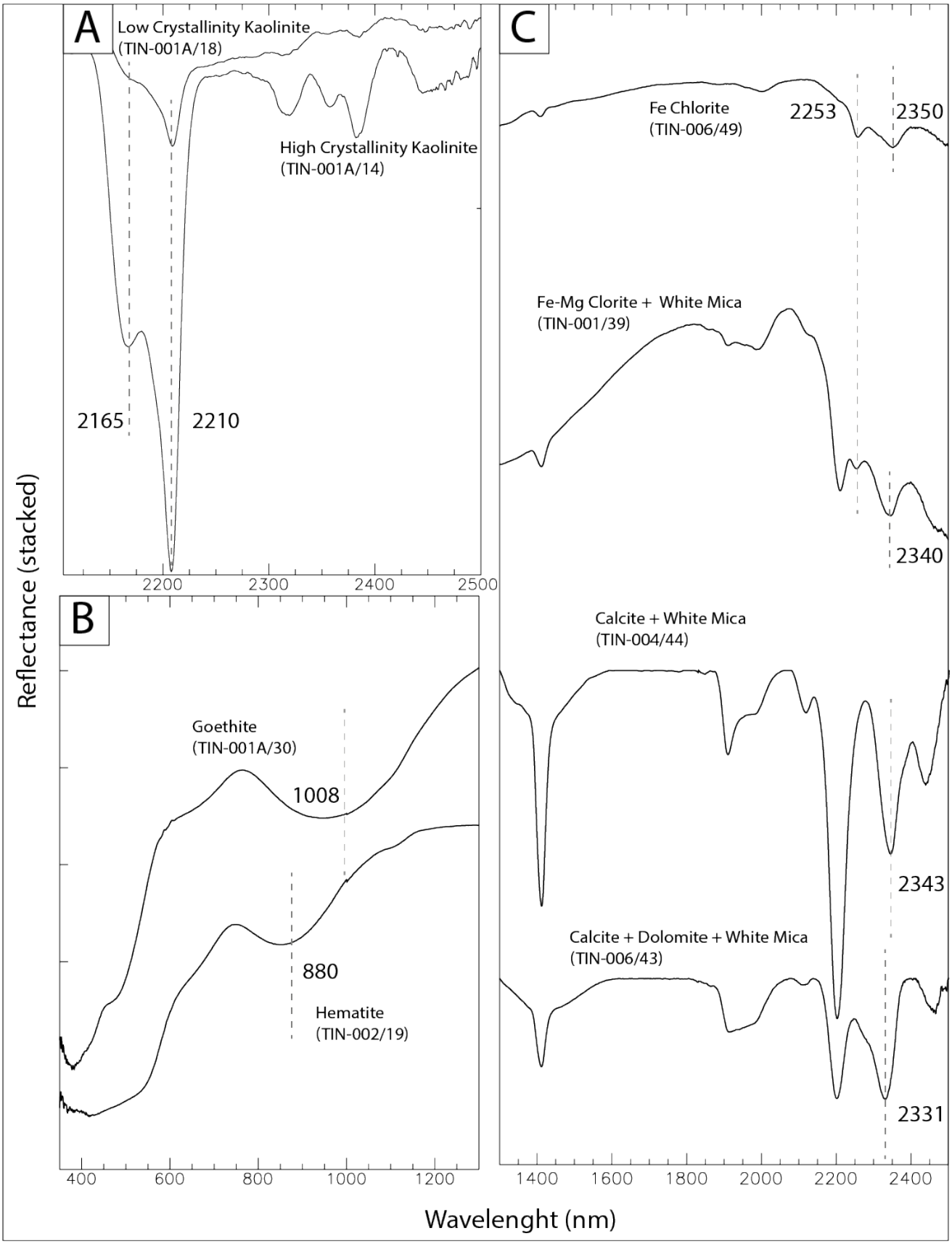

Figure 30: Cutoffs from the spectra of all endmembers of the mineral groups, iron oxides and hydroxides (B), carbonates (C), kaolinite (A) and chlorite (C) found in the samples. The image shows the name of the hole and the sample number for each spectrum. The spectra had the continuum removed to enable a better visualization.

The minerals of the kaolinite group have a set of absorption features at 2208 nm and another between the 2160 and 2190 nm region due to the Al-OH bonds (Bishop *et al*., 2008). In this specific study, the diagnostic features are at 2165 nm and 2210 nm (Figure 30A), while depth is correlated with crystallinity: the deeper, the greater the crystallinity value. There are also three features of lower intensity and depth characteristic of kaolinite, in 2310, 2350 and 2380 nm regions, which are well defined in the high crystallinity spectrum shown in Figure 30A.

The carbonate group is the least abundant in the samples analyzed, and has two main diagnostic features: one between 2500 and 2550 nm and another between 2300 and 2350 nm (Figure 30 C) due to the CO^{2-}_3 present in the mineral structure. The main diagnostic features were determined at 2343 nm for calcite and 2331 nm for the calcite-dolomite mixture. Figure 30 C shows these endmembers and the interference due to the mica present in the samples. No sample with an abundance of pure dolomite was obtained. It is noted that in the studied area, calcite concentration is higher compared to the calcite-dolomite mixture, which has less than ten occurrences in the samples.

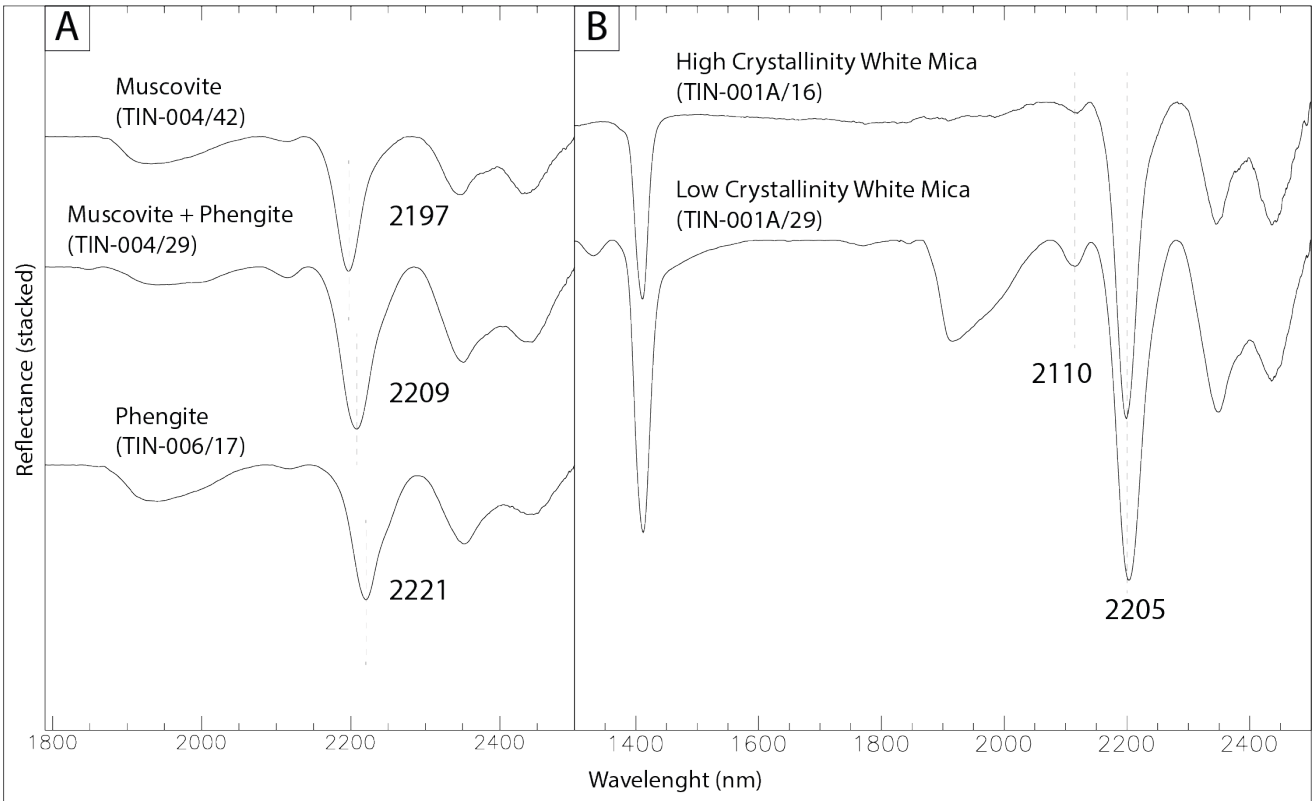

Figure 31: Cutoffs of spectra of all endmembers of the white mica mineral group found in the analyzed samples. A) It emphasizes its compositional contrasts and variety and B) its crystallinity. The image shows the drillhole name and the sample number for each spectrum. The spectra were removed from the continuum to enable a better visualization.

The members of the white mica mineral group present diagnostic features in the spectrum regions from 2197 nm to 2221 nm (Figure 31A) related to the presence of AlOH in their mineral structure. Also, two more discrete features usually occur in the 2340 nm and 2430 nm region,

characterizing two minerals with a very similar mineral structure: muscovite and phengite, but phengite has a more magnesian chemical character. Consequently, this crystallo-chemical difference ends up defining the regions of the spectrum: values above 2200 nm classify only as muscovite, from 2208 nm to 2216 nm as a muscovite and phengite mixture while greater than 2216 nm as phengite. The migration of the main absorption feature between muscovite and phengite is characterized by the Tschermak replacement (Wang *et al.,* 2017).

For muscovite, the depth of the absorption features and the AlOH vs H_2O relationship determine the crystallinity degree (Figure 31 B). Most samples in this study have high crystallinity, but the quartz interference in the rock increases the depth of the H_2O feature at 1900 nm, interfering with the crystallinity diagnosis. The histogram in Figure 32 shows the frequency of the mineral group endmembers, in which muscovite is predominant and the muscovite and phengite mixture occurs moderately. Phengite, on the other hand, is much less abundant compared to the other components. Figures 33, 34 and 35 show scatter plots of all analyzed mineral groups regarding rock lithology versus depth of the TIN-001, TIN-001A, TIN-002, TIN-004, and TIN-006 drill cores.

The most superficial soil and saprolite levels had a low abundance of the analyzed groups, including the TIN-001 and TIN-001A samples with no recorded occurrence. In the TIN-002 drill core, these levels are characterized by the presence of oxides and hydroxides with a mixed composition between hematite and goethite. In the TIN-004 and TIN-006 core cores, in addition to the presence of hematite-goethite, there are also mineral occurrences of the white mica group whose composition tends to phengite. The breccia, present only in the TIN-001 and TIN-001A drill cores, is also characterized by the occurrence of the same mineral groups. Where iron oxide-hydroxides tend to have more hematite, and white mica tends to exhibit an intermediate composition of phengite and muscovite, with crystallinity values reaching up to 11.74.

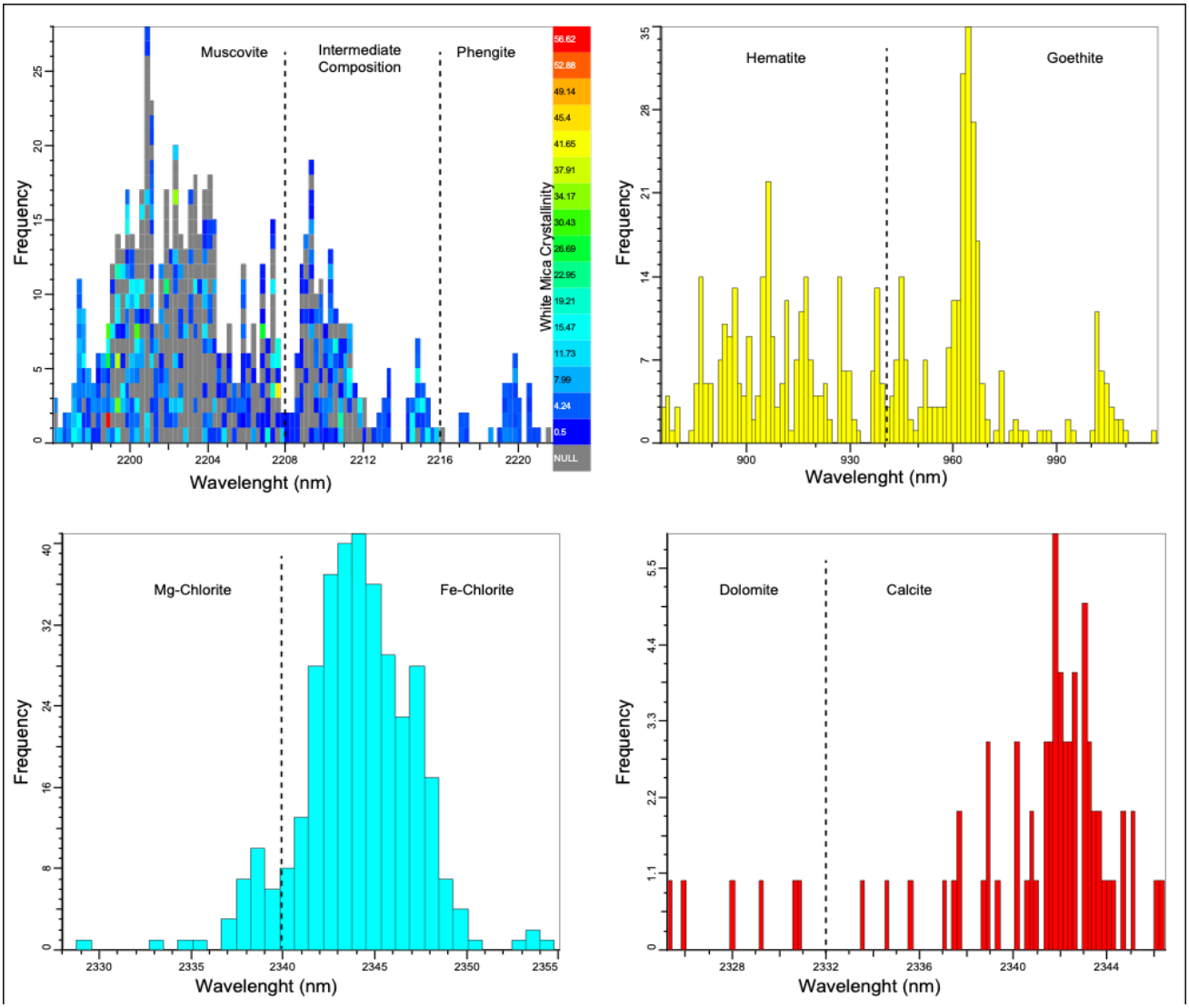

Figure 32: Histograms showing the frequency of samples versus the spectrum region where the main endmembers are concentrated.

Muscovite schist (TIN-001 and TIN-001A) is a mixture of minerals from the group of iron oxides and hydroxides while the white micas tend to muscovite, whose crystallinity can reach 7. TIN-002 core exhibits a greater compositional range of minerals from the group of iron oxides and hydroxides, with occurrences of hematite, goethite and intermediate phases. White mica tends to muscovite, and there is also Fe-chlorite. Likewise, in TIN-004, minerals from the group of iron oxides and hydroxides are present similarly to TIN-002, with a predominant intermediate phase of white mica minerals, and high crystallinity values reaching up to 45. In TIN-006, occasional occurrences of high crystallinity kaolinite are observed, the minerals from the group of iron oxides and hydroxides have an intermediate composition, whereas the composition of white micas tends to phengite.

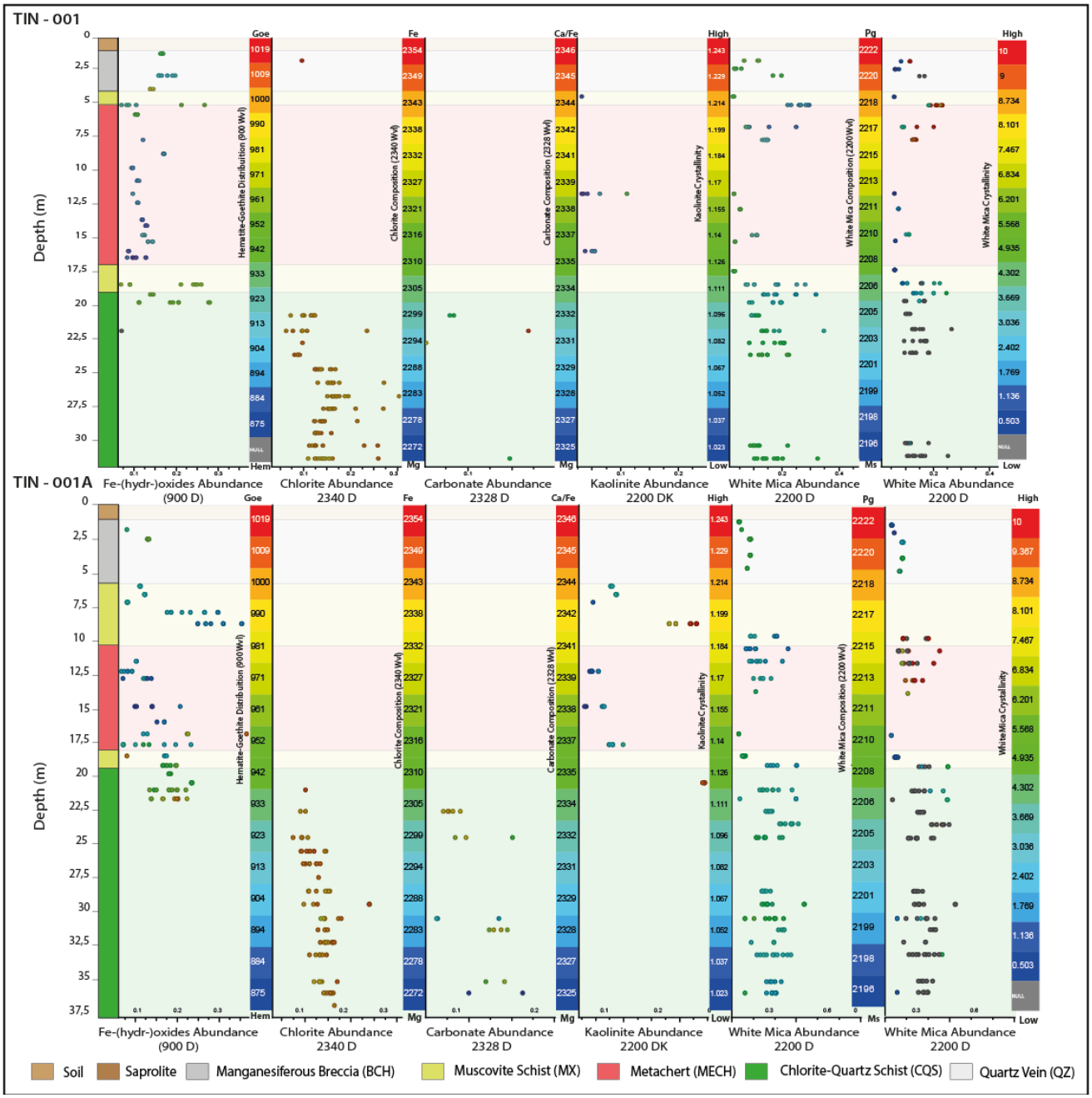

Figure 33: Scatter Plots showing how abundance and mineral composition vary with the depth of TIN-001 and TIN-001A drill cores.

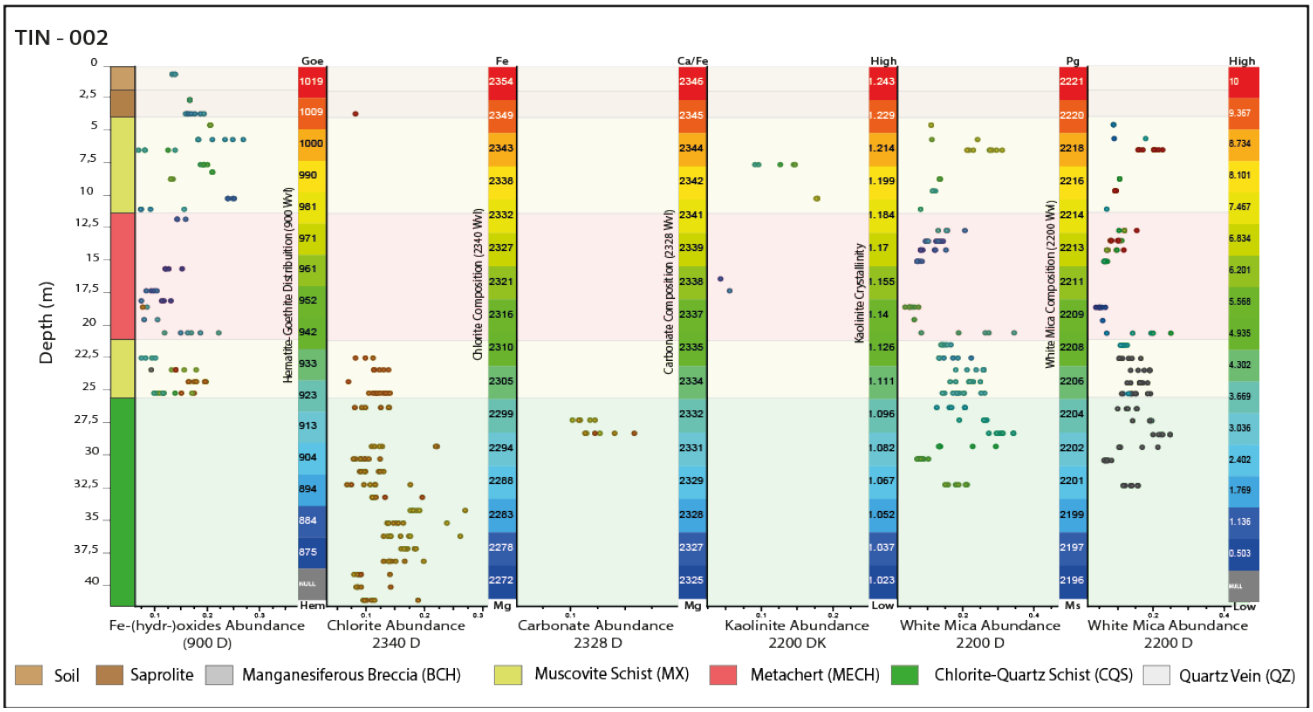

Figure 34: Scatter Plots showing how abundance and mineral composition vary with the depth of TIN-002 drill core.

The minerals of the groups of iron oxides and hydroxides in the metachert (TIN-001, TIN-001A and TIN-002) are predominantly composed of hematite, with an intermediate composition at some levels. The kaolinite has low crystallinity and occurs locally, while the white mica has high crystallinity (50) and tends to muscovite. Iron oxides and hydroxides have a hematite and goethite mixed composition (TIN 004), and, occasionally, a Fe-chlorite occurrence (TIN06). The spectral data on chlorite-quartz schist (CQS) reveals this is the only analyzed lithotype with abundant Fe-chlorite and calcite. Occasionally, white mica tending to muscovite was mapped. Quartz veins (QZ) have levels enriched in muscovite, and also altered by the hematite halo. Minerals from the iron oxide-hydroxide group (with intermediate hematite-goethite composition) and also minerals from the white mica group were mapped.

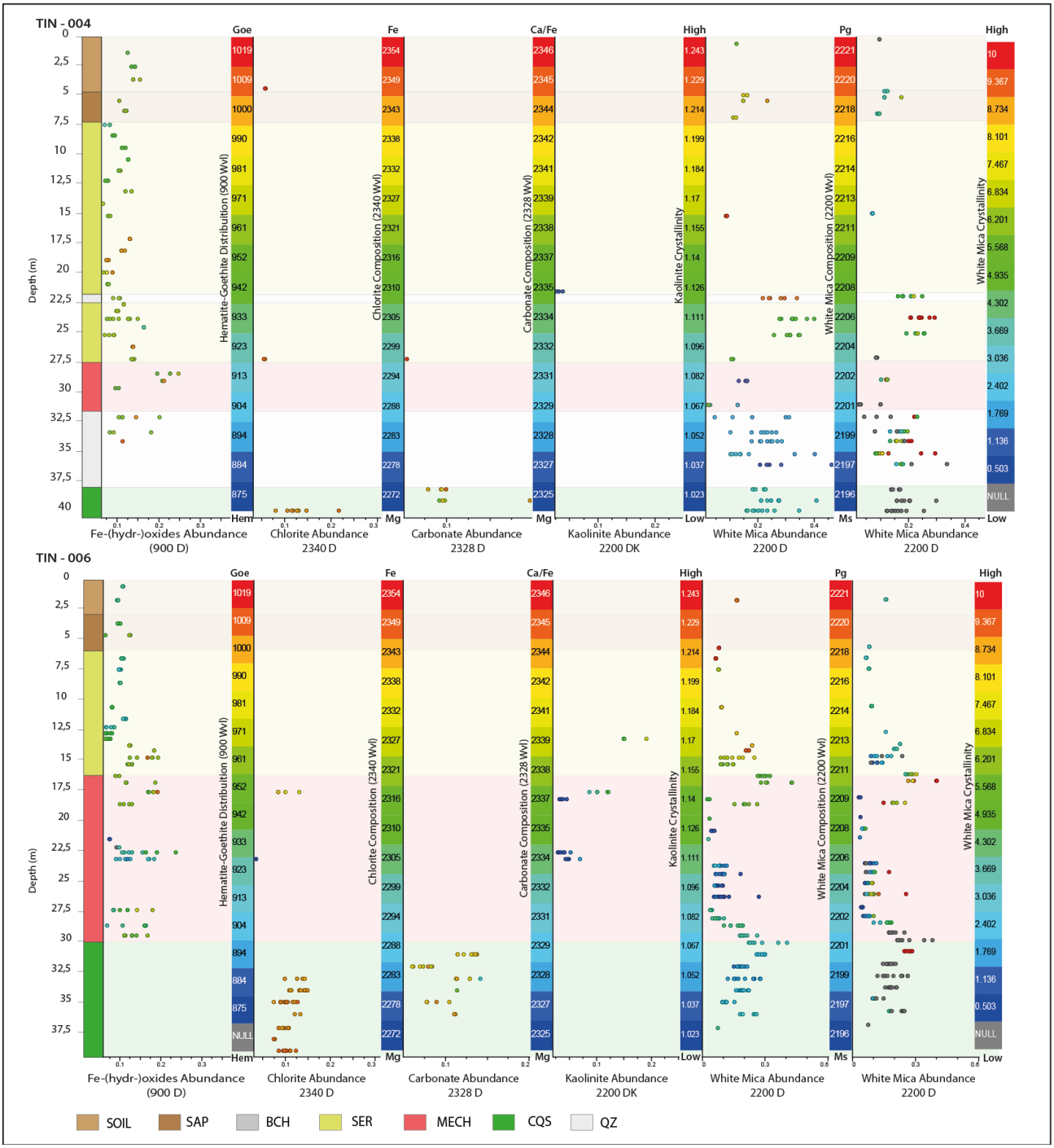

Figure 35: Scatter Plots showing how abundance and mineral composition vary with the depth of TIN-004 and TIN-006 drill cores.

4.2 Geochemical Data

The potential of the Tinteiro target was discovered from the results of geochemical soil sampling grids carried out by the Orinoco Gold Limited and later discussed in Campos *et al*. (2017). The samples from the North Tinteiro target have up to 50% of Fe and up to 10.25 ppm of Au. The gold mineralization shows a strong correlation with anomalous values of Fe, Cr, Ba, Ni (up to 2.05 ppm), and in some samples, Cu. Samples from the Central Tinteiro target have the highest contents of the

following elements: Au (23.9 ppm), Co (10,000 ppm), Cu (3,995 ppm), Mn (168,200 ppm), Ni (5,600 ppm), Pb (216 ppm) and Zn (2,580 ppm). These mineral contents do not appear to be spatially correlated, as they occur dispersed in the region. The Southeast Tinteiro domain has the highest occurrence of manganese breccias with the main anomalous contents of Ag (4.234 ppm) and Li (560 ppm), and also other relevant values for Ba, Co, Cu, Li, Mn, Ni, V and Zn. The soil samples from the South Tinteiro target indicate content up to 59.3% Fe and 5.930 ppm V, as well as anomalous values of Ag, Ba, Co, Cu, Li and Mn.

The TIN-001, TIN-001A and TIN-002 drillholes were drilled in the target region of the Southeast Tinteiro whereas the TIN-004 and TIN-006 cores are in the target region of the Central Tinteiro. The rocks sampled in the process were sent for geochemical analysis to deepen the delimitation and correlation of these elements with anomalous contents, as well as to determine the dimensions of the mineralizations and hydrothermal alteration zones. Scatter plots were built to show how major and minor elements obtained by geochemical analysis of whole-rock vary with the depth of all drill cores studied. These graphs are shown in figures 36, 37, 38 and 39, the first two refer to major elements as oxides, and the following ones refer to minor elements selected based on their relevance in the system.

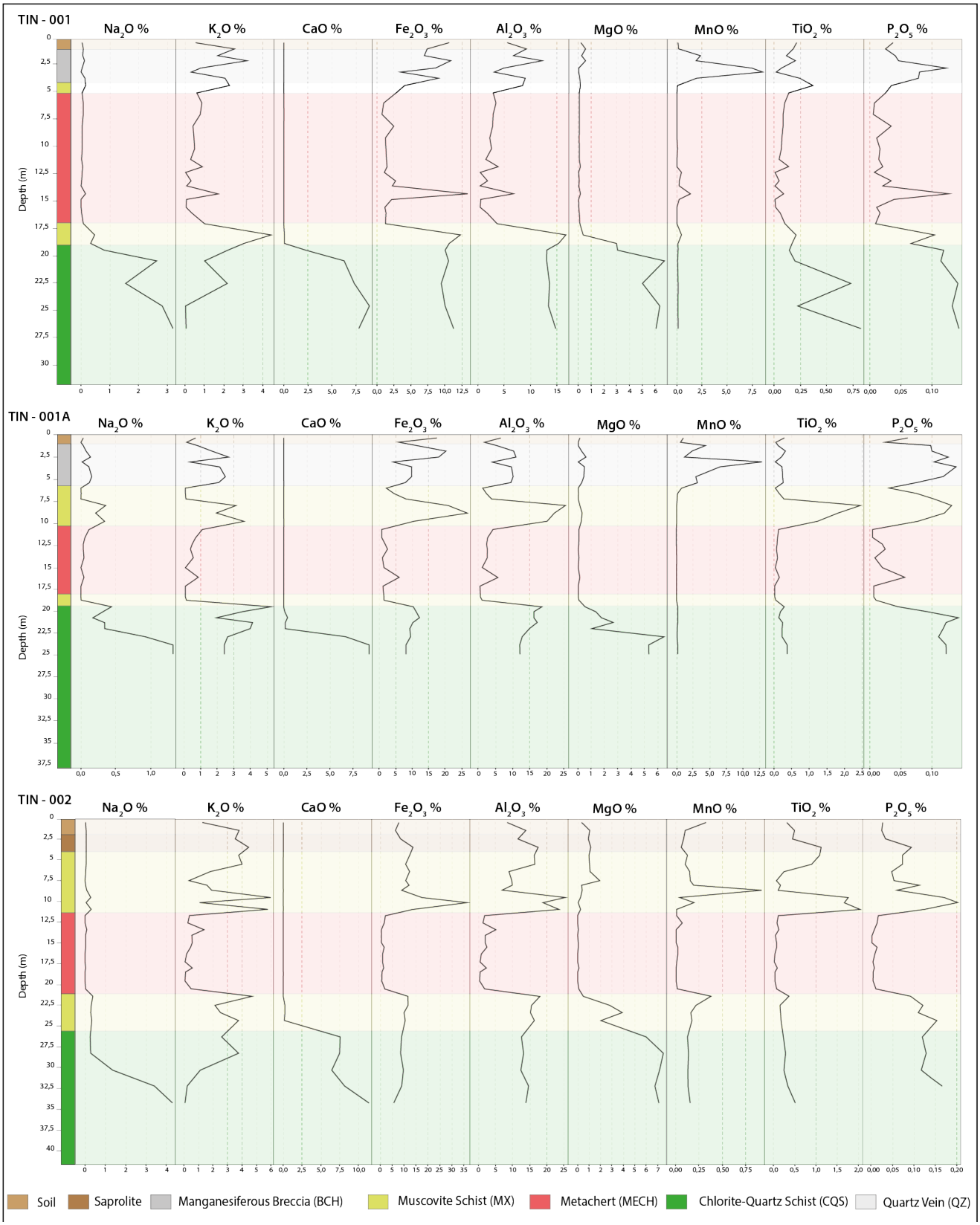

Figure 36: Chemical analysis of major elements from drillcores TIN-001 to TIN-002. Percent Na, K, Ca, Fe, Al, Mg, Mn, Ti and P oxides in the Southeast Tinteiro System.

Figure 37: Chemical analysis of major elements from drillcores TIN-004 and TIN-006. Percent Na, K, Ca, Fe, Al, Mg, Mn, Ti and P oxides in the Central Tinteiro System.

The major elements are found in greater abundance in the assemblage of minerals and rocks, reflecting what the petrography describes and are compatible with the Tinteiro system alterations: the Fe_2O_3 percentage is directly correlated with the hematite alteration, and the same is observed for the percentages of K_2O and Al_2O_3 regarding the muscovite-rich alteration.

The samples collected in the most superficial levels of soil and saprolite exhibit average contents of 10 to 15% Fe_2O_3, 5 to 15% Al_2O_3, 2 to 5% K_2O, and 1 to 2% MgO. The manganese breccia unit (BCH) has the highest contents of MnO ranging from 2.5 to 12.5% and Fe_2O_3 from 5 to 20%. These contents and those of Al_2O_3 and K_2O (5 to 13% and 1 to 3%, respectively) agree with the mineralogical assemblage described in the petrography. The unaltered metachert (MECH) is marked by low percentages of other elements since it is mostly composed of quartz. Thus, it is also the best unit/element to map the hydrothermal alteration zones, reaching up to 35% Fe_2O_3, and 25% Al_2O_3 is in the TIN-002 drillhole. Muscovite schist (MX) has high K_2O (2 to 7%) and Al_2O_3 (10 to 20%) and

when intercepted by hematite alteration levels, it also shows anomalous Fe_2O_3 values (5 to 10%). Chlorite-quartz schist (CQS) has the greatest chemical contrast among the analyzed rocks, the elements that best distinguish this unit are CaO (5 to 10%), MgO (5 to 7%), and Na_2O (up to 4 %) since they are practically absent in all other lithologies. Levels intercepted by quartz veins (QZ) present low values of practically all elements, except for mica rich domains.

The minor elements were chosen based on their abundance and relevance to the system. The maximum value obtained for Au was 1.07 ppm in sample 002/13 from the TIN-002 core. The rest of the samples showed, on average, values lower than 0.10 ppm, as indicated at the beginning of this item/section, the highest levels of gold were found in soil and outcropping rocks scattered over the targets of the Tinteiro system.

The mineralized zone, is where the highest Ba, Li, Co, Ni and Zn levels are concentrated. Barium concentrations reach up to 10,000 ppm, lithium up to 300 ppm, cobalt up to 2,500 ppm, nickel up to 1,500 ppm and zinc up to 200 ppm. The more superficial levels of soil and saprolite, due to supergenic enrichment, sporadically present anomalous contents regarding the background of certain elements, such as Ag (up to 40 ppm), Co (300 ppm), and Li (50 ppm). In the other units, the chemical contents are mainly controlled by the proximity between their contacts, allowing to identify traces of the Tinteiro system acting on the enclosing rocks. At these levels, there are anomalous levels of Ag (200 ppm), Ba (2,200 ppm), Li (80 ppm), Co (100 ppm), Ni (1,500 ppm), Cr (2,200 ppm), As (1,000 ppm), Zn (150 ppm), which coincide with the hematite alteration zones. And the chlorite-quartz schist unit presents As, Cu, Li and Ba anomalies associated with the levels where sulfides and magnetite are present.

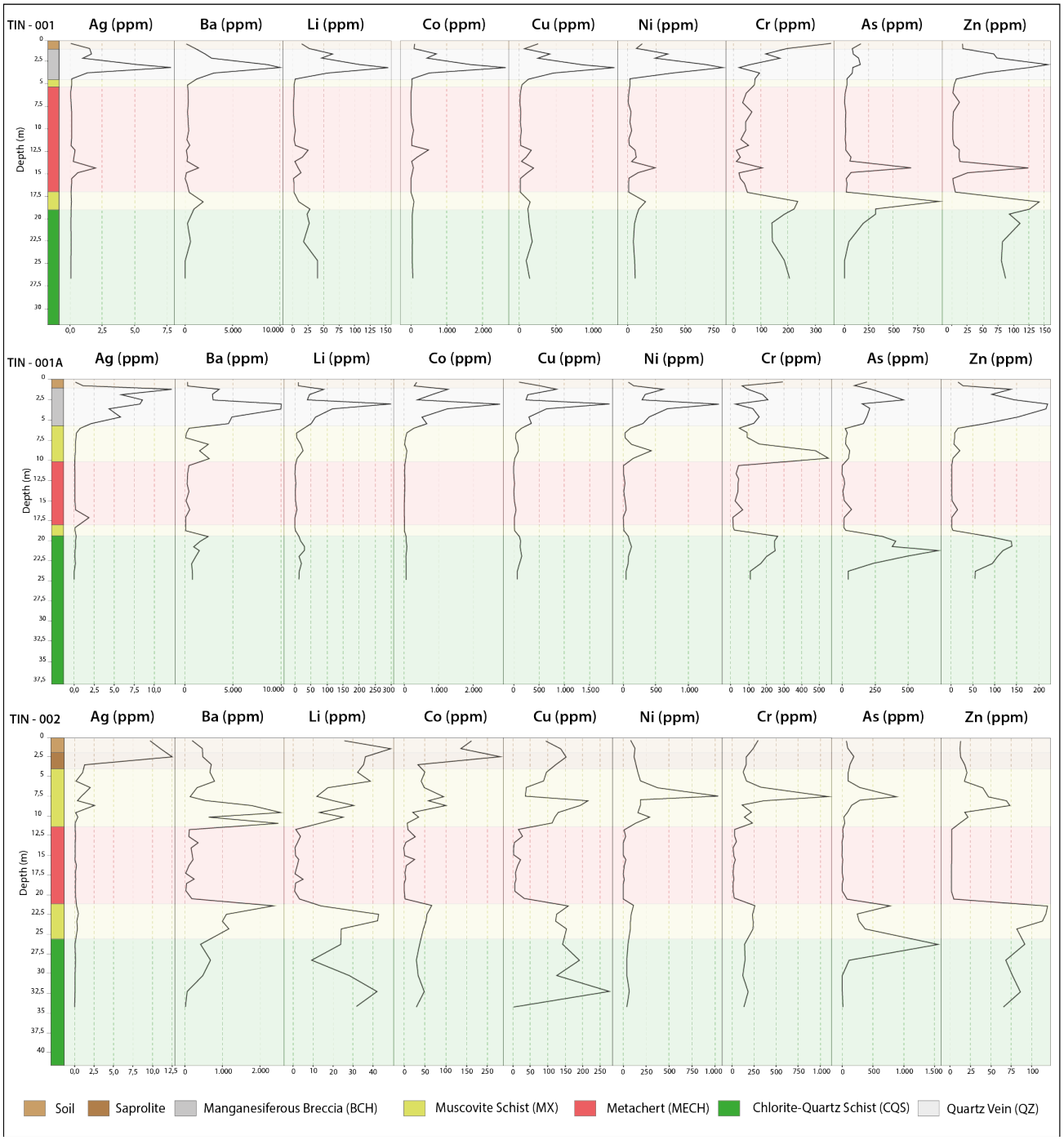

Figure 38: Chemical analysis of minor elements from drillcores TIN-001 to TIN-002 (Southeast Tinteiro). Characterization in ppm of the following elements: Ag, Ba, Li, Co, Cu, Ni, Cr, As and Zn.

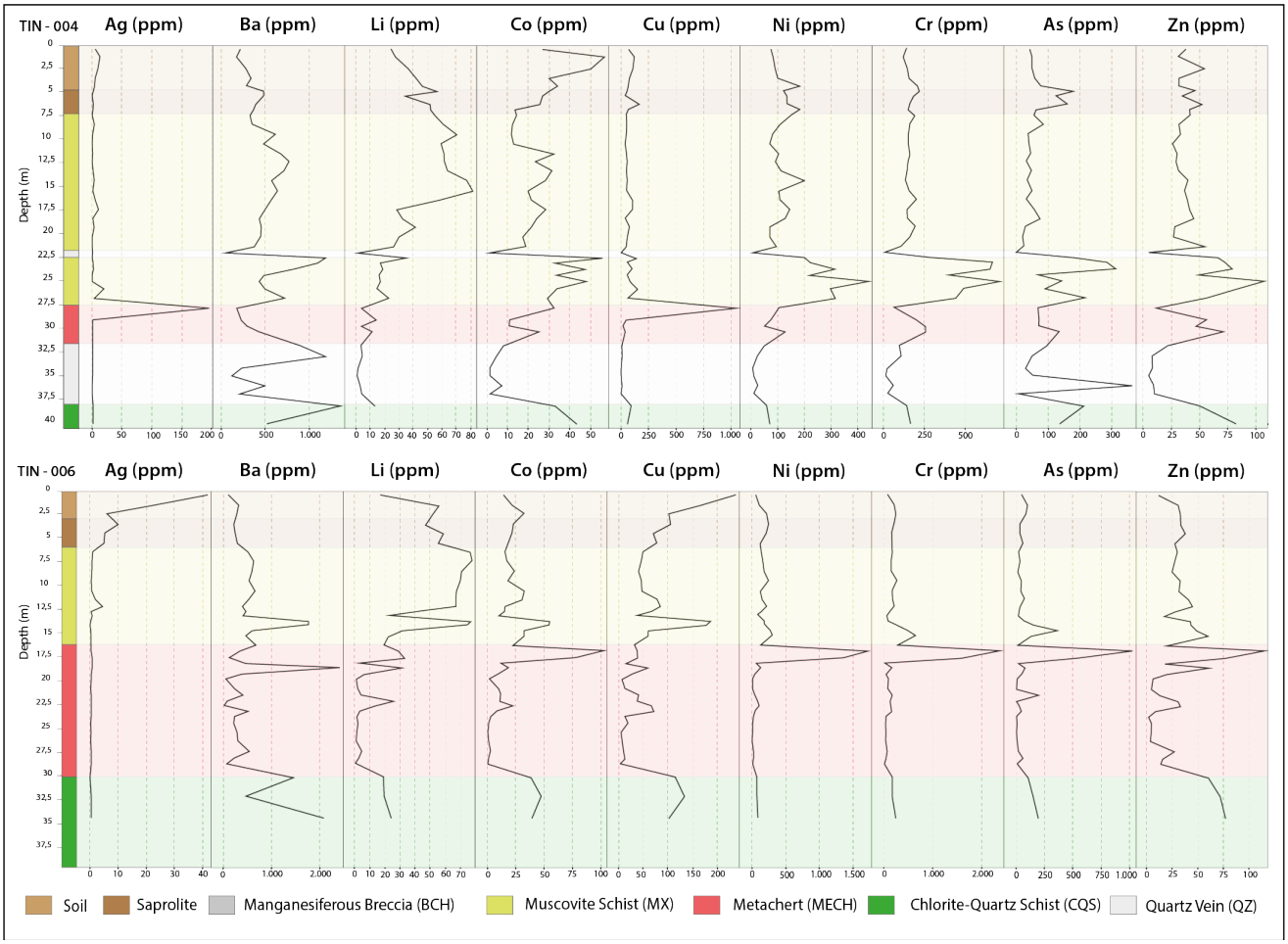

Figure 39: Chemical analysis of minor elements from drillcores TIN-004 and TIN-006 (Central Tinteiro). Characterization in ppm of the following elements: Ag, Ba, Li, Co, Cu, Ni, Cr, As and Zn.

4.3 Physical Properties of Rocks

The behavior of rock physical properties is directly associated with their mineralogical assemblage features, textures and structures. Therefore, this analysis is relevant for mineral exploration, since it serves as a parameter when interpolated to airborne data and derivative, and it is also a very effective tool to individualize geological units and their respective hydrothermal alteration zones. This work concentrates on analyses directed to two physical properties: magnetic susceptibility and density.

4.3.1 Magnetic Susceptibility

The magnetic susceptibility (MS) values of the analyzed samples vary between 0.016 and 67.633x10^{-3} SI. Table 3 shows the mean, median, minimum, maximum and range MS values and the total number of samples (count) for all analyzed units. Figure 40 presents strip log graphs of MS versus the depth of all sampled drillcores, and figure 41 is a boxplot of all units and their properties illustrating the statistical relationships shown in table 3.

Table 3: Maximum, minimum and mean magnetic susceptibility values of the main lithologies analyzed in the drillholes.

	SOIL/SAP	BCH	MECH	MX	CQS	QZ
Mean (SI)	1.642×10^{-3}	0.524×10^{-3}	0.182×10^{-3}	0.236×10^{-3}	4.23×10^{-3}	0.297×10^{-3}
Median (SI)	0.855×10^{-3}	0.421×10^{-3}	0.074×10^{-3}	0.224×10^{-3}	0.719×10^{-3}	0.079×10^{-3}
Range	8.725	1.634	2.675	0.778	67.553	1.503
Minimum (SI)	0.185×10^{-3}	0.016×10^{-3}	0.015×10^{-3}	0.019×10^{-3}	0.077×10^{-3}	0.007×10^{-3}
Maximum (SI)	8.91×10^{-3}	1.65×10^{-3}	2.69×10^{-3}	0.797×10^{-3}	67.63×10^{-3}	1.51×10^{-3}
Sample Count	21	12	60	62	63	7

The highest MS value (67.633×10^{-3} SI) was obtained from a sample of the chlorite-quartz schist unit (CQS), with abundant euhedral magnetite crystals. The wide range of values in this unit is due to the very well-defined levels containing the ferromagnetic mineral. The soil and saprolite levels also exhibit higher MS values, an average of 1.642×10^{-3} SI, compared to other lithologies. Samples of manganesiferous breccia (BCH) with preserved sulfide crystals, may have MS values up to 1.650×10^{-3} SI, and an average of 0.524×10^{-3} SI.

The remaining units (MX, MECH and QZ) consist mostly of either quartz or phyllosilicates, which are mostly diamagnetic, with mean values ranging from 0.182 to 0.297×10^{-3} SI, the lowest MS values determined.

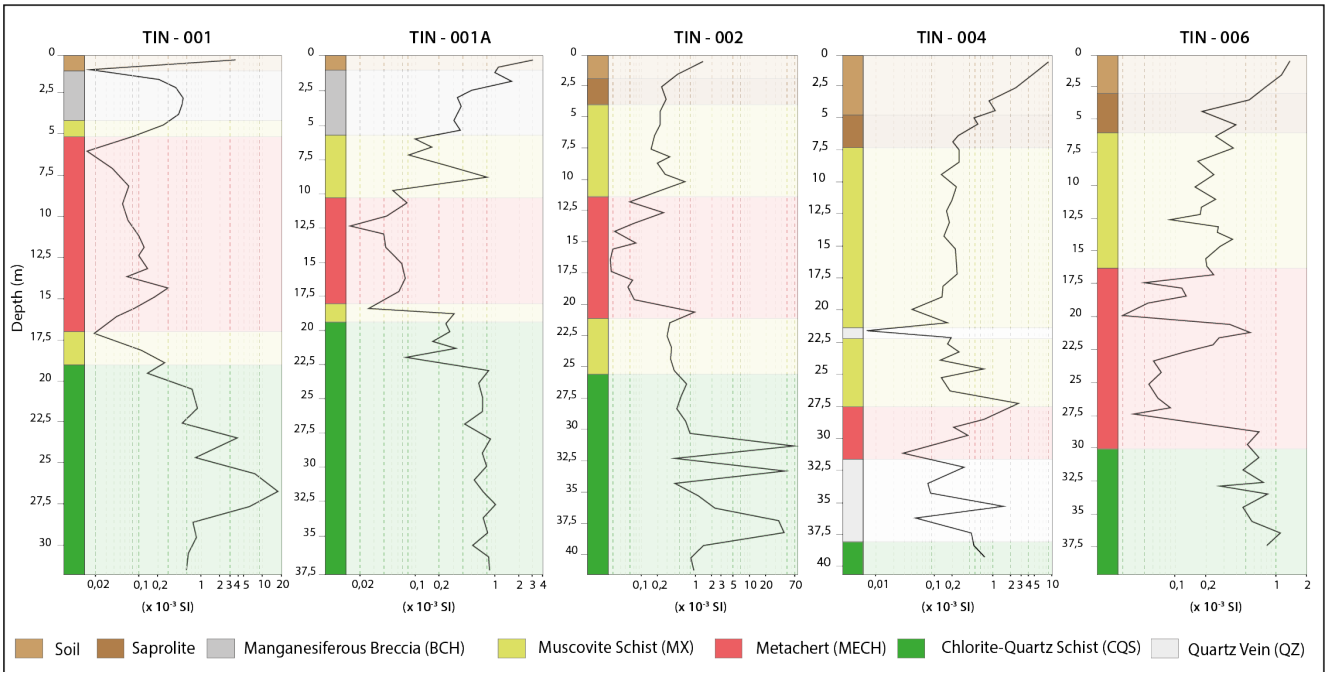

Figure 40: Strip log of magnetic susceptibility for the lithologies intercepted by drill holes TIN-001 to TIN-006.

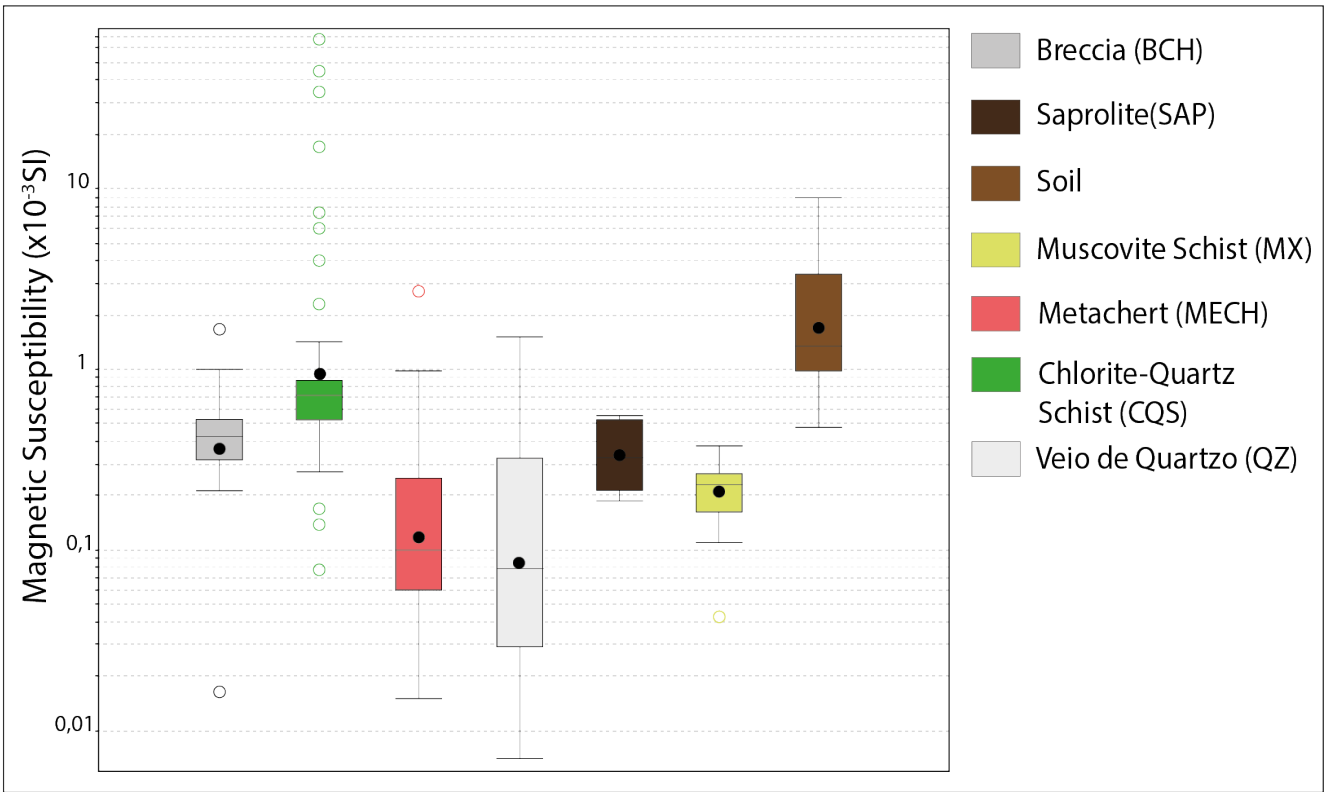

Figure 41: Box plot showing the magnetic susceptibility measurement ranges, averages and outliers of each studied unit of the TIN drillcores.

4.3.2 Density

Rock density, defined as the mass to volume ratio, is directly influenced both by the mineral paragenesis that makes up the lithology and by its structures, whether primary (porosity) or secondary

(foliation, fracturing, weathering, etc.). The rock density was determined in consolidated rock samples using a hydrostatic balance to determine first the weight of dry samples, and subsequently, after submersion in water, to calculate sample natural density (Hinze, 2013). However, because part of the samples collected for this study are unconsolidated due to supergenic processes and the lithological texture itself, their density was determined by another method, using the pentapycnometer. In this case, as there are no longer primary or secondary textural features preserved in the samples, the result is based only on the density of the minerals that compose them and configure the absolute density (Hinze, 2013).

Tables 4 and 5 present the mean, maximum and minimum values, and median of the measured density. Table 4 refers to consolidated samples, determined by the hydrostatic balance while table 5 refers to the friable material sampled, determined by the pentapycnometer method. The strip log graphs show the density versus depth of the drillholes. Figure 42 shows the results of the consolidated samples for all five drillcores. Figure 43 shows the results of the unconsolidated samples for four drill cores, except for TIN-001, which had very few samples and was not included in the graph. Figure 44 shows two box plot graphs for both methods used to illustrate the density behavior of the studied samples. The density values range from 1.61 to 2.93 g/cm^3 for the hydrostatic balance method and from 2.69 to 3.37 g/cm^3 for the pentapycnometer method. The absolute density is always higher (or at most equal) since it is assumed that there are no empty spaces and/or filled by other materials (liquid, gases, or both), which consequently entails lower values.

Table 4: Density obtained by the hydrostatic balance method for the studied lithologies.

	BCH	MECH	MX	CQS	QZ
Mean	2,21 g/cm^3	2,56 g/cm^3	2,25 g/cm^3	2,7 g/cm^3	2,63 g/cm^3
Median	2,31 g/cm^3	2,58 g/cm^3	2,32 g/cm^3	2,74 g/cm^3	2,65 g/cm^3
Range	0,81	0,62	1,16	0,76	0,51
Minimum	1,74 g/cm^3	2,19 g/cm^3	1,61 g/cm^3	2,11 g/cm^3	2,42 g/cm^3
Maximum	2,55 g/cm^3	2,81 g/cm^3	2,77 g/cm^3	2,87 g/cm^3	2,93 g/cm^3
Count	7	45	30	61	7

Table 5: Density obtained by the pentapycnometer method for the studied lithologies.

	SOIL/SAP	BCH	MECH	MX	CQS
Mean	2,79 g/cm^3	2,89 g/cm^3	2,74 g/cm^3	2,84 g/cm^3	2,81 g/cm^3
Median	2,79 g/cm^3	2,87 g/cm^3	2,72 g/cm^3	2,81 g/cm^3	2,81 g/cm^3
Range	0,19	0,33	0,19	0,66	0,01
Minimum	2,72 g/cm^3	2,78 g/cm^3	2,69 g/cm^3	2,71 g/cm^3	2,8 g/cm^3
Maximum	2,9 g/cm^3	3,11 g/cm^3	2,88 g/cm^3	3,37 g/cm^3	2,81 g/cm^3
Count	21	6	15	38	2

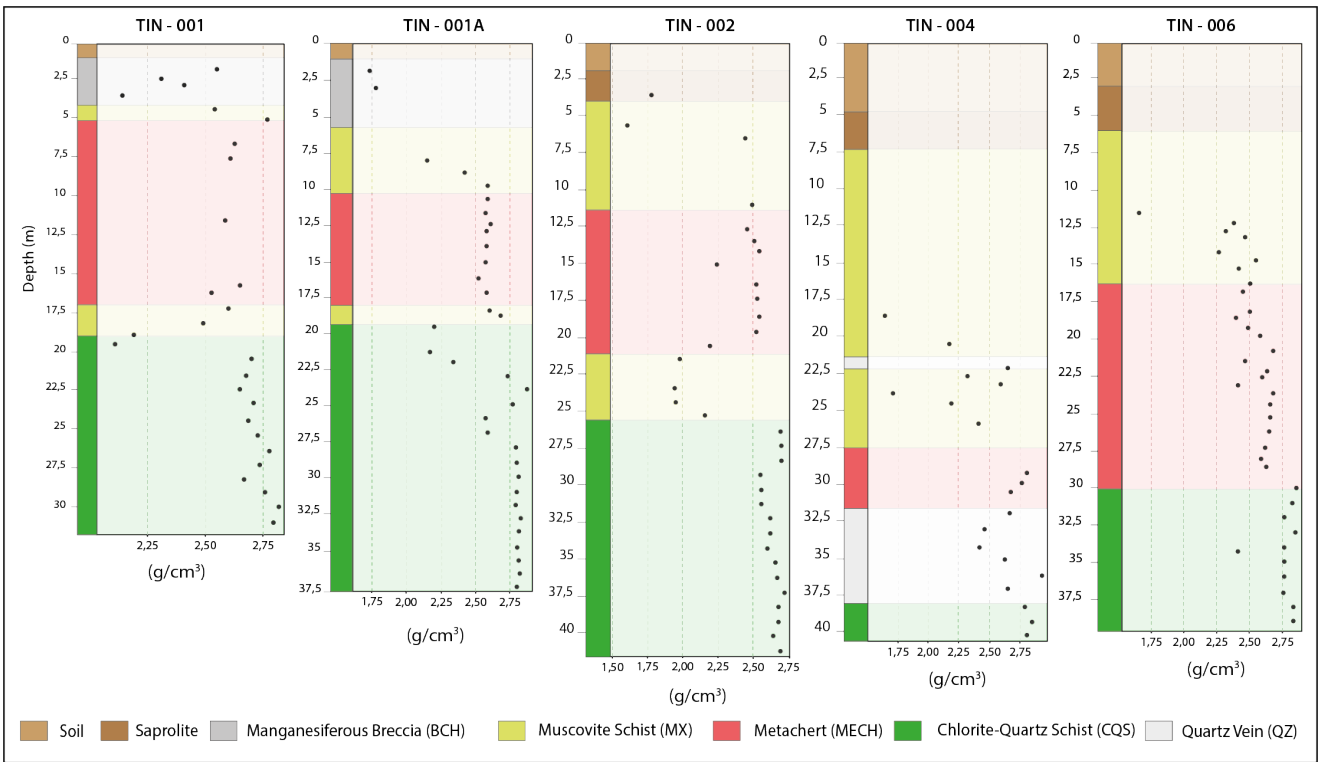

Figure 42: Strip logs of the lithological sections of the TIN-001, TIN-001A, TIN-002, TIN-004, and TIN-006 cores, and respective density values versus the drillhole depth (m).

The manganese breccia (BCH) has an average natural density of 2.21g/cm^3 and an average absolute density of 2.89g/cm^3. This anisotropic unit is very fractured with levels with many quartz fragments and quite weathered, which generates varied results. These factors result in low density, despite having the highest mean absolute density of the analyzed samples. Muscovite shale (MX) behaves similarly to BCH, since it is also a very friable rock, with a mineral framework consisting of not very resistant and dense phyllosilicates. The metachert (MECH) consists practically of only quartz, but as it is a very porous rock, the average density of 2.56 g/cm^3 can fluctuate in the most altered levels where sericite and/or hematite are observed. The average absolute density of 2.74 g/cm^3 is close to that of the mineral quartz (2.7 g/cm^3).

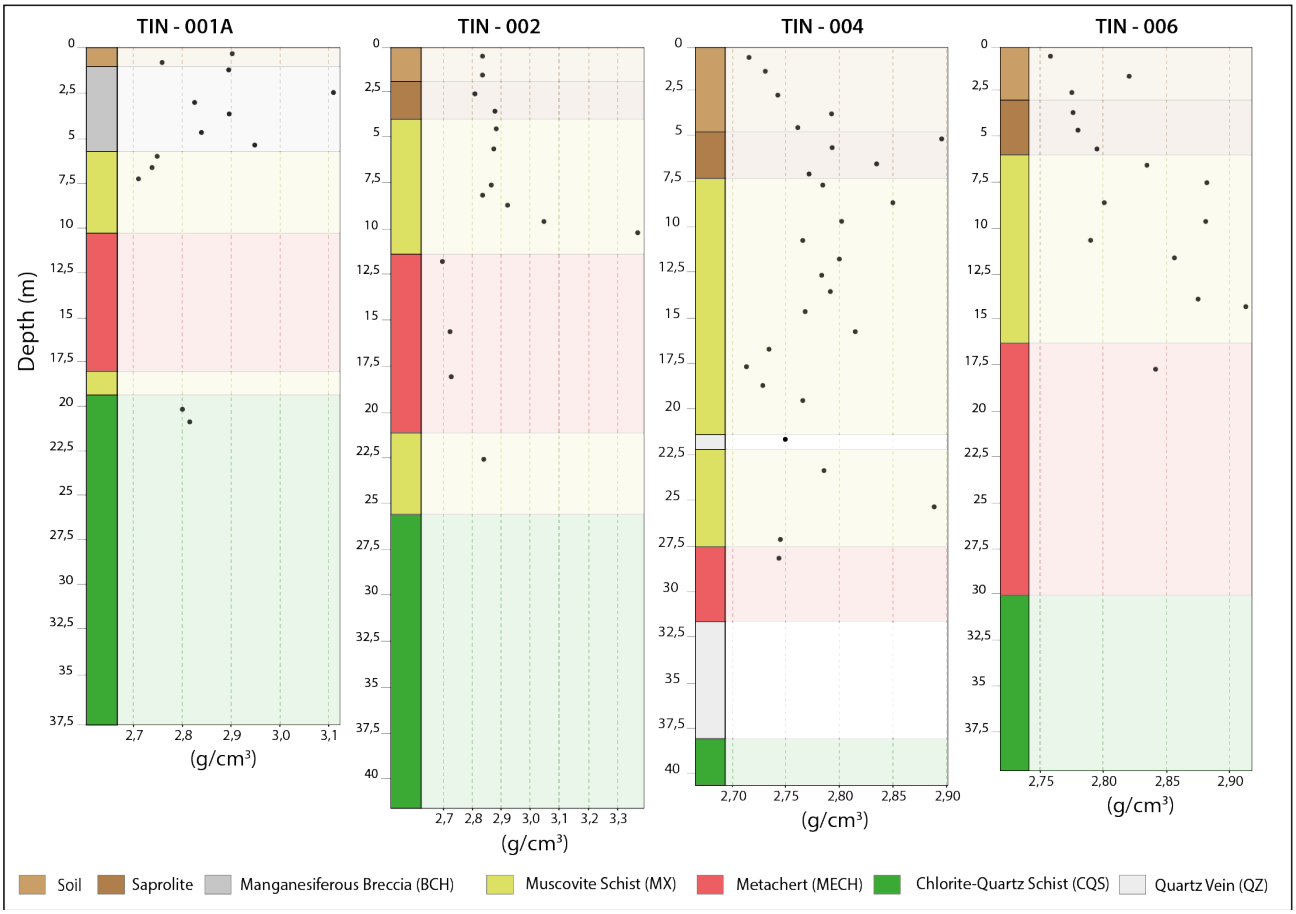

Figure 43: Strip logs of the lithological sections of the TIN-001A, TIN-002, TIN-004 and TIN-006 cores, and respective mineral density values versus drillhole depth (m).

Chlorite-quartz schist occurs in the deepest portions of the drillcores studied, and, consequently, is very little altered by the supergenic interaction. Additionally, this rock is very compact with dense minerals (oxides and sulfides) in the composition, and the highest average density (2.7g/cm^3) of the studied samples. Similar to the chlorite-quartz schist, the density of rocks in the quartz vein levels (QZ) is also high since these levels are isotropic, massive and not weathered.

Compared to the magnetic susceptibility values, it is noteworthy that the density values vary much less because they are physical parameters measured in different orders of magnitude. Figure 45

presents a scatter plot of magnetic susceptibility versus density of the analyzed rocks for each unit. It should be noted that both parameters individualize two units in different zones with high precision: the metachert (MECH) and the chlorite-quartz schist (CQS), whereas the other units are more dispersed in the chart.

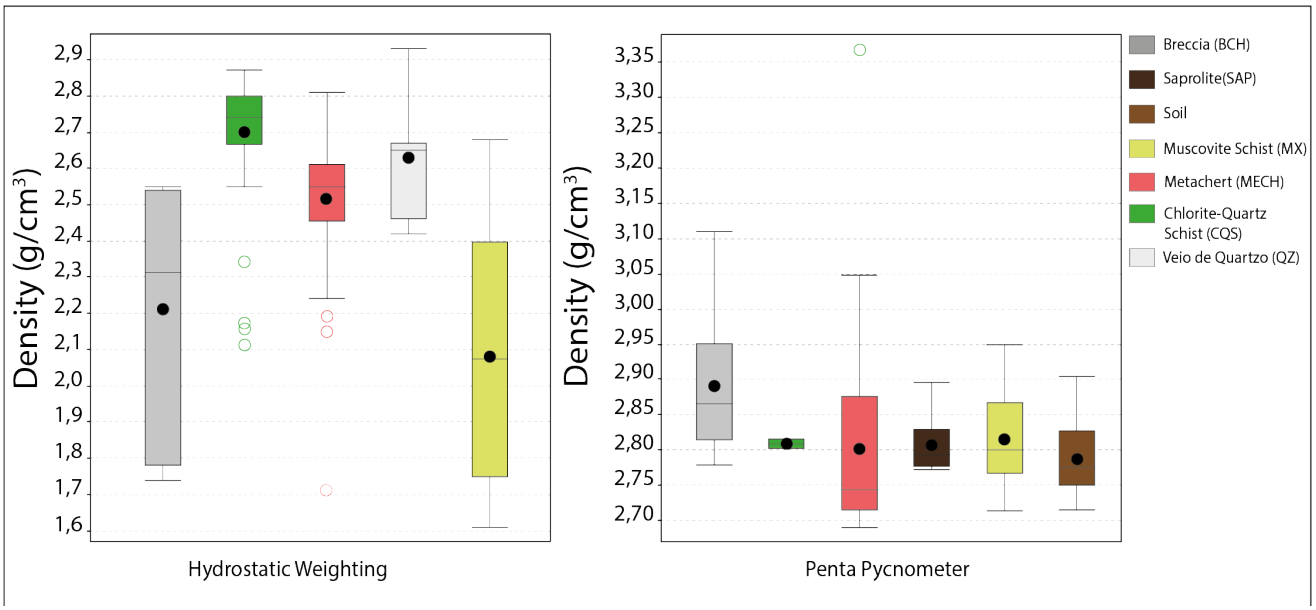

Figure 44: Box plot illustrating the measurement ranges, averages and outliers for density and mineral density of each unit found in the drillcores.

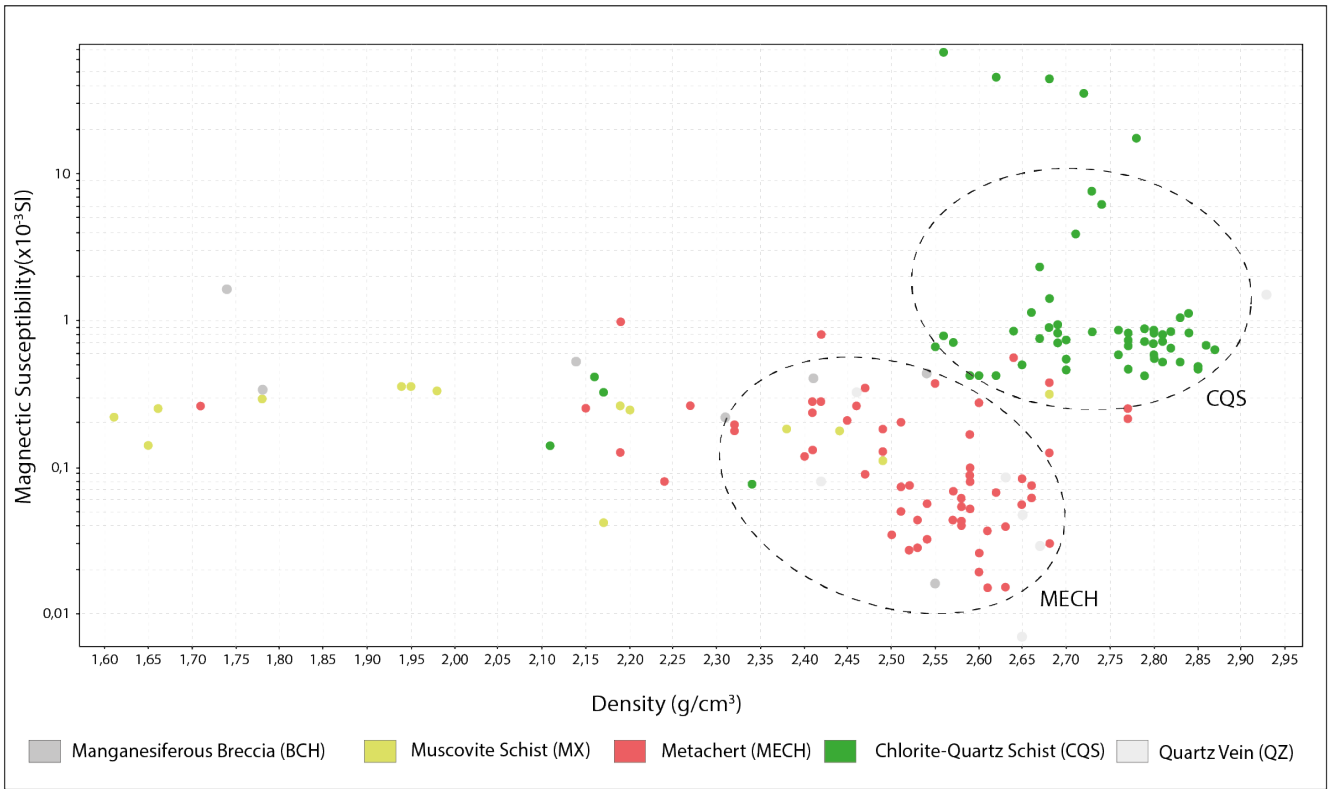

Figure 45: Diagram of magnetic susceptibility versus natural density of the studied rocks. The chlorite-quartz schist (CQS) and metachert (MECH) are predominantly found in the two domains marked by the circles.

5. Discussions

The Tinteiro system polymetallic mineralization in the area of the TIN-001 to TIN-006 drillholes was defined by manganesiferous breccia (BCH) occurences with various mineral phases in its composition that were identified by the various analytical methods used. The TIN-001A/5 sample (Figure 18) was chosen as the best representative of this rock and characterized by optical petrography and X-ray diffraction (Figure 21) in this study, as well as mineral chemistry analysis in Campos *et al*. (2017). The paragenesis of manganese oxides and hydroxides found is common to weathering systems, supergene enrichment, and low-temperature hydrothermal systems (Mota Silva *et al*., 2012). This paragenesis is represented by the following low crystallinity minerals: Lithiophorite $(Al,Li)MnO_2(OH)_2$, Hollandite $[(Ba(Mn_6Mn_2)O_{16})]$, Romanechite $[(Ba,H_2O)_2(Mn,Mn)_5O_{10}]$ and psilomelane $[(Ba,H_2O)_2Mn_5O_{10}]$. Post (1999) discusses the abundant variety of manganese oxides and hydroxides, attributing it to the fact that Mn occurs naturally in three oxidation states: +2, +3, and +4. This factor gives rise to a very wide range of valence phases and also great diversity in atomic architecture that can easily accommodate a whole range of other metallic cations. Manganese is a common element in most geological systems, and it can form minerals under the most varied chemical and temperature conditions.

Lithiophorite is a manganese and lithium hydroxide, commonly found in paragenesis with the mineral asbolane (cobalt and manganese hydroxide, in which cobalt can be replaced by nickel) since both are low-temperature hydrothermally altered Mn minerals with the same structure, and can coexist in mixed particle forms such as clay minerals, in layers (Post & Appleman, 1994). Whole-rock geochemistry shows that these samples have high MnO (12.9%), Co (2,790 ppm), and Ni (1,460 ppm). Chemical analysis of lithiophorite grains shows that the lithium content can vary from 0.2 to 3% while transition metals Ni, Cu and Co are recurrent substitutes in its structure (Campos *et al*., 2017).

Hollandite is a basic Mn-oxide with Ba in the structure that can be replaced by K, Pb, and Na. These minerals can compose important phases in oxidized zones of manganese deposits and are typically found forming masses of fibrous crystals compacted in aggregates of botryoidal habit (Post, 1999). Romanechite is found in circumstances close to hollandite, also in botryoidal masses in oxidized zones of manganese-rich deposits (Turner & Post, 1988). Post (1999) points out that these two minerals commonly intergrow in a very fine scale, in which both crystallochemical structures are interconnected by octahedral double chains whereas romanechite transforms into hollandite above 550°C. Psilomelane is commonly found in mineral paragenesis of oxidized-type manganese deposits, such as the Chiatura deposit in Georgia (Sasmaz *et al*. 2020) and in the Odisha state, India (Bhoja *et al*., 2021). Based on mineral chemistry analysis, Campos *et al.* (2017) concluded that part of the goethite found in this

system results from the oxidation of preexisting arsenopyrite crystals. The mineral mapping of the samples also showed that iron oxides and hydroxides have an intermediate composition between goethite and hematite whereas the white mica group minerals have an intermediate composition between muscovite and phengite, with a high degree of crystallinity.

However, the comparative analysis between spectral and geochemical data requires a lot of attention due to the methodological contrasts of the techniques, since the first performs a partial scan of the sample, that is, it only analyzes its surface (qualitative result) and the second performs the chemical characterization (quantitative result) of a volumetric sample of up to 10 cm^3. Nevertheless, the interpolation of these parameters allowed to differentiate very relevant patterns that reflect even mineralogical variations in the samples (Figure 46). Samples with higher Fe content (>15%) were interpreted as hematite (from 880 to 940 nm) by reflectance spectroscopy. The identified members of the white mica group are muscovite (2196 nm to 2208 nm) and phengite (2216 nm to 2222 nm) and were compared with the MgO, Al_2O_3 and K_2O percentages. In all graphs, the samples with phengite present at least above 1% of these elements whereas those with muscovite have a much wider range of contents. This result is predominantly because only muscovite schist samples were classified as phengite and, therefore, the chemical percentage result is homogeneous as it corresponds to only one of the studied lithotypes. For example, in samples with phengite and muscovite, the MgO content ranges from 1 to 2.5% and from 0 to 7%, respectively.

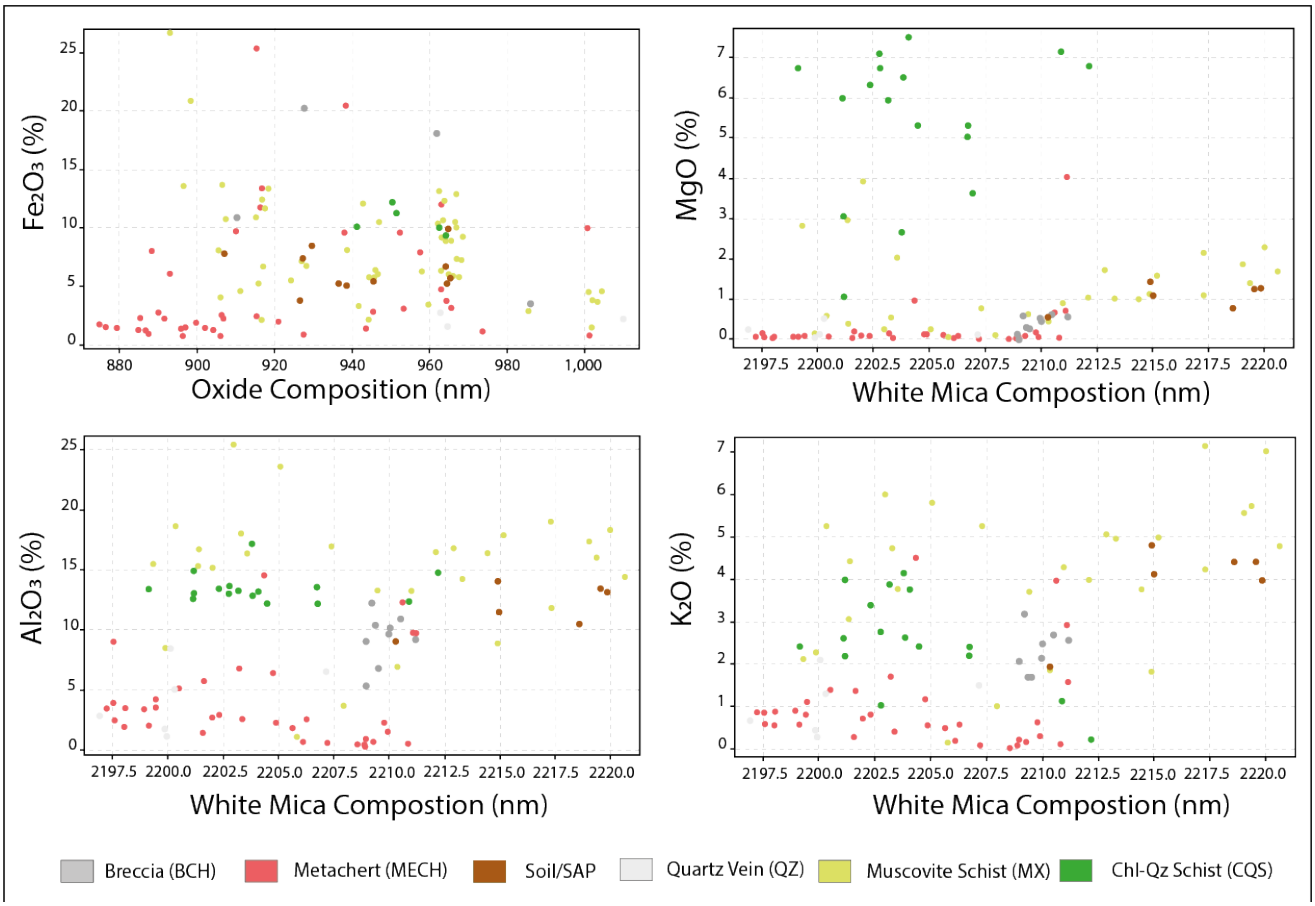

Figure 46: Scatterplots of reflectance spectroscopy versus whole-rock geochemistry. The composition of oxides/hydroxides is compared to Fe_2O_3, and the composition of white mica is compared to MgO, Al_2O_3 and K_2O.

The comparison of intervals with hydrothermal alteration traces of the manganese breccia shows conformity in the anomalous elements that contrast with the background, but even so, the values are discrepant, as if these levels were "trails" of the system with lower contents (Figure 47). The intervals, where hematite alteration with chemical traces of the mineralized zone occurs, have much lower MnO content (<1%) and no specific formation of manganese oxides and hydroxides, or the contents are below the detection level of the methods used.

The TIN-001A/27 sample was selected to characterize the hematite hydrothermal alteration zones using X-ray diffraction (Figure 31). Of the identified mineral phases, members of the smectite, kaolinite and chlorite groups stand out, in addition to iron oxides and hydroxides already discussed. Corrensite $[(Mg,Fe)_9((Si,Al)_8O_{20}(OH)_{10}.nH_2O]$ is a clay mineral of the smectite group that results from the transformation of saponite $[Ca_{0.25}(Mg,Fe)_3((Si,Al)_4O_{10})(OH)_2.nH_2O]$, submitted to temperatures from 80 to 300°C (Roberson *et al.,* 1999). Post (1984) reports that these minerals are common in clayey halos of hydrothermal alteration, probably an alteration product of dolomitic limestone, which acts as a source of Mg. Clinochlore $[(Mg, Fe)_5AlSi_3AlO_{10}(OH)_8]$ is an endmember of the chlorite group

minerals (Welch & Marshall, 2001), rich in Fe^{2+}, and common in environments of contact metamorphism, hydrothermal alterations, and regional metamorphism of mafic minerals.

The textural and positional arrangements between structures that overlap each other (Figures 23 and 24) confirm the late character of the Tinteiro system. On a larger scale, due to the deformation events of D_4, brittle structures are formed creating an intense system of hydraulic breccias and adjacent to this, an entire system of venulations and veins filled with hematite is formed and distributed/scattered in the rocks found in the Faina greenstone belt. The integration of the data compiled here allowed us to trace the main vectors that characterize the footprint of the Tinteiro system (Figure 47). Figure 48 also shows schematically the behavior of these vectors regarding the analyzed lithologies, ranging from distal (CQS) to proximal (MX), and mineralized zone (BCH).

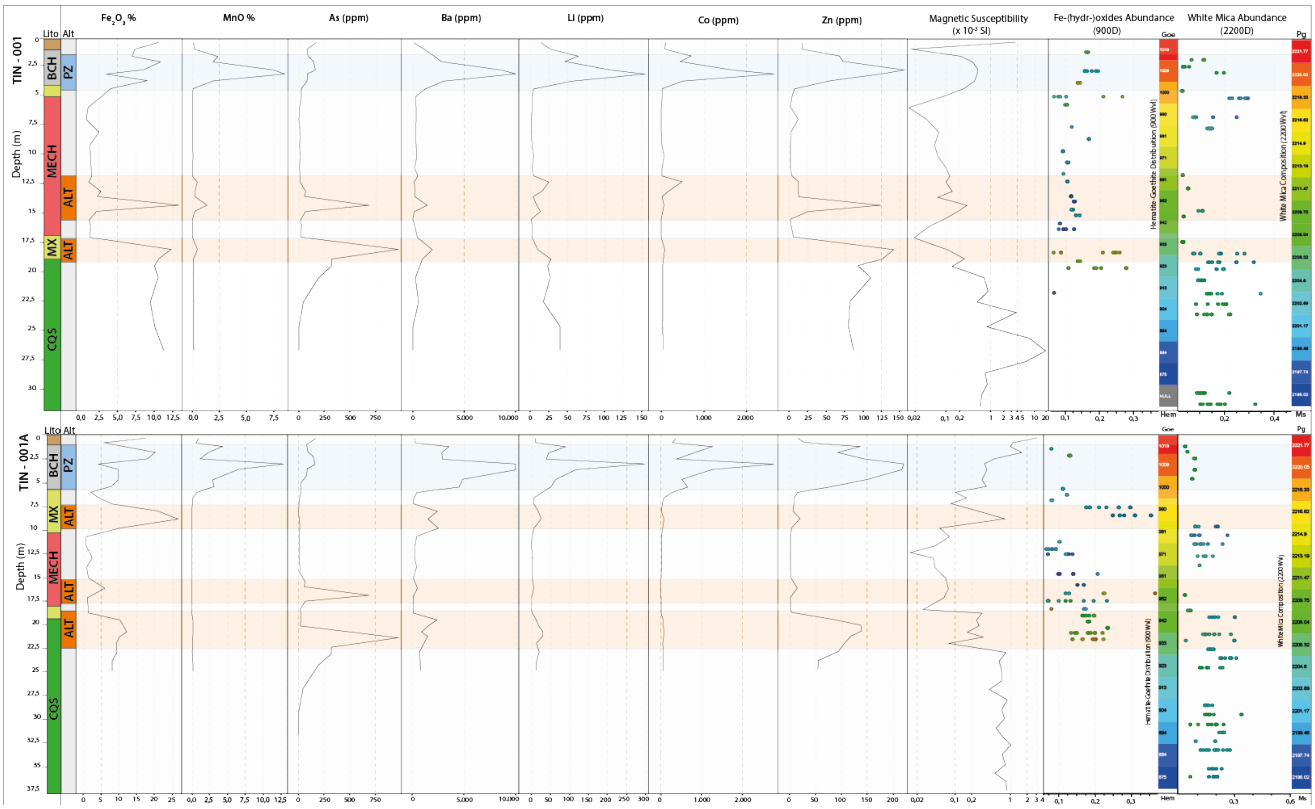

Figure 47: Lithological section reinterpreted according to the geochemical, petrophysical and spectral data that define the footprint of the Tinteiro system and the hematite hydrothermal alteration halo.

Chlorite-quartz schist (CQS) has the highest values of magnetic susceptibility, and after its occurrence, the demagnetization of rocks towards mineralization begins. This is the only lithology in which reflectance spectroscopy identified abundance of minerals of the chlorite and carbonate groups without brittle structures and deformations, having only magnetite and sulfides as indicators of tardi-tectonic events. The metachert unit (MECH) records the beginning of hematite and muscovite alteration occurrences that intensify towards mineralization. These more intense alteration levels are marked by peaks of anomalous values of pathfinder elements such as As, Zn, Cr, Ni and Cu. Muscovite

schist (MX) is the proximal unit of the mineralized zone and marks the increase of the absolute density values towards rock mineralization. On the other hand, the natural density decreases due to the increasing occurrence of brittle structures, which tend to generate breccia features and, consequently, empty spaces in the rocks. Crystallinity also increases (>10) in the members of white mica groups, whose intermediate composition is between phengite and muscovite. The mineralized lithology of manganese breccia (BCH) marks a drop in the abundance of iron oxides and hydroxides (<0.22) which is contrasted by the increase in manganese oxides and hydroxides. This unit is the most deformed and fractured by brittle structures, and also, because it is located in shallow pedological levels, the rocks are extremely affected by weathering action (Figure 48).

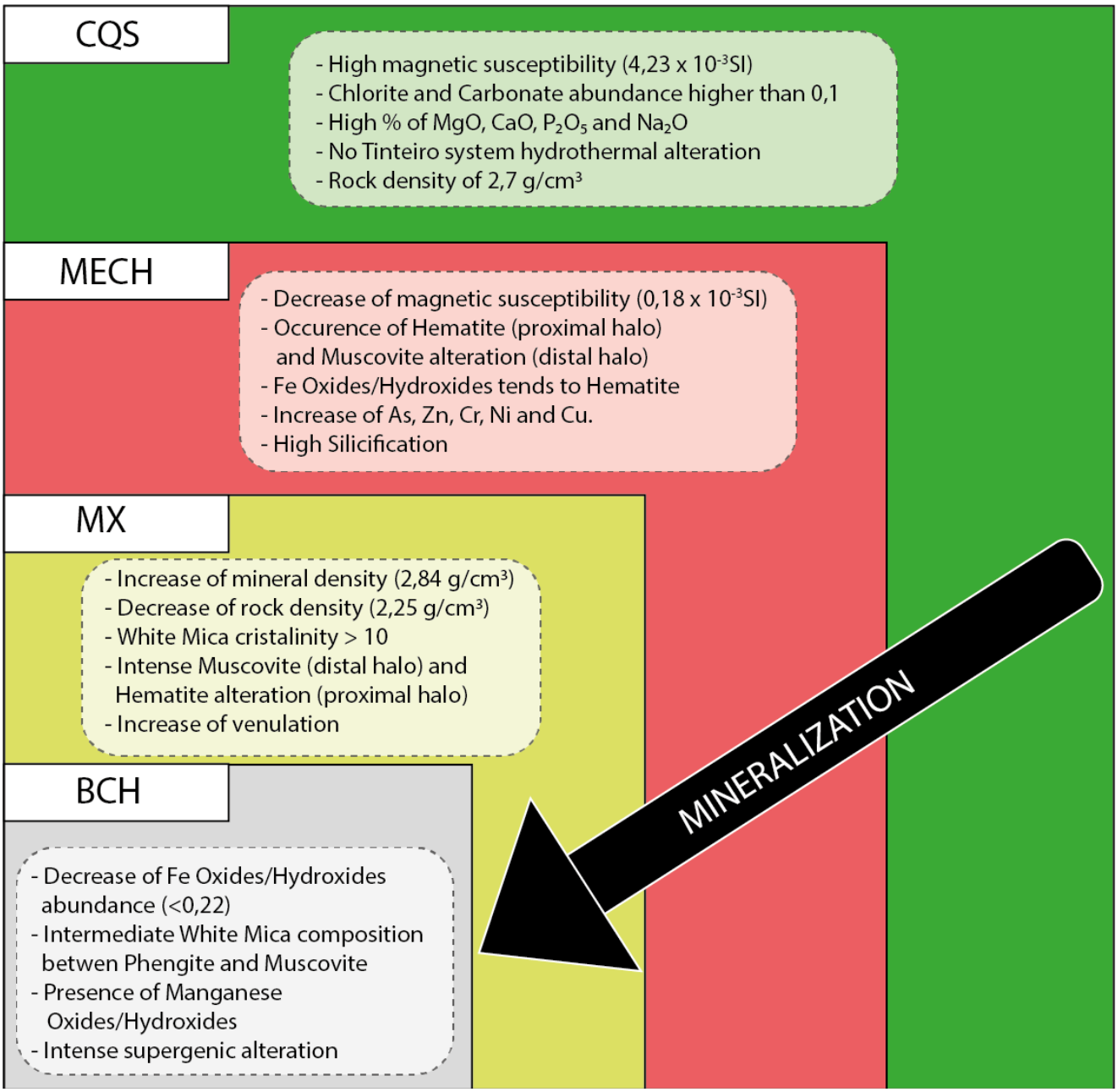

Figure 48: Schematic model of vectors that define the mineralization footprint of the Tinteiro system.

6. Conclusions

The methodological routine proposed in this work was based on the discoveries reported by the Orinoco Gold, and the publications by Campos *et al*. (2017) and Bogossian *et al*. (2020), who presented questions regarding the Tinteiro system and its polymetallic signature. Based on the already known geology and the availability of drillholes, systematic sampling was carried out aimed at applying several methods to produce a diverse database from various sources that can be applied in a follow-up stage and to define possible applications of new geophysical and geological methods to understand this system in greater depth. The integration of the applied methods allowed us to identify which techniques have the greatest affinity of responses with the system and to guide possible new discoveries in the Faina greenstone belt.

Therefore, the following conclusions are highlighted:

- The main characteristics of the Tinteiro system mineralized zone – the manganese breccia – are determined by a mineral paragenesis consisting of quartz, muscovite, hematite, goethite, psilomelane, romanechite, and hollandite. Reflectance spectroscopy indicates that iron oxides and hydroxides have an intermediate composition between goethite and hematite while the minerals of the white mica group have an intermediate composition between muscovite and phengite, with a high degree of crystallinity. Chemical anomalies up to 9% Fe_2O_3, 13% MnO, 2790 ppm Co, 10000 ppm Ba, 1890 ppm Cu and 1460 ppm Ni, average natural density and absolute density values of 2.21 and 2 .89 g/cm^3, respectively, and 0.524 x 10^{-3} SI magnetic susceptibility, were observed.

- The distal hydrothermal alteration halo, rich in muscovite, is quite pervasive and occurs subtly, marked by muscovite lamellae filling preexisting planes in the rocks, to exuberantly generating metric levels of muscovite schist intervals in the mineralization direction. This alteration interferes with the chemical composition of the rocks, and also reflects the drop in both natural density and magnetic susceptibility values.

- The proximal hydrothermal alteration halo, rich in hematite, also occurs in preexisting planes and structures in the rocks but intensifies in veins and venules that are discordant with the structure of the Paleoproterozoic foliation. This alteration carries small-scale chemical traces

of certain elements from the mineralized zone, and also presents anomalous Zn and As contents that behave as pathfinder elements of the system.

- In addition to the mineralized zone, the density and magnetic susceptibility results individualize/characterize effectively the lithotypes intercepted by the drillcores. The average natural density and magnetic susceptibility values are, respectively, 2.56 g/cm^3 and 0.182 x 10^{-3} SI for metachert; 2.7 g/cm^3 and 4.23 x 10^{-3} SI for chlorite-quartz schist; and 2.25 g/cm^3 and 0.236 x 10^{-3} SI for muscovite schist.

- Samples with higher Fe contents (>15%) showed a direct correlation with the abundance of minerals from the iron oxide and hydroxide groups analyzed by reflectance spectroscopy and are characterized by hematite (from 880 to 940 nm).

7. Acknowledgments

This study was financed in part by the Coordenação de Aperfeiçoamento de Pessoal de Nível Superior - Brasil (CAPES) - Finance Code 001. The author thanks CNPq for the master's scholarship, and also the Orinoco Gold Limited for allowing to publish this work and the support provided in the field stages. The author also thanks Prof. Álvaro Penteado Crósta of the IG/UNICAMP for loaning the TSG software license. A.M. Silva and C.L.B. Toledo are also grateful to CNPq for the research productivity grant.

Referências Bibliográficas

Beghelli Junior, L.P., 2012. Charnockitos e ortognaisses da porção centro-oeste do Bloco Arqueano de Goiás: Dados geoquímicos e isotópicos. Dissertação de Mestrado, Instituto de Geociências, Universidade de Brasília, 87 pp.

Borges, C. C. A., Toledo, C. L. B., Silva, A. M., Junior, F. C., Jost, H., & de Carvalho Lana, C. (2017). Geochemistry and isotopic signatures of metavolcanic and metaplutonic rocks of the Faina and Serra de Santa Rita greenstone belts, Central Brazil: Evidences for a Mesoarchean intraoceanic arc.Precambrian Research, 292, 350-377.

Bogossian, J., Hagemann S.G., Rodrigues V.G., Lobato L.M., Roberts M., 2020. Hydrothermal Alteration and Mineralization in the Faina greenstone belt: evidence from the Cascavel and Sertão orogenic gold deposits. Ore Geol. Rev. 119, 10323.

Brant, R.A.P., Souza, V.S., Dantas, E.L., Jost, H., Rodrigues, V.G., Carvalho, M.J., Araújo, K.C., 2015. Contribuição ao estudo de proveniência sedimentar com base em dados U-Pb para o greenstone belt de Faina, Goiás. In: SBG, XIV Simpósio de Geologia do Centro-Oeste, Brasília, Anais, pp. 30-33.

Campos, D. S., Silva, A. M., Toledo, C.L.B., Carvalho, M.J., Araujo, K. (2017). Prospectivity analysis of gold and iron oxide copper-gold-(silver) mineralizations from the Faina Greenstone Belt, Brazil, using multiple data sets. Brazilian Journal of Geology, São Paulo, v. 47, n. 4, p. 561-590, out./dez.

Campos, L.M. Caracterização das zonas de alteração hidrotermal associadas à mineralização de ouro no greenstone belt Crixás – GO. 2019. xix, 165 il. Dissertação (Mestrado em Geologia) — Instituto de Geociências, Universidade de Brasília, Brasília.

Carvalho M.J., Rodrigues V.G., Jost H. 2013. Formação Arraial Dantas: depósito aurífero detrítico glacíge- no do greenstone belt de Faina, Goiás. In: UFRGS, Simpósio Brasileiro de Metalogenia, 3, Gramado, Re- sumo em DF, 2 pgs.

DNPM – Departamento Nacional de Produção Mineral. Relatório de Planejamento e Arrecadação. Goiânia, 2007.

De Wit M.J., Ashwal L.D. 1995. Greenstone belts: what are they? South African Journal of Geology 98:504–519.

Dentith, M., and Mudge,T.S., 2014, Geophysics for the Mineral Exploration Geoscientist: London, Cambridge University Press, 454p.

Fortes, P.T.F.O., 1996. Metalogênese dos depósitos auríferos Mina III, Mina Nova e Mina Inglesa, greenstone belt de Crixás, GO. Tese de Doutorado, Instituto de Geociências, Universidade de Brasília, 176 pp.

Fortes, P.T.F.O., Pimentel, M.M., Santos, R.V., Junges, S., 2003. Sm-Nd study of the Crixás greenstone belt, Brazil: implications for the age of deposition of the upper sedimentary rocks and associated Au mineralization. Journal of South American Earth Sciences 16, 503-512.

Jost H., Fuck R.A., Dantas E.L., Rancan C.C., Rezende D.B., Santos E., Portela J.F., Mattos L., Chiarini M.F.N., Oliveira R.C., Silva S.E. 2005. Geologia e geocro- nologia do Complexo Uvá, bloco arqueano de Goi- ás. Rev. Brasil. Geociências, 35:559-572.

Jost, H.; Dussin, I. A.; Chemale Jr., F.; Tassinari, C. C. G.; Junges, S., 2008a. U-Pb and Sm-Nd constraints for the Paleoproterozoic age of the metasedimentary sequences of the Goiás Archean greenstone belts. VI SOUTH AMERICAN SYMPOSIUM ON ISOTOPE GEOLOGY, 6, San Carlos de Bariloche, 2008, Argentina, 2008a., Proceedings in CD, 4 p.,

Jost H., Chemale Junior F., Fuck R.A., Dussin I.A. 2013. Uvá complex, the oldest orthogneisses of the Archean-Paleoproterozoic terrane of central Brazil. Journal of South American Earth Sciences, 47:201-212.

Jost, H., Carvalho, M.J., Rodrigues, V.G., Martins, R., 2014. Metalogênese dos greenstone belts de Goiás. In: Silva, M.G., Neto, M.B.R., Jost, H., Kuyumjian,114 R.M. (Orgs.), Metalogênese das províncias tectônicas brasileiras, Belo Horizonte, CPRM, pp. 141-168.

Marques J.C., Jost H., Creaser R.A., Frantz J.C., Osório R.G. 2013. Age of arsenopyrite gold-bearing massi- ve kenses of the Mina III and its implication on ex- ploration, Crixás greenstone belt, Goiás, Brazil. In UFRGS, Simp. Bras. Metalongenia, 3, Gramado, Resumo em CD, 32 pgs.,

Orinoco Gold Limited (ASX:OGX), 2014 to 2018. Annual reports. Available at: https://orinocogold.com/shareholder-centre/financial-reports/annual-reports.

Patten, C.G.C, Pitcairn, I.K., Molnár, F., Kolb, J., Beaudoin, G., Guilmette, C., Peillod, A.; Gold mobilization during metamorphic devolatilization of Archean and Paleoproterozoic metavolcanics rocks. Geology 2020; 48 (11): 1110–1114.

Pearce, Julian. 2014. Geochemical Fingerprinting of the Earth's Oldest Rocks. Geology. 42. 175-176.

Pereira, H.S., 2017. Integração de dados geológicos, geoquímicos, espectrorradiométricos e de propriedades físicas de rocha: o estudo de caso do Corpo N5S, Província Mineral de Carajás. 150 f., il. Dissertação (Mestrado em Geologia) —Universidade de Brasília, Brasília.

Pimentel M.M., Fuck R.A., Jost H., Ferreira Filho C.F., Araújo S.M., 2000. The basement of the Brasília Fold Belt and the Goiás Magmatic Arc. In: Cordani UG, Milani EJ, Thomaz Filho A, Campos DA (eds) Tectonic evolution of South America, international geological congress, Rio de Janeiro, pp 195–232.

Pimentel, M.M., Jost, H., Fuck, R.A., Armstrong, R.A., Dantas, E.L., Potrel, A., 2003. Neoproterozoic anatexis of 2.9 Ga old granitoids in the Goiás-Crixás block, Central Brazil: evidence from new SHRIMP U-Pb data and Sm-Nd isotopes. Geol. USP, Sér. Cient. 3, 1-12.

Pimentel, M.M., Jost, H., Fuck, R.A., 2004. O embasamento da Faixa Brasília e o Arco Magmático de Goiás. In: Mantesso-Neto, V., Bartorelli, A., Carneiro, C.D.R., Neves, B.B.B. (Eds.), Geologia do Continente Sul-Americano: evolução da obra de Fernando Fávio Marques de Almeida. Beca Produções Culturais Ltda, São Paulo, pp. 356-368.

Pimentel, M.M., 2016. The tectonic evolution of the Neoproterozoic Brasília Belt, central Brazil: a geochronological and isotopic approach. Braz. J. Geol. 46, 67-82.

Prado, Elias., Silva, A., Ducart, D., Toledo, C., Assis, L., 2016. Reflectance spectroradiometry applied to a semi-quantitative analysis of the mineralogy of the N4ws deposit, Carajás Mineral Province, Pará, Brazil. Ore Geology Reviews. 78.

Post, J.L. Saponite from Near Ballarat, California. Clays Clay Miner. 32, 147–153 (1984).

Post, J. E. and Appleman, D. E.; 1994. Crystal structure refinement of lithiophorite. American Mineralogist; 79 (3-4): 370–374.

Post, J. E., 1999. Manganese oxide minerals: Crystal structures and economic and environmental significance. Proceedings of the National Academy of Sciences Mar 1999, 96 (7) 3447-3454.

Queiroz C.L., Jost H., Silva L.C., McNaughton N.J. 2008. U-Pb SHRIMP and Sm-Nd geochronology of granite- gneiss complexes and implications for the evolution of the central Brazil Archean terrain. J. South Am. Earth Sci., 26:100-124.

Resende M.G., Jost H., Osborne G.A., Mol A.G., 1998. Stratygraphy of the Goiás and Faina greenstone belts, Central Brazil: a new proposal. Revista Brasileira de Geociencias, 28, 77-94.

Resende M.G., Jost H., Lima B.E.M., Teixeira A.A. 1999. Proveniência e idades-modelo Sm-Nd de rochas siliciclásticas arqueanas dos greenstone belts de Faina e Santa Rita, Goiás. RBG, 29:281-290.

Roberson, H.E., Reynolds, R.C. & Jenkins, D.M. 1999. Hydrothermal Synthesis of Corrensite: A Study of the Transformation of Saponite to Corrensite. Clays Clay Miner. 47, 212–218.

Rodrigues V.G. 2011. Geologia do depósito aurífero do Caiamar, greenstone belt de Guarinos: um raro depósito associado a albitito sódico. Dissertação de Mestrado. IG/UnB, 79 pgs.

Santos R.V., Oliveira C.G., Souza V.H.V., Carvalho M.J., Andrade T.V., Souza H.G.A. 2008. Correlação isotópica baseada em isótopos de Carbono entre os greenstone belts de Goiás. In: SBG, Congr. Bras. Geol., 44, Curitiba, Volume de Resumos, pg. 52.

Silva, M. P., Rocha, C., 2008. Caracterização da Mineração Aurífera em Faina, Goiás, em um Contexto Ambiental Histórico e Atual. Ambiente & Sociedade. Campinas, v. XI, n. 2.

da Silva, P.J.M.; Horbe, A.M.C e Horbe, M.A., 2012. Mineralogia e geoquímica de ocorrências manganesíferas da bacia Alto Tapajós, sudeste do estado do Amazonas, Brasil. Bol. Mus. Para. Emilio Goeldi Cienc. Nat. [online]., vol.7, n.1, pp.11-28. ISSN 1981-8114.

Silva, P. J. M., Horbe, A. M. C. & M. A. Horbe, 2012. Mineralogia e geoquímica de ocorrências manganesíferas da bacia Alto Tapajós, sudeste do estado do Amazonas, Brasil. Boletim do Museu Paraense Emílio Goeldi. Ciências Naturais 7(1): 11-28.

Tassinari C.G., Jost H., Santos J., Nutman A, Bennell M.R. 2006. Pb and Nd isotope signatures and SHRIMP U-Pb geochronological evidence of Paleoproterozoic age for Mina III gold mineralization, Crixás District, Central Brazil. V SAGI CD-ROM, pp. 527-529

Turner S., and Post J E, American Mineralogist, 73 (1988). p.1155-1161, Refinement of the substructure and superstructure of romanechite

Post Jeffrey E., & Appleman. 1994. Crystal structure refinement of lithiophorite. American Mineralogist, Volume 79, pages 370-374.

Smithies, R.H., Ivanic, T.J., Lowrey, J.R; Morris, P.A., Barnes, S.J., Wyche, S ; Lu, Y. 2018. Two distinct origins for Archean greenstone belts. Earth and Planetary Science Letters. 487. 106-116.

Toledo, C.L.B.; Silva, A.M.; Chemale Jr, F.; Almeida, T.; Garnier, J.; Araujo Filho, J.O.; Hauser, N.; Botelho, N.F.; Jost, H.; Bernardi, G.B.; Paiva, R.G.; Magaldi, T.T.; Ferreira, V.H.C.S.; Magalhães, H.V.B.; Araujo, B.V.B.; Silva, L.B.C.; Bastos, Y.M.M.; Teixeira, C.D.; Vieira, H.A.; Moraes, F.G.M.; Neiva Jr, F.B.; Mansur, E.T.; Soares, T.M.; Valle, R.S.C.; Silva, S.P.; Oliveira, A.L.; Martins, P.L.G.; Franco, G.S.; Lamblém, H.S.; Leite, A.M.; Fazio, G.; Topan, J.G.O.; Daldegan, L.C.B.; Cassemiro, R.B., 2014. Projeto Faina-Goiás – Mapeamento Geológico na escala 1:25.000. Trabalho de Formatura da UnB.

Wang, R., Cudahy, T., Laukamp, C., Walshe, J. L., Bath, A., Mei, Y., … Laird, J. (2017). White Mica as a Hyperspectral Tool in Exploration for the Sunrise Dam and Kanowna Belle Gold Deposits, Western Australia. Economic Geology, 112(5), 1153–1176.

Welch, M. D. & Marshall, W. G. 2001. High-pressure behavior of clinochlore. American Mineralogist, Volume 86, pages 1380–1386, 2001.

CAPÍTULO IV – DISCUSSÕES FINAIS

1. Considerações finais e sugestões para trabalhos futuros

A presente dissertação de mestrado foi realizada com o intuito de investigar e caracterizar vetores que possam viabilizar melhor compreensão do sistema polimetálico Tinteiro presente no *greenstone belt* de Faina que é uma descoberta relativamente recente, e ainda foi muito pouco estudado. A rotina aplicada baseou-se em técncias de análise direta de cinco furos que interceptam este sistema, tais quais caracterização microscópica de detalhe, difratometria de raios-x, mapeamento espectral, geoquímica e petrofísica das rochas. Foram definidas duas zonas de alterações principais, uma rica em muscovita, e outra rica em hematita, e foram respectivamente definidas como halo distal e halo proximal do sistema, e por fim, a zona mineralizada. Comprovando assim, a eficácia da metodologia proposta na caracterização de sistemas polimetálicos hospedados em *greenstone belts*.

A integração dos multiparâmetros coletados identifica que o *footprint* da zona distal do sistema é caracterizada por alta susceptibilidade magnética (valor médio de 4,23 x 10^{-3} SI), abundancia de clorita e carbonato superior a 0,1, teores superiores a 5% de MgO, Cao, P_2O_5 e Na_2O e pouca incidência de estruturas rúpteis. O *footprint* do halo proximal do sistema evidencia uma queda nos valores de densidade e susceptibilidade magnética das rochas ao sentido da mineralização, a composição dos minerais do grupo dos óxidos e hidróxidos de ferro é de hematita e a cristalinidade dos minerais membros do grupo das micas brancas atingem valores superiores a 10, e quanto maior a proximidade da porção mineralizada, maior a intensidade de feições de venulações e fraturas. O *footprint* da zona mineralizada é caracterizado por queda da abundancia de minerais do grupo dos óxidos e hidróxidos de ferro (menor que 0,22), queda nos valores da densidade da rocha, mas altos valores de densidade absoluta e a susceptibilidade magnética aumenta em relação às zonas proximais (média de 0,542 x 10^{-3} SI).

A identificação de fases minerais componentes das rochas mineralizadas do sistema Tinteiro (brechas manganesíferas) foi bem definida pelo método de difratometria de raios-x, principalmente a paragênese dos óxidos e hidróxidos de manganês, uma vez que estes compõem mais de 1% de parte das amostras (limite de detecção da técnica) (Vyverberg *et al.*, 2018). Recomenda-se um estudo mais detalhado com uma malha de maior adensamento em afloramentos e amostras de brechas manganesíferas e suas diversas ocorrências no *greenstone belt* de Faina com o uso do método de *Rietveld* para a quantificação das principais fases minerais.

Este estudo comprovou que a densidade é um importante vetor petrofísico na identificação do sistema Tinteiro. Este parâmetro quando analisado em relação a densidade absoluta das amostras apresenta aumento proporcional em função da intensidade de alteração hidrotermal hematítica, e o oposto ocorre com os valores de densidade natural das rochas. Com este fato em mente, recomenda-se

a aplicação do método de gravimetria gradiométrica para possibilitar a identificação de novos alvos (espaçamento de 100 metros) no polígono da área deste trabalho. Com base nos resultados da inversão dos dados gravimétricos gradiométricos é possível projetar uma malha de sondagem de furos mais profundos que possam avançar no entendimento desse sistema Tinteiro polimetálico em profundidade. Adicionalmente, com dados de uma futura campanha de sondagem mais profunda, poderão ser adquiridos novos dados petrofísicos e de mapeamento mineral e espectral para o refinamento dos vetores. Estes vetores poderão ser integrados por técnicas de *machine learning* com o intuito de promover a geração de cenários prospectivos mais robustos na região do *greenstone belt* de Faina.

REFERÊNCIAS BIBLIOGRÁFICAS

Adams, J.B., 1974. Visible and near-infrared diffuse reflectance: spectra of pyroxenes as applied to remote sensing of solid objects in the solar system. J. Geophys. Res. 79, 4829–4836.

Beghelli Junior, L.P., 2012. Charnockitos e ortognaisses da porção centro-oeste do Bloco Arqueano de Goiás: Dados geoquímicos e isotópicos. Dissertação de Mestrado, Instituto de Geociências, Universidade de Brasília, 87 pp.

Borges, C.C.A., Toledo, C.L.B., Silva, A.M., Junior, F. C., Jost, H., & de Carvalho Lana, C., 2017. Geochemistry and isotopic signatures of metavolcanic and metaplutonic rocks of the Faina and Serra de Santa Rita greenstone belts, Central Brazil: Evidences for a Mesoarchean intraoceanic arc.Precambrian Research, 292, 350-377.

Bogossian, J., Hagemann S.G., Rodrigues V.G., Lobato L.M., Roberts M., 2020. Hydrothermal Alteration and Mineralization in the Faina greenstone belt: evidence from the Cascavel and Sertão orogenic gold deposits. Ore Geol. Rev. 119, 10323.

Brant, R.A.P., Souza, V.S., Dantas, E.L., Jost, H., Rodrigues, V.G., Carvalho, M.J., Araújo, K.C., 2015. Contribuição ao estudo de proveniência sedimentar com base em dados U-Pb para o greenstone belt de Faina, Goiás. In: SBG, XIV Simpósio de Geologia do Centro-Oeste, Brasília, Anais, 30-33.

Burns, R.G., 1993. Origin of electronic spectra of minerals in the visible and near-infrared region. In: Pieters, C.M., Englert, P.A.J. (Eds.), Remote Geochemical Analysis: Elemental and Mineralogical Composition. Cambridge University Press, New York, 3–30.

Byrne, K., Lesage, G, Gleeson S.A., Piercey, S.J., Lypaczewski, P, Kyser, K.; Linking Mineralogy to Lithogeochemistry in the Highland Valley Copper District: Implications for Porphyry Copper Footprints. Economic Geology 2020;; 115 (4): 871–901. doi: https://doi.org/10.5382/econgeo.4733

Campos, D. S., Silva, A. M., Toledo, C.L.B., Carvalho, M.J., Araujo, K. 2017. Prospectivity analysis of gold and iron oxide copper-gold-(silver) mineralizations from the Faina Greenstone Belt, Brazil, using multiple data sets. Brazilian Journal of Geology, São Paulo, v.47, n. 4, 561-590.

Campos, L.M, 2019. Caracterização das zonas de alteração hidrotermal associadas à mineralização de ouro no greenstone belt Crixás – GO. xix, 165 il. Dissertação (Mestrado em Geologia) — Instituto de Geociências, Universidade de Brasília, Brasília.

Carvalho M.J., Rodrigues V.G., Jost H. 2013. Formação Arraial Dantas: depósito aurífero detrítico glacíge- no do greenstone belt de Faina, Goiás. In: UFRGS, Simpósio Brasileiro de Metalogenia, 3, Gramado, Re- sumo em DF, 2 pgs.

DNPM – Departamento Nacional de Produção Mineral. 2007. Relatório de Planejamento e Arrecadação. Goiânia.

de Jong, S. M., & van der Meer, F. D. 2004. Remote sensing image analysis : including the spatial domain. (Remote sensing and digital image processing; Vol. 5). Kluwer Academic.

Dentith, M., and Mudge,T.S., 2014, Geophysics for the Mineral Exploration Geoscientist: London, Cambridge University Press, 454p.

De Wit M.J., Ashwal L.D., 1995. Greenstone belts: what are they? South African Journal of Geology 98:504–519.

Fortes, P.T.F.O., 1996. Metalogênese dos depósitos auríferos Mina III, Mina Nova e Mina Inglesa, greenstone belt de Crixás, GO. Tese de Doutorado, Instituto de Geociências, Universidade de Brasília, 176p.

Fortes, P.T.F.O., Pimentel, M.M., Santos, R.V., Junges, S., 2003. Sm-Nd study of the Crixás greenstone belt, Brazil: implications for the age of deposition of the upper sedimentary rocks and associated Au mineralization. Journal of South American Earth Sciences 16, 503-512.

Goetz A.F.H., Barrett N. Rock, Lawrence C. Rowan; Remote sensing for exploration; an overview. Economic Geology 1983;; 78 (4): 573–590.David I. Groves, Frank P. Bierlein, Lawrence D. Meinert, Murray W. Hitzman; Iron Oxide Copper-Gold (IOCG) Deposits through Earth History: Implications for Origin, Lithospheric Setting, and Distinction from Other Epigenetic Iron Oxide Deposits. Economic Geology 2010;; 105 (3): 641–654. doi: https://doi.org/10.2113/gsecongeo.105.3.641

Hastie, Evan C.G.; Daniel J. Kontak, Bruno Lafrance; Gold Remobilization: Insights from Gold Deposits in the Archean Swayze Greenstone Belt, Abitibi Subprovince, Canada. Economic Geology 2020;; 115 (2): 241–277. doi: https://doi.org/10.5382/econgeo.4709

Hinze, William & vonFrese, Ralph & Saad, Afif. 2013. Gravity and Magnetic Exploration, Principles, Practices, and Applications by Hinze, vonFrese and Saad.

Hunt, G. R., 1977. Spectral signatures of particulate minerals in the visible and near infrared. Geophysics. 42(3), 501-513.

Jost H., Fuck R.A., Dantas E.L., Rancan C.C., Rezende D.B., Santos E., Portela J.F., Mattos L., Chiarini M.F.N., Oliveira R.C., Silva S.E. 2005. Geologia e geocro- nologia do Complexo Uvá, bloco arqueano de Goi- ás. Rev. Brasil. Geociências, 35:559-572.

Jost, H.; Dussin, I. A.; Chemale Jr., F.; Tassinari, C. C. G.; Junges, S., 2008a. U-Pb and Sm-Nd constraints for the Paleoproterozoic age of the metasedimentary sequences of the Goiás Archean greenstone belts. VI SOUTH AMERICAN SYMPOSIUM ON ISOTOPE GEOLOGY, 6, San Carlos de Bariloche, 2008, Argentina, 2008a., Proceedings in CD, 4 p.,

Jost H., Chemale Junior F., Fuck R.A., Dussin I.A. 2013. Uvá complex, the oldest orthogneisses of the Archean-Paleoproterozoic terrane of central Brazil. Journal of South American Earth Sciences, 47:201-212.

Jost, H., Carvalho, M.J., Rodrigues, V.G., Martins, R., 2014. Metalogênese dos greenstone belts de Goiás. In: Silva, M.G., Neto, M.B.R., Jost, H., Kuyumjian,114 R.M. (Orgs.), Metalogênese das províncias tectônicas brasileiras, Belo Horizonte, CPRM, pp. 141-168.

Katz, L. R., Kontak, D. J., Dubé B., McNicoll, V., Creaser, R., Petrus, J. A., 2020. An Archean Porphyry-Type Gold Deposit: The Côté Gold Au(-Cu) Deposit, Swayze Greenstone Belt, Superior Province, Ontario, Canada. Economic Geology;; 116 (1): 47–89. doi: https://doi.org/10.5382/econgeo.4785

Kreuzer, Oliver P., Mahyar Yousefi, Vesa Nykänen. Introduction to the special issue on spatial modelling and analysis of ore-forming processes in mineral exploration targeting, Ore Geology Reviews, Volume 119, 2020, 103391, ISSN 0169-1368, https://doi.org/10.1016/j.oregeorev.2020.103391.

Mathieu, L., Snyder, D. B., Bedeaux, P., Cheraghi, S., Lafrance, B., Thurston, P., & Sherlock, R. (2020). Deep into the Chibougamau area, Abitibi greenstone belt: Structure of a Neoarchean crust revealed by seismic reflection profiling. Tectonics, 39, e2020TC006223. https://doi.org/10.1029/2020TC006223

Marques J.C., Jost H., Creaser R.A., Frantz J.C., Osório R.G. 2013. Age of arsenopyrite gold-bearing massi- ve kenses of the Mina III and its implication on ex- ploration, Crixás greenstone belt, Goiás, Brazil. In UFRGS, Simp. Bras. Metalongenia, 3, Gramado, Resumo em CD, 32 pgs.,

Meer, F.D. van der., Jong, S. M. D. (Eds.). 2002. Imaging Spectrometry. Remote Sensing and Digital Image Processing. doi:10.1007/978-0-306-47578-8

Meneses P.R., Netto M.S.J., Moraes L.M.E., Ponzoni J.F., Junior F.G.L., Galvão S.L.(Eds.) 2001. Sensoriamento remoto, reflectância dos alvos naturais. 1 ed., 262 pp.

Orinoco Gold Limited (ASX: OGX), 2014 to 2018. Annual reports. Available at: https://orinocogold.com/shareholder-centre/financial-reports/annual-reports.

Patten, C.G.C, Pitcairn, I.K., Molnár, F., Kolb, J., Beaudoin, G., Guilmette, C., Peillod, A.; Gold mobilization during metamorphic devolatilization of Archean and Paleoproterozoic metavolcanics rocks. Geology 2020; 48 (11): 1110–1114.

Pearce, Julian. (2014). Geochemical Fingerprinting of the Earth's Oldest Rocks. Geology. 42. 175-176.

Pereira, H. S., 2017. Integração de dados geológicos, geoquímicos, espectrorradiométricos e de propriedades físicas de rocha: o estudo de caso do Corpo N5S, Província Mineral de Carajás. 2017. 150 f., il. Dissertação (Mestrado em Geologia) —Universidade de Brasília, Brasília, 2017.

Pimentel M.M., Fuck R.A., Jost H., Ferreira Filho C.F., Araújo S.M., 2000. The basement of the Brasília Fold Belt and the Goiás Magmatic Arc. In: Cordani UG, Milani EJ, Thomaz Filho A, Campos DA (eds) Tectonic evolution of South America, international geological congress, Rio de Janeiro, pp 195–232.

Pimentel, M.M., Jost, H., Fuck, R.A., Armstrong, R.A., Dantas, E.L., Potrel, A., 2003. Neoproterozoic anatexis of 2.9 Ga old granitoids in the Goiás-Crixás block, Central Brazil: evidence from new SHRIMP U-Pb data and Sm-Nd isotopes. Geol. USP, Sér. Cient. 3, 1-12.

Pimentel, M.M., Jost, H., Fuck, R.A., 2004. O embasamento da Faixa Brasília e o Arco Magmático de Goiás. In: Mantesso-Neto, V., Bartorelli, A., Carneiro, C.D.R., Neves, B.B.B. (Eds.), Geologia do Continente Sul-Americano: evolução da obra de Fernando Fávio Marques de Almeida. Beca Produções Culturais Ltda, São Paulo, pp. 356-368.

Pimentel, M.M., 2016. The tectonic evolution of the Neoproterozoic Brasília Belt, central Brazil: a geochronological and isotopic approach. Braz. J. Geol. 46, 67-82.

Prado, Elias & Silva, Adalene & DUCART, DIEGO & Toledo, Catarina & Assis, Luciano. (2016). Reflectance spectroradiometry applied to a semi-quantitative analysis of the mineralogy of the N4ws deposit, Carajás Mineral Province, Pará, Brazil. Ore Geology Reviews. 78.

Post, J.L., 1984. Saponite from Near Ballarat, California. Clays Clay Miner. 32, 147–153.

Post, J. E. and Appleman, D. E.; 1994. Crystal structure refinement of lithiophorite. American Mineralogist; 79 (3-4): 370–374.

Post, J. E., 1999. Manganese oxide minerals: Crystal structures and economic and environmental significance. Proceedings of the National Academy of Sciences Mar 1999, 96 (7) 3447-3454.

Queiroz C.L., Jost H., Silva L.C., McNaughton N.J. 2008. U-Pb SHRIMP and Sm-Nd geochronology of granite- gneiss complexes and implications for the evolution of the central Brazil Archean terrain. J. South Am. Earth Sci., 26:100-124.

Rieger, P., Joseph M. Magnall, Sarah A. Gleeson, Anja M. Schleicher, Marie Bonitz, Richard Lilly. The mineralogical and lithogeochemical footprint of the George Fisher Zn-Pb-Ag massive sulphide deposit in the Proterozoic Urquhart Shale Formation, Queensland, Australia, Chemical Geology, Volume 560, 2021, 119975, ISSN 0009-2541, https://doi.org/10.1016/j.chemgeo.2020.119975.

Resende M.G., Jost H., Osborne G.A., Mol A.G., 1998. Stratygraphy of the Goiás and Faina greenstone belts, Central Brazil: a new proposal. Revista Brasileira de Geociencias, 28, 77-94.

Resende M.G., Jost H., Lima B.E.M., Teixeira A.A. 1999. Proveniência e idades-modelo Sm-Nd de rochas siliciclásticas arqueanas dos greenstone belts de Faina e Santa Rita, Goiás. RBG, 29:281-290.

Roberson, H.E., Reynolds, R.C. & Jenkins, D.M., 1999. Hydrothermal Synthesis of Corrensite: A Study of the Transformation of Saponite to Corrensite. Clays Clay Miner. 47, 212–218.

Rodrigues V.G. 2011. Geologia do depósito aurífero do Caiamar, greenstone belt de Guarinos: um raro depósito associado a albitito sódico. Dissertação de Mestrado. IG/UnB, 79 pgs.

Santos R.V., Oliveira C.G., Souza V.H.V., Carvalho M.J., Andrade T.V., Souza H.G.A. 2008. Correlação isotópica baseada em isótopos de Carbono entre os greenstone belts de Goiás. In: SBG, Congr. Bras. Geol., 44, Curitiba, Volume de Resumos, pg. 52.

Silva, M. P., Rocha, C. (2008). Caracterização da Mineração Aurífera em Faina, Goiás, em um Contexto Ambiental Histórico e Atual. Ambiente & Sociedade. Campinas, v. XI, n. 2.

da Silva, P.J.M.; Horbe, A.M.C e Horbe, M.A., 2012. Mineralogia e geoquímica de ocorrências manganesíferas da bacia Alto Tapajós, sudeste do estado do Amazonas, Brasil. Bol. Mus. Para. Emilio Goeldi Cienc. Nat. [online]., vol.7, n.1, pp.11-28. ISSN 1981-8114.

Silva, P. J. M., Horbe, A. M. C. & M. A. Horbe, 2012. Mineralogia e geoquímica de ocorrências manganesíferas da bacia Alto Tapajós, sudeste do estado do Amazonas, Brasil. Boletim do Museu Paraense Emílio Goeldi. Ciências Naturais 7(1): 11-28.

Smithies, R. H., Ivanic, T. J., Lowrey, J. R., Morris, P. A., Barnes, S. J., Wyche, S., & Lu, Y. - J. (2018). Two distinct origins for Archean greenstone belts. Earth and Planetary Science Letters, 487, 106-116. https://doi.org/10.1016/j.epsl.2018.01.034

Tassinari C.G., Jost H., Santos J., Nutman A, Bennell M.R. 2006. Pb and Nd isotope signatures and SHRIMP U-Pb geochronological evidence of Paleoproterozoic age for Mina III gold mineralization, Crixás District, Central Brazil. V SAGI CD-ROM, pp. 527-529

Tassinari, C.G., Jost, H., Santos, J., Nutman, A., Bennell, M.R., 2006. Pb and Nd isotope signatures and SHRIMP U-Pb geochronological evidence of Paleoproterozoic age for Mina III gold mineralization, Crixás District, Central Brazil. 5th South American Symposium on Isotope Geology, Punta Del Este, Uruguay, Short Papers Volume, p. 527-529.

Turner S., and Post J E, 1988 American Mineralogist, 73. p.1155-1161, Refinement of the substructure and superstructure of romanechite.

Schön, J. H. 2011. Physical Properties of Rocks, A Workbook. Volume 8, 1-494.

Jeffrey E. Post, Daniel E. Appleman. 1994. Crystal structure refinement of lithiophorite· American Mineralogist, Volume 79, pages 370-374.

Smithies, R & Ivanic, Tim & Lowrey, Jack & Morris, Paul & Barnes, Stephen & Wyche, Stephen & Lu, Yong-jun. (2018). Two distinct origins for Archean greenstone belts. Earth and Planetary Science Letters. 487. 106-116.

Thompson, A.J.B., Hauff, P.L. & Robitaille, A.J., 1999. Alteration Mapping in Exploration: Application of Short-Wave Infrared (SWIR) Spectroscopy. Econ. Geol. Newlsetter, #39, October 1999.

Toledo, C.L.B.; Silva, A.M.; Chemale Jr, F.; Almeida, T.; Garnier, J.; Araujo Filho, J.O.; Hauser, N.; Botelho, N.F.; Jost, H.; Bernardi, G.B.; Paiva, R.G.; Magaldi, T.T.; Ferreira, V.H.C.S.; Magalhães, H.V.B.; Araujo, B.V.B.; Silva, L.B.C.; Bastos, Y.M.M.; Teixeira, C.D.; Vieira, H.A.; Moraes, F.G.M.; Neiva Jr, F.B.; Mansur, E.T.; Soares, T.M.; Valle, R.S.C.; Silva, S.P.; Oliveira, A.L.; Martins, P.L.G.; Franco, G.S.; Lamblém, H.S.; Leite, A.M.; Fazio, G.; Topan, J.G.O.; Daldegan, L.C.B.; Cassemiro, R.B., 2014. Projeto Faina-Goiás – Mapeamento Geológico na escala 1:25.000. Trabalho de Formatura da UnB.

Van der Meer, F. (2000). Spectral curve shape matching with a continuum removed CCSM algorithm. International Journal of Remote Sensing. 21. 3179-3185. 10.1080/01431160050145063.

Vyverberg, K. L., Jaeger, J. M., & Dutton, A. (2018). Quantifying Detection Limits and Uncertainty in X-ray Diffraction Mineralogical Assessments of Biogenic Carbonates. Journal of Sedimentary Research, 88(11), 1261–1275. doi:10.2110/jsr.2018.63

Williams P.J., Barton M.D., Johnson D.A., Fonteboté L., Haller A., Mark G., Oliver N.H.S., Marschik R. 2005. Iron Oxide Copper-Gold Deposits: Geology, Space-Time Distribution, and Possible Modes of Origin. Economic Geology 100th Anniversary Volume. p. 371-405.

Wang, R., Cudahy, T., Laukamp, C., Walshe, J. L., Bath, A., Mei, Y., … Laird, J. (2017). White Mica as a Hyperspectral Tool in Exploration for the Sunrise Dam and Kanowna Belle Gold Deposits, Western Australia. Economic Geology, 112(5), 1153–1176.

Welch, M. D. & Marshall, W. G. 2001. High-pressure behavior of clinochlore. American Mineralogist, Volume 86, pages 1380–1386.